MECHANICAL CHARACTERIZATION AND STRUCTURAL ANALYSIS OF NORMAL AND REMODELED CARDIOVASCULAR SOFT TISSUE

A Dissertation

by

AKHILESH A. KOTIYA

Submitted to the Office of Graduate Studies of
Texas A&M University
in partial fulfillment of the requirements for the degree of

DOCTOR OF PHILOSOPHY

May 2008

Major Subject: Biomedical Engineering

MECHANICAL CHARACTERIZATION AND STRUCTURAL ANALYSIS OF NORMAL AND REMODELED CARDIOVASCULAR SOFT TISSUE

A Dissertation

by

AKHILESH A. KOTIYA

Submitted to the Office of Graduate Studies of
Texas A&M University
in partial fulfillment of the requirements for the degree of

DOCTOR OF PHILOSOPHY

Approved by:

Chair of Committee,	John C. Criscione
Committee Members,	Jay D. Humphrey
	Christopher M. Quick
	Rudolph Stewart
Head of Department,	Gerard L. Cote'

May 2008

Major Subject: Biomedical Engineering

ABSTRACT

Mechanical Characterization and Structural Analysis of Normal and Remodeled Cardiovascular Soft Tissue. (May 2008)

Akhilesh A. Kotiya, B.En, Mumbai University; M.S., Texas A&M University

Chair of Advisory Committee: Dr. John C. Criscione

Characterization of multiaxial mechanical properties of cardiovascular soft tissue is essential in order to better understand their growth and remodeling in homeostatic conditions and in response to injury or pathological conditions. Though numerous phenomenological models have been proposed to characterize such multiaxial mechanical behavior, the approach has certain drawbacks regarding experimental determination of the model coefficients. We propose a method that aims to overcome these drawbacks. The approach makes use of orthogonal polynomials to fit the biaxial test data and suggests a way to derive the strain energy function from these analytical fits by way of minimizing the deviation of the behavior from hyperelastic ideal. Using the proposed method, a strain energy function for a lymphatic vessel is derived and the method is compared with traditional ones that used non-orthogonal polynomials as independent variables in the functional form for strain energy. The unique coefficient values obtained using the proposed method, for the first time gives us an opportunity to attribute a physical characteristic of the material to the coefficient values. The method also provides a way to assess two different material behaviors by way of comparing their deviation from the hyperelastic behavior when a similar test protocol is used to collect the data, over a similar deformation range and the order of polynomial function is chosen so as to give a similar error of fit. The behavior of mesenteric lymph vessels from normal cows, cows subjected to sham surgery and those subjected to 3 days of edematous conditions by venous occlusion are compared using this method. To be able to better understand the changes in mechanical behavior, morphological analysis of the vessels was carried out and the geometric and structural changes in these vessels were studied. We found that the behavior of bovine mesenteric lymph vessels subjected to a

high flow condition shows a small difference in their mechanical behavior as compared to the vessels from normal a cow and a cow subjected to sham surgery. The geometry and structure of these vessels also showed marked differences from the other two. The thickness to radius ratio increased and a rise in percentage of area occupied by smooth muscle cells and medial collagen was observed. Though not all the differences were statistically significant, we conclude that the behavior and the morphology are suggestive of the remodeling of the vessel in response to altered hemodynamic conditions and require further investigation.

DEDICATION

To my Teachers, Family and Friends

ACKNOWLEDGEMENTS

I would like to thank my committee chair, Dr. John C. Criscione, and my committee members, Dr. Humphrey, Dr. Quick, and Dr.Stewart, for their guidance and support throughout the course of this research.

Thanks also go to my friends and colleagues and the department faculty and staff for making my time at Texas A&M University a great experience

Finally, thanks to my mother and father for their encouragement and my sister and cousins for their support throughout these years.

TABLE OF CONTENTS

LIST OF FIGURES

FIGURE Page

FIGURE Page

LIST OF TABLES

TABLE Page

CHAPTER I
INTRODUCTION

Background

The Lymphatic System

The lymphatic system consists of lymphatic vessels and lymph nodes and is primarily involved with maintaining interstitial fluid balance by returning the net outflow of micro-vascular filtrate from the interstitial space to circulation. The lymphatic vessels were observed as early as 400 BC by Hippocrates and the lymphatic system itself was described by Gasparo Aselli in 1672 (Swartz 2001). The name lymphatic is derived from the almost transparent fluid (lympha-water) that these vessels carry.

Apart from maintaining interstitial fluid at homeostatic levels these vessels form an important part of immune system as the leukocytes and antigen-presenting cells are transported with lymph to lymph node where they initiate proliferation of white blood cells (Rockson 2005). As a result swollen lymph nodes are commonly observed when body is fighting some infection. Some of the lymphatic vessels are also involved with specific function such as those of intestine, called lacteals that absorb fatty acids and cholesterol from the mucosal cells of the gut (Swartz 2001).

The lymphatic system is implicated in tumor metastasis too. The highly permeable initial lymphatic vessels provide an easily accessible conduit for migration of malignant cells and the nodes provide a healthy/desirable environment for their proliferation (Trappen and Pepper 2001). They also play a key role in inflammation associated with asthma and are believed to be involved with pathologies such as psoriasis, rheumatoid arthritis and with medical problems such as transplant rejection.

Anatomy

Though the development of the lymphatic vessels, de-novo formation /lymphangiogenesis or sprouting and transdifferentitation from venules, is debatable

---

This dissertation follows the style of Journal of Biomechanics.

(Nagase et al., 2005) they are as widespread as the blood vessels. These thin walled transparent vessels are found in almost all organs except in cartilages, nails, cuticle and hair. They can be classified as superficial and deep vessels (Grays 1901) and are organized as initial lymphatics also called lymphatic capillaries or terminal lymphatics, collecting vessels, trunks and lymphatic ducts (Swartz 2001).

The superficial vessels lie immediately under the integument while the deep vessels are situated in submucous arerolar tissue throughout the length of gastro pulmonary and genitor urinary tracts and in subserous tissue in cranial, thoracic and abdominal cavities (Grays 1901). The initial lymphatic consists of single layer of non-fenestrated highly attenuated endothelial cells that are attached to the ECM collagen by the so called anchoring filaments. These blind ended vessels that are usually larger than blood capillaries carry the lymph (interstitial fluid, plasma proteins and other macromolecules) into the collecting vessels. The collecting vessel wall consists of a single layer of endothelial cells lining the luminal volume. The wall itself has few layers of SMC and has unidirectional valves that separate the vessel into segments called lymphangions.

The collecting vessels usually pass through a cluster of lymph node and can be termed as afferent and efferent depending upon if they enter into a lymph node or exit from one. The efferent vessels empty into lymphatic trunk that drains into the lymphatic duct. All the collecting vessels except for those from right side of head, neck and thorax, right lung and upper extremities, right side of heart and convex surface of liver empty themselves into thoracic duct (Grays 1901). The duct originates from the receptaculum chyli and ends at the root of the neck where it joins left subclavian vein at its junction with the left internal jugular vein. The other collecting vessels empty into the right lymphatic duct that is connected to the right subclavian vein near the bifurcation with the right internal jugular vein (Grays 1901). The vessels from intestinal, hepatic and lumbar area do not drain directly into the thoracic duct but they drain into cisterna chyli/ receptaculum chili.

Histology

The terminal lymphatic vessels are made of a single layer of attenuated endothelial cells that often overlap each other to form open junctions. The cells are attached to the ECM with help of so called anchoring filaments made of fibrillin (Scavelli et al., 2004). The anchoring filaments are attached to the outer membrane of the endothelial cells that form the open junction. The basement membrane is either discontinuous or absent (Pepper and Skobe 2003).

The vessel wall of the collecting lymphatics can be divided into three layers. The innermost layer or intima is a single layer of endothelial cells surrounded by basement membrane. The middle layer or media consists of few layers of SMC with collagen and elastin fibers. The amount and arrangement of SMC within this layer is dependent on the size of the vessel. The smaller vessels have smaller amounts of SMC and lack any particular organization whereas the larger vessels have more ordered SMC oriented in circumferential direction. The outer layer or adventitia consists of connective tissue elements along with nerves and the fibroblasts (Von Der Weid 2001). The unidirectional valves are made of elastic fibers with endothelial cells lining both the sides. (Hargen and Schmid-Schonbein 2000).

Physiology-Lymph Formation, Absorption and Propulsion

The net flux of blood plasma (that forms the interstitial fluid) out of blood capillaries and that of interstitial fluid into initial lymphatic vessels is often described by Starlings law (Swartz 2001, Hargen and Schmid-Schonbein 2000) as given below,

$$J = L_p A(\Delta P - \sigma \Delta \pi) \qquad (1.1)$$

Where J is the trans-capillary filtration (blood: J_c or lymphatic: J_l), A the capillary surface area, L_p the permeability of capillary wall, ΔP the local hydrostatic pressure difference across capillary wall, $\Delta \pi$ the local osmotic pressure difference across the capillary wall and σ the capillary osmotic reflection coefficient.

It should be noted that the two fluxes need not be the same at a given moment and that persistent difference among them ($J_c > J_l$) will eventually result in a pathological condition called edema.

The interstitial fluid flows into the lumen of the initial lymphatics through the open junctions formed by the overlapping endothelial cells and is propelled forward into the collecting lymphatics by compression (predominantly passive). Once into the collecting lymphatic the retrograde flow of lymph is blocked by the unidirectional valves that are usually bicuspid (some with single flap and tricuspid have also been observed) (Swartz 2001). The lymph is propelled further by the intrinsic constriction of the vessel lumen due to spontaneous contraction of SMC. Along with this active mechanism some of the passive mechanisms that aide in propulsion of lymph through the lymphatic vessels and nodes are motion of surrounding skeletal muscle and those of the blood vessels, the intrathoracic pressure differential created by breathing and that in the subclavian veins due to blood flow (Von Der Weid 2001).

Lymphedema

Edema is a condition that results from interstitial fluid imbalance and is characterized by local accumulation of excess proteins and fluid, increased number of fibroblasts, adipocytes and keratinocytes in interstitial space that gives rise to increased collagen deposition and outgrowth of adipose and connective tissue eventually resulting in fibrosis (Rockson 2005). The condition is a result of either high output failure or low output failure. In case of high output failure the lymphatic system is overwhelmed i.e. there is excess filtration of blood plasma and macromolecules than a healthy lymphatic system can handle. The resulting condition as observed during inflammation is commonly called oedema. On the other hand the low output failure generally termed as Lymphedema is a consequence of compromised functionality of the lymphatic vessels and nodes. Lymphedema is further classified as primary lymphedema and secondary lymphedema

The primary lymphedema is generally caused due to genetic/chromosomal defect with praecox lymphedema being the most common form of primary edema that occurs

predominantly in female population (10:1 female to male ratio). It is further classified as congenital (occurs before age 2), praecox (occurs sometime after puberty upto third decade of life) and tarda (occurs after age 35). *Some of the known primary lymphedema are: Noonan Syndrome, Noone-Milroy Hereditary Lymphedema, Meige Lymphedema, Lymphedema Distichiasis, Cholestasis-Lymphedema Syndrome, Lymphedema-microcephaly-Cho etc (Rockson 2005).*

Secondary lymphedema occurs due to compromised lymphatic vessels and nodes as a result of trauma, diseases, surgery and radiotherapy. American cancer society claims that of the 2 million treated for breast cancer 400,000 develop lymphedema. World wide about 90 million suffer from the disease.

Lymphedema often result in thickening of skin, lipidosis and fibrosis due to excessive accumulation of collagen fiber, disruption of the immune system (Rockson 2005), repeated episodes of bacterial infections like cellulites or lymphangitis (Lymphology 2003) etc. Although not fatal such complication are associated with a variety of psychological and social issues, may result in impaired organ function, pain and unsatisfactory cosmesis (Brennan and Miller 1998).

Diagnosis

In most of the cases the clinical history and physical examination suffices to diagnose lymphedema but for cases where the pathology is secondary to certain other conditions such as morbid obesity, venous insufficiency etc, other diagnostic tools might or should be used. The isotope lymphography also called as lymphoscintigraphy or lymphangioscintigraphy has been most successful to accurately determine a lymphatic abnormality. Other imaging tools available to better understand the disease are magnetic resonance imaging (MRI), ultrasonography (US), computed tomography (CT), lymphography (IL), fluorescent microlymphangiography(FM), phlebography etc. Genetic testing can also be used to identify gene mutation associated with certain primary lymphedema such as lymphedema-distichiasis (FOXC2) and Milroy disease (VEGFR-3). Biopsy and fine needle aspiration with cytological examination are other alternatives but should be used only as a last resort.

Treatment Strategies to Resolve Lymphedema

The options available for resolution of lymphedema can be classified into conservative or non-operative and operative. The conservative approaches include combined physical therapy (CPT) and drug therapy where as the operative approaches include resection and microsurgical procedure.

The combined physical therapy also known as complex decongestive physiotherapy is a two phase treatment. Phase 1 consists of skin care, manual massage, exercise and use of compression bandages while phase 2 is aimed at maintaining the results obtained at the end of phase 1. Along with this pneumomassage, regular massage, simple elevation and thermal therapy can also be used to manage the lymphedema. The drug therapy consists of use of diuretics (usually at the initial stages of CPT), Benzopyrones that helps the absorption of tissue proteins into the lymphatic vessels by hydrolyzing them, antimicrobials: antibiotics in case of cellulites or erysipelas and antimycotic drugs for fungal infections, and drugs such as diethylcarbamazine, Albendazole or Ivermectin used to counter the microfilariae in blood.

Operative procedures are not widely accepted and are usually employed when the non operative procedures fail to show any significant improvement in lymphedema resolution. Resection involves simple operations such as removal of excess skin, omental transposition, enteromesenteric bridge operation, liposuction etc. Microsurgical approaches include reconstructive method such as autologous vein or lymph vessel transplantation and derivative method such as lympho-venous and lympho-nodal venous anastamosis/shunt (Campisi et al, 2001, Matsubara et al., 2006).

Although a wide variety of approaches have been developed to resolve lymphedema there has been little progress in treating this pathology (Swartz 2001). For the development of novel treatment strategies as well as refinement of the existing ones, both surgical and pharmaceutical, it is essential that one understands the changes in the structure and hence the function of the lymphatic vessels due to the pathological condition (lymphedema). The research presented in the following chapters has been motivated predominantly by this idea. The main goals of the study were as follows,

- Develop a methodology to derive, from experimental data, a constitutive equation do describe biaxial mechanical behavior (inflation-extension) for thin walled vessels in terms of Criscione's strain attributes.
- Study the mechanical behavior of normal lymph vessels and those subjected to edematous conditions using the methodology developed.
- Study the morphological changes in the lymph vessels subjected to edematous condition.

A way to determine strain energy function from the biaxial experimental data is described in chapter II. Use of such methodology allows one to determine error of definition or the error associated with the assumption of hyperelastic behavior and hence allows one to compare two different test protocols. We use 2 dimensional orthogonal polynomials to fit the experimental data which not only simplifies parameter estimation using least square analysis but also yields unique parameter values. Such uniqueness allows one a way to assign a physical meaning to parameter and to correlate them with the underlying structure. Finally derivation of strain energy function in terms of Criscione's strain attributes leads to orthogonal response functions and hence minimal error propagation.

Chapter III briefly discusses a custom built biaxial test device and illustrates the use of theory developed in chapter I to describe and compare the biaxial mechanical behavior of normal lymph vessels and those subjected to edematous conditions. Both comparison of error of definition and of parameter values is used to study the difference between the mechanical behaviors of the two kinds of vessels.

The morphological changes in the lymph vessels subjected to edematous conditions are discussed in chapter IV. We compare the vessel geometry to study the changes in wall thickness and histological analysis is carried out to determine the changes in microstructure of the vessels.

CHAPTER II
ON THE BIAXIAL MECHANICAL BEHAVIOR OF THIN WALLED VESSELS – THEORY

Introduction

Characterization of multiaxial mechanical properties of cardiovascular soft tissue is essential in order to better understand their growth and remodeling in homeostatic conditions and in response to injury or pathological conditions (Humphrey 2003). Such information is also beneficial towards research and development of novel cardiovascular devices and would certainly be useful to improve surgical interventions especially those carried out with use of robotic manipulators.

Numerous phenomenological models have been proposed to characterize such multiaxial mechanical behavior. The common practice in developing these models is to assume that the tissue behavior is hyperelastic or Green elastic and hence existence of a strain energy function W. The functional form of W is guessed a priori and its parameters are estimated from the multiaxial test data using linear or nonlinear regression analysis (Humphrey et al., 1990).

This procedure has certain drawbacks regarding experimental determination of the parameters of the assumed functional form of W. Since the assumption of hyperelastic behavior is seldom verified a wide variety of soft tissues are modeled using a single functional form without any regards to the appropriateness of using the model. Also a variety of test protocols are used to collect data from which to estimate the parameter values of the assumed functional form W. Since the parameters estimated are dependent on the experimental protocol (Humphrey et al., 1990) one might end up with two completely different set of parameters for the same assumed function form for two specimens that are exactly the same which is not desirable.

Also the most commonly used strain measures, namely Green Strain E and its invariants I, give rise to covariant response functions and hence result in a significant propagation of experimental error (Criscione 2003, 2004). Finally the functional forms guessed often have non orthogonal independent variables that might lead to some issues

in regression analysis (Shacham and Brauner 1997) and over-parameterization of W. Such collinearity also results in non unique parameter values that vary with the order of the assumed functional form (Yin et al.,1986, Fung et al., 1979).

The aim of this study is 1. To fit the biaxial test data with analytical function that uses orthogonal polynomials in two variables as independent variables. 2. Propose a measure to quantify the deviation of the mechanical behavior of the vessel under combined loading from the hyperelastic ideal 3. Infer, based on the biaxial test data, a strain energy function in terms of Criscione strain attributes that minimizes this measure for a given experimental protocol.

Use of orthogonal polynomials in terms of Criscione strain attributes to fit the experimental data results in minimizing error propagation, results in response functions that do not covary, avoid over-parameterization, and give unique parameter values i.e. independent of the order of the polynomial function. It also simplifies regression analysis as matrix (X^TX) of normal equation reduces to a diagonal matrix and hence does not have to be inverted.

A measure that quantifies the deviation of behavior from the hyperelastic ideal would help us to verify the assumption of hyperelastic or Green elastic behavior and hence give us an idea about the efficacy of the model in its application to certain real life problems. It would also help us to compare different experimental protocols that are commonly used to model the biaxial behavior of the vessel and help us to identify one that ensures that the behavior is as close to being hyperelastic as possible. This protocol can then be used as a standard protocol to test a vessel under assumption that its behavior is hyperelastic.

The functional form of W that we propose is motivated both by theory and experimental data. Though the approach is similar to the one suggested by Rivlin and Saunders (Rivlin and Saunders 1951) to model biaxial behavior of rubber and that employed by Humphrey and Yin to model the passive biaxial behavior of myocardium (Humphrey et al., 1990), it is not exactly the same. Similar to these approaches the theory helps to determine the Criscione strain attributes that W would depend on but W

in terms of these attributes is derived directly from the surface fits to the biaxial experimental data That is rather than starting with a functional form for W and then determining the parameters by fitting the response function to the experimental data, we begin by fitting the experimental data with separate analytical functions in terms of orthogonal polynomials and determine W from these functions hence allowing one to separate error of fit from error of definition.

Theoretical Preliminaries

Kinematics of Combined Inflation and Extension of a Thin Walled Tube

Let B_0 be the fixed reference configuration of a tubular continuum as shown in the figure 2.1. The geometric region occupied by the continuum can then be defined in terms of cylindrical polar coordinates (**R, Q, Z**) as (Ogden 1997)

$$R_{in} < R < R_{out} \qquad 0 < Q < 2\pi \qquad 0 < Z < L \tag{2.1}$$

Where R_{in} and R_{out} is the inner and outer radius of the vessel and L is its initial unstretched length. Let deformation χ: $B_0 \in R^3$, that for the current case represents combined inflation and extension, transform a material point of interest **X** in reference configuration to position **x** in current/deformed configuration B_t such that $\boldsymbol{x}=\chi(\boldsymbol{X}) \in B$. The deformation gradient for the transformation/deformation is given by $F = \frac{\partial x}{\partial X}$ and the current configuration of the vessel in terms of coordinates (**r, q, z**) can be defined as

$$r_{in} < r < r_{out} \qquad 0 < q < 2\pi \qquad 0 < z < l \tag{2.2}$$

Where r_{in} and r_{out} are inner and outer radius of the vessel in the current configuration and $l = \lambda_z L$ is its current length. λ_z is the axial stretch ratio. The deformation χ is given as

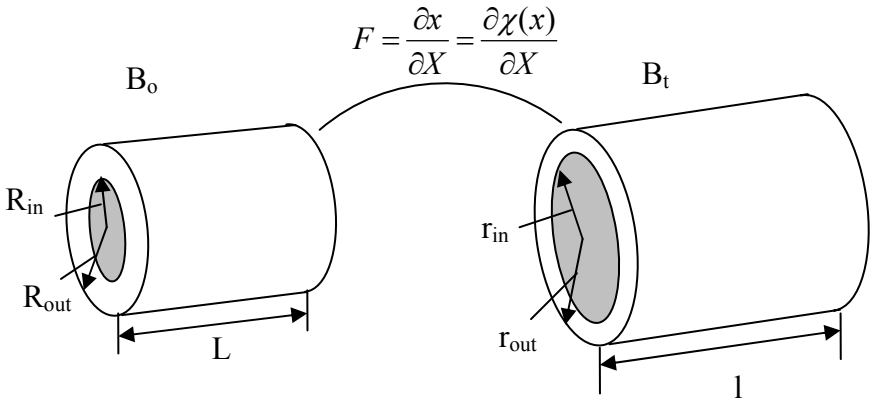

Figure 2.1: Combined inflation and extension of a thin walled axis-symmetric tube. B_o is the reference configuration and B_t is the current configuration. The deformation is given by $\mathbf{x}=\chi(\mathbf{X})$ with deformation gradient as F.

The circumferential stretch ratio is a function of radial position R in reference configuration and is given as,

$$\lambda_Q^2(R) = \lambda_Z^{-1} + \left(\lambda_Q^2(R_{out}) - \lambda_Z^{-1}\right)\frac{R_{out}^2}{R^2} \tag{2.3}$$

The deformation gradient F for the above deformation is also a function of R and is given as,

$$F(R) = \begin{bmatrix} \lambda_Z^{-1}\lambda_Q(R)^{-1} & 0 & 0 \\ 0 & \lambda_Q(R) & 0 \\ 0 & 0 & \lambda_Z \end{bmatrix}_{R,Q,Z} \tag{2.4}$$

For combined inflation-extension of an incompressible axis-symmetric vessel that after deformation can still be assumed as axis-symmetric, the coordinates for reference and current configuration stay the same i.e. **r=R**, **q=Q** and **z=Z.** The Criscione strain attributes for such deformation are given as (Criscione 2004)

$$\begin{aligned} &\gamma_1 = 0, \quad \gamma_2 = \ln\lambda_Z^{3/2}, \quad \gamma_3 = \ln\lambda_Q^2(R) + \ln\lambda_Z, \\ &\gamma_4 = 0, \quad \gamma_5 = 0, \quad \gamma_6 = 0, \end{aligned} \tag{2.5}$$

Stress Power Law and Constitutive Relation

Hyperelastic or Green Elastic materials are defined as those for which there exists a scalar function of strain attributes called the strain energy potential or elastic potential function W (Malvern pg 282). Such materials conserve as strain energy any mechanical work that is performed on them. For simple material acted on by negligible body forces and undergoing mechanical processes that are isothermal, quasistatic and that result in negligible body couples and reversible heat conduction, the conservation of energy and stress power gives,

$$\dot{W} = \mathrm{J}\, t : \dot{F}\, F^{-1} \tag{2.6}$$

Substituting for **F** in terms of Crisione's strain attributes it can be shown that (Criscione 2004)

$$\mathrm{W} = \mathrm{W}\left(\gamma_1, \gamma_2, \gamma_3, \gamma_4, \gamma_5, \gamma_6\right) \tag{2.7}$$

For the case of combined inflation and extension of a thin walled incompressible vessel the above form of strain energy function can be further reduced to,

$$\mathrm{W} = \mathrm{W}\left(\gamma_2, \gamma_3\right) \tag{2.8}$$

The Cauchy stress **t** can then be defined as a sum of response terms each consisting of a derivative of W with respect to one of the Criscione strain attributes multiplied by a kinematic tensor,

$$t = -\mathrm{p}\, I + \frac{1}{\mathrm{J}} \sum_{\mathrm{i}=2}^{3} \frac{\partial \mathrm{W}}{\partial \gamma_{\mathrm{i}}} A_{\mathrm{i}} \tag{2.9}$$

Where Ai are given as (Criscione 2004)

$$A_1 = I, \qquad A_2 = z \otimes z - \frac{1}{2} q \otimes q - \frac{1}{2} r \otimes r, \qquad A_3 = q \otimes q - r \otimes r \tag{2.10}$$

p is the Lagrange Multiplier whose value is determined from appropriate boundary conditions.

Though complete characterization of an incompressible, orthotropic thin walled vessel would require $\mathrm{W} = \mathrm{W}\left(\gamma_2, \gamma_3, \gamma_4, \gamma_5, \gamma_6\right)$, the dependence of strain energy function on $\gamma_{4\text{-}6}$ cannot be determined from combined inflation-extension test. Characterization of

such dependence would require one to perform tests that can subject the vessel to combined inflation, extension, torsion, telescopic shear and circumferential shear. Though one can perform combined torsion, inflation and extension test on thin walled vessel (Humphrey1993) we are unaware of any test device that can induce telescopic shear and circumferential shear on thin walled vessels. Also it should be noted that inflation and extension are the most prominent deformation that most of the thin walled vessels undergo in-vivo.

Equilibrium Equations

In absence of body forces (weight of the vessel being supported by buoyant force while immersed in a tissue bath), couple moments and inertial forces (use of test protocol that ensures slow deformation of the test specimen) the conservation of mass and linear momentum requires

$$\nabla . t = 0 \tag{2.11}$$

For symmetric **t** and in absence of variation of stress components along axial and circumferential directions the above relation reduces to,

$$\begin{aligned} &\frac{dt_{rr}}{dr} + \frac{t_{rr} - t_{\theta\theta}}{r} = 0 \\ &\frac{dt_{r\theta}}{dr} + 2\frac{t_{r\theta}}{r} = 0 \\ &\frac{dt_{rz}}{dr} + \frac{t_{rz}}{r} = 0 \end{aligned} \tag{2.12}$$

From equation above and considering that $-t_{rr}(r_{in})=P_{in}$ and $-t_{rr}(r_{out})=P_{out}$ where P_{in} and P_{out} are internal and external pressure respectively it can be shown that (Criscione 2004)

$$P_{in} - P_{out} = \int_{r_{in}}^{r_{out}} \frac{2}{rJ}\frac{\partial W}{\partial \gamma_3} dr \tag{2.13}$$

Considering the global equilibrium in the axaial direction one can derive the following equation for the measured load,

$$L_z = 3\pi \int_{r_{in}}^{r_{out}} \frac{1}{J}\frac{\partial W}{\partial \gamma_2} r dr \tag{2.14}$$

For a thin walled incompressible vessel the above two equation can be further reduced to

$$P_{in} - P_{out} = 2\frac{\partial W}{\partial \gamma_3}\frac{h}{r_{avg}} \qquad (2.15\ a)$$

$$L_z = 3\pi \frac{\partial W}{\partial \gamma_2} r_{avg} h \qquad (2.15\ b)$$

Where r_{avg} is the average radius of the vessel and h is the thickness of the vessel wall.

Data Fitting

Typical experimental measurements for a combined inflation extension loading of the thin walled vessel include that of luminal pressure, axial load, outside diameter of the vessel and axial stretch ratio. Using these measured values one can estimate the quantities $\left(\frac{\partial W_{\gamma_2}}{\partial \gamma_2}\right)_{\exp}$ and $\left(\frac{\partial W_{\gamma_3}}{\partial \gamma_3}\right)_{\exp}$ as defined in equation below,

$$\left(\frac{\partial W_{\gamma_3}}{\partial \gamma_3}\right)_{\exp} = \frac{(P_{in} - P_{out}).r_{avg}}{2.h} \qquad \left(\frac{\partial W_{\gamma_2}}{\partial \gamma_2}\right)_{\exp} = \frac{L_z}{3\pi r_{avg} h} \qquad (2.16)$$

Where $(P_{in} - P_{out})$, is the transmural pressure difference, L_z is the measured load, r_{avg} is the average radius of the vessel wall and h is the thickness of the vessel wall

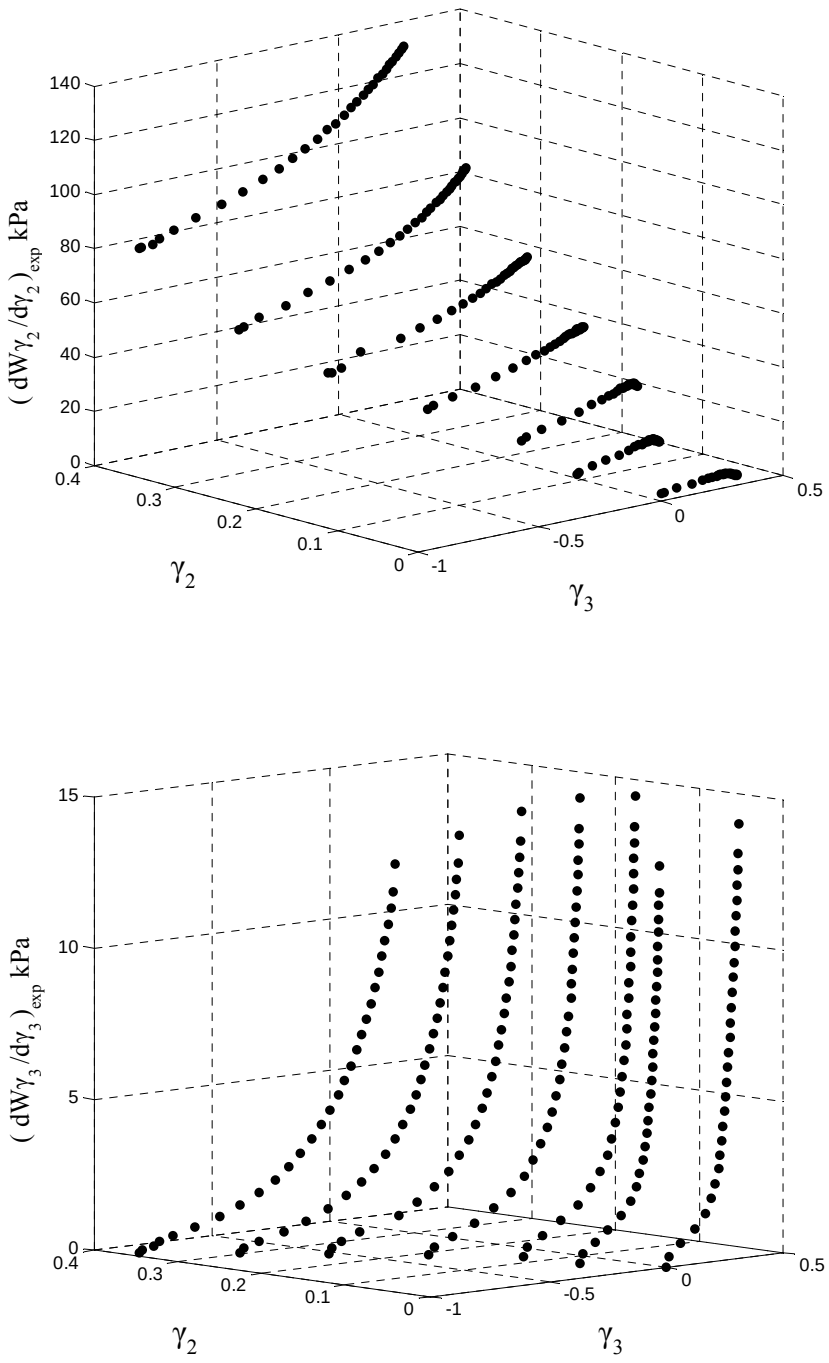

Figure 2.2: The variation of $\left(\partial W_{\gamma_2}/\partial\gamma_2\right)_{exp}$ and $\left(\partial W_{\gamma_3}/\partial\gamma_3\right)_{exp}$ with respect to γ_2 and γ_3. The variation is obtained from the inflation extension test on a lymphatic vessel assumed to be incompressible with orthotropic material behavior.

It must be noted that both the entities in equation 2.16 are experimentally measured entities and by $\left(\frac{\partial W_{\gamma_k}}{\partial \gamma_k}\right)_{\exp}$ we do not imply that the material behavior under the prescribed multiaxial loading is hyperelastic or Green elastic. Typical variation of $\left(\frac{\partial W_{\gamma_2}}{\partial \gamma_2}\right)_{\exp}$ and $\left(\frac{\partial W_{\gamma_3}}{\partial \gamma_3}\right)_{\exp}$ with respect to γ_2 and γ_3 as obtained from the inflation extension test on a lymphatic vessel shown in figure 2.2 and can be approximated in terms of orthogonal polynomials as follows,

$$\left(\frac{\partial W_{\gamma_k}}{\partial \gamma_k}\right)_{Fit} = \sum_{i=1}^{n}\sum_{j=1}^{m} a_{ij}\phi_i(\gamma_2)\phi_j(\gamma_3) \qquad k = 1,2 \tag{2.17}$$

Where, n and m are the order of the orthogonal polynomials used and a_{ij} are the unknown coefficients. The orthogonal polynomials can be obtained using the Gram-Schmidt process and are given as follows, (Forsythe 1957)

$$\begin{aligned}\phi_{r+1}(\gamma_k) = &\left(\gamma_k - \sum_{p=1}^{N}(\gamma_k)_p\phi_r^2(\gamma_k)_p \Big/ \sum_{p=1}^{N}\phi_r^2(\gamma_k)_p\right)\phi_r(\gamma_k) \\ &-\left(\sum_{p=1}^{N}\phi_r^2(\gamma_k)_p \Big/ \sum_{p=1}^{N}\phi_{r-1}^2(\gamma_k)_p\right)\phi_{r-1}(\gamma_k)\end{aligned} \tag{2.18}$$

Such that, $\phi_0(\gamma_k) = 1 \quad \phi_1(\gamma_k) = (\gamma_k - \bar{\gamma}_k)$, $\sum_{p=1}^{N}\left[\phi_i(\gamma_2)\phi_j(\gamma_3)\phi_r(\gamma_2)\phi_s(\gamma_3)\right]_p = \kappa\delta_{ir}\delta_{js}$, and N is the number of data points.

The coefficients a_{ij} can be estimated using least square method and minimizing the objective function

$$e = \sum_{p=1}^{N}\left[\left(\frac{\partial W_{\gamma_k}}{\partial \gamma_k}\right)_{\exp} - \sum_{i=1}^{n}\sum_{j=1}^{m} a_{ij}\phi_i(\gamma_2)\phi_j(\gamma_3)\right]_p^2 \tag{2.19}$$

Following the standard procedure of least square analysis (Forsythe 1957) it can be shown that the coefficients a_{ij} can be obtained from the normal equations as follows

$$[\phi_i(\gamma_2)\phi_j(\gamma_3)]^T_{p\times(n+m)}[\phi_r(\gamma_2)\phi_s(\gamma_3)]_{p\times(n+m)}[\mathbf{a}_{ij}]_{(n+m)\times 1} = \left[\left(\frac{\partial W_{\gamma_k}}{\partial \gamma_k}\right)_{\exp}\right]_{1\times p}[\phi_i(\gamma_2)\phi_j(\gamma_3)]_{p\times(n+m)} \quad (2.20)$$

For orthogonal polynomials $\phi_i(\gamma_2)$ and $\phi_j(\gamma_3)$ the above equation can be further reduced to,

$$[\mathbf{A}_{ij}]_{(n+m)\times(n+m)}[\mathbf{a}_{ij}]_{(n+m)\times 1} = [\mathbf{B}_{ij}]_{1\times(n+m)} \quad (2.21)$$

where,

$$\mathbf{A}_{ij} = \sum_{p=1}^{N}[\phi_i(\gamma_2)\phi_j(\gamma_3)\phi_i(\gamma_2)\phi_j(\gamma_3)]_p \quad and \quad B_{ij} = \sum_{p=1}^{N}\left[\left(\frac{\partial W_{\gamma_k}}{\partial \gamma_k}\right)_{\exp}\phi_i(\gamma_2)\phi_j(\gamma_3)\right]_p$$

It should be evident that $\mathbf{A}_{ij}$ is a diagonal matrix and hence we have

$$a_{ij} = B_{ij} / A_{ij} \quad (2.22)$$

For **A** to be a diagonal matrix the distribution of γ_2 and γ_3 should confirm to certain conditions as given below,

$$\begin{aligned}
&\sum_{p=1}^{N}(\gamma_2 - \bar{\gamma}_2)_p \approx 0 \\
&\sum_{p=1}^{N}(\gamma_3 - \bar{\gamma}_3)_p \approx 0 \\
&\sum_{p=1}^{N}(\gamma_2 - \bar{\gamma}_2)_p(\gamma_3 - \bar{\gamma}_3)_p \approx 0
\end{aligned} \quad (2.23)$$

Failure of γ_2-γ_3 distribution to confirm to these conditions gives rise to collinearity amongst the independent variables $\phi_i(\gamma_2)\phi_j(\gamma_3)$. This could result in overparameterisation of the fit and the coefficients determined will not be unique. In many cases the experimental setup does not allow precise control over the γ_2-γ_3 values and hence the distribution would fail to confirm to the above conditions. It will be

required then that one use appropriate method to select new values of γ_2 - γ_3 that confirm to the condition in equation (2.23) and allows one to estimate the corresponding values of $\left(\frac{\partial W_{\gamma_k}}{\partial \gamma_k}\right)_{\exp}$ from the original ones.

To determine the goodness of fit we use the following two measures (Hu et al., 2007).

$$\varepsilon = \frac{1}{mean\left(\frac{\partial W_{\gamma_k}}{\partial \gamma_k}\right)_{\exp}} \sqrt{\frac{e_{\gamma_k}}{(N-q)}}$$

$$AIC = N \ln\left(\frac{e_{\gamma_k}}{N}\right) + 2.q \tag{2.24}$$

Where, q is the number of parameters/coefficients $(n \times m)$, N is the number of data points, and $e_{\gamma_k} = \sum_{p=1}^{N}\left[\left(\frac{\partial W_{\gamma_k}}{\partial \gamma_k}\right)_{\exp} - \left(\frac{\partial W_{\gamma_k}}{\partial \gamma_k}\right)_{fit}\right]_p^2$. It must be noted that mean of $\frac{\partial W_{\gamma_k}}{\partial \gamma_k}$ is used for normalization of standard error ε instead of reference value of $\frac{\partial W_{\gamma_k}}{\partial \gamma_k}$ as in Hu 2007, owing to the fact that there is significant error associated with determination of $\frac{\partial W_{\gamma_k}}{\partial \gamma_k}$ at the reference configuration.

Deviation from Hyperelastic Behavior

If the material behavior under the combined loading were hyperelastic then from the results of equation 2.15 it would be possible to determine a strain energy function using the analytical fit $\left(\frac{\partial W_{\gamma_k}}{\partial \gamma_k}\right)_{fit}$. For instance the strain energy function W can be inferred from the $\left(\frac{\partial W_{\gamma_2}}{\partial \gamma_2}\right)_{fit}$ and $\left(\frac{\partial W_{\gamma_3}}{\partial \gamma_3}\right)_{fit}$ using the following equation

$$W = \int \left(\frac{\partial W_{\gamma_2}}{\partial \gamma_2} \right)_{Fit} d\gamma_2 + \int \left(\frac{\partial W_{\gamma_3}}{\partial \gamma_3} \right)_{Fit} d\gamma_3 \Bigg|_{\gamma_2 = 0} \tag{2.25}$$

The second term in the above equation is added to account for the γ_3 terms that would equate to zero when one takes partial of W with γ_2. One can then obtain an analytical function $\left(\frac{\partial W_{\gamma_3}}{\partial \gamma_3} \right)_{predict}$ to predict the data $\left(\frac{\partial W_{\gamma_3}}{\partial \gamma_3} \right)_{\exp}$ by taking the partial of W in equation 2.25 with γ_3 as follows,

$$\left(\frac{\partial W_{\gamma_3}}{\partial \gamma_3} \right)_{predict} = \frac{\partial W}{\partial \gamma_3} = \frac{\partial}{\partial \gamma_3} \left(\int \left(\frac{\partial W_{\gamma_2}}{\partial \gamma_2} \right)_{Fit} d\gamma_2 + \int \left(\frac{\partial W_{\gamma_3}}{\partial \gamma_3} \right)_{Fit} d\gamma_3 \Bigg|_{\gamma_2 = 0} \right) \tag{2.26}$$

Similarly one can derive W from $\left(\frac{\partial W_{\gamma_2}}{\partial \gamma_2} \right)_{fit}$ and $\left(\frac{\partial W_{\gamma_3}}{\partial \gamma_3} \right)_{fit}$ and hence $\left(\frac{\partial W_{\gamma_2}}{\partial \gamma_2} \right)_{predict}$ using equations below,

$$W = \int \left(\frac{\partial W_{\gamma_3}}{\partial \gamma_3} \right)_{Fit} d\gamma_3 + \int \left(\frac{\partial W_{\gamma_2}}{\partial \gamma_2} \right)_{Fit} d\gamma_2 \Bigg|_{\gamma_3 = 0} \tag{2.27}$$

$$\left(\frac{\partial W_{\gamma_2}}{\partial \gamma_2} \right)_{predict} = \frac{\partial W}{\partial \gamma_2} = \frac{\partial}{\partial \gamma_2} \left(\int \left(\frac{\partial W_{\gamma_3}}{\partial \gamma_3} \right)_{Fit} d\gamma_3 + \int \left(\frac{\partial W_{\gamma_2}}{\partial \gamma_2} \right)_{Fit} d\gamma_2 \Bigg|_{\gamma_3 = 0} \right) \tag{2.28}$$

If the behavior were truly hyperelastic then the error in predicting the data using the function $\left(\frac{\partial W_{\gamma_k}}{\partial \gamma_k} \right)_{predict}$ would be near zero or comparable to the error of fit. Therefore the sum of square of difference between the values predicted by $\left(\frac{\partial W_{\gamma_k}}{\partial \gamma_k} \right)_{predict}$ and those by $\left(\frac{\partial W_{\gamma_k}}{\partial \gamma_k} \right)_{fit}$ at all the data points (γ_2, γ_3) can be used as an indicator of deviation from the hyperelastic ideal. With this motivation we define following measures to quantify the

deviation from hyperelastic behavior of the vessel under combined loading of inflation and extension,

$$\Delta_{\varepsilon} = \frac{2}{mean\left(\frac{\partial W_{\gamma_2}}{\partial \gamma_{\gamma_2}}\right)_{\exp} + mean\left(\frac{\partial W_{\gamma_3}}{\partial \gamma_{\gamma_3}}\right)_{\exp}} \sqrt{\frac{e_{\gamma_2} + e_{\gamma_3}}{(2N - q_{\gamma_2} - q_{\gamma_3})}} \tag{2.29}$$

$$\Delta_{AIC} = 2N \ln\left(\frac{e_{\gamma_2} + e_{\gamma_3}}{2N}\right) + 2.q_{\gamma_2} + 2.q_{\gamma_3} \tag{2.30}$$

Where, $e_{\gamma_k} = \sum_{p=1}^{N}\left[\left(\frac{\partial W_{\gamma_k}}{\partial \gamma_k}\right)_{predict} - \left(\frac{\partial W_{\gamma_k}}{\partial \gamma_k}\right)_{fit}\right]_p^2$, $mean\left(\frac{\partial W_{\gamma_k}}{\partial \gamma_{\gamma_k}}\right)_{\exp} = \frac{1}{N}\sum_{p=1}^{N}\left[\left(\frac{\partial W_{\gamma_k}}{\partial \gamma_{\gamma_k}}\right)_{\exp}\right]_p$, N is the no. of data points and q_{γ_k} is the number of parameters/coefficients.

Strain Energy Function

Once the analytical fits $\left(\frac{\partial W_{\gamma_2}}{\partial \gamma_2}\right)_{fit}$ and $\left(\frac{\partial W_{\gamma_3}}{\partial \gamma_3}\right)_{fit}$ are determined one can obtain two different strain energy functions using equation 2.25 and 2.27. Since the hyperelasticity assumption requires existence of a single valued potential we propose one as follows

$$W = \omega\left[\int\left(\frac{\partial W_{\gamma_2}}{\partial \gamma_2}\right)_{Fit} d\gamma_2 + \int\left(\frac{\partial W_{\gamma_3}}{\partial \gamma_3}\right)_{Fit} d\gamma_3\Big|_{\gamma_2=0}\right] + (1-\omega)\left[\int\left(\frac{\partial W_{\gamma_3}}{\partial \gamma_3}\right)_{Fit} d\gamma_3 + \int\left(\frac{\partial W_{\gamma_2}}{\partial \gamma_2}\right)_{Fit} d\gamma_2\Big|_{\gamma_3=0}\right] \tag{2.31}$$

Where weight ω is a value between 0 and 1, with value of 0 indicating that the strain energy function is same as that obtained by using equation 2.25 and that of 1 indicating it is as obtained using equation 2.27. Once the $\left(\frac{\partial W_{\gamma_2}}{\partial \gamma_2}\right)_{fit}$ and $\left(\frac{\partial W_{\gamma_3}}{\partial \gamma_3}\right)_{fit}$ are determined for the data obtained using a particular biaxial test protocol, Δ_{ε} and Δ_{AIC} is estimated for

each weight ω varying from 0 to 1 in steps of 0.1 and the ω that gives the minimum Δ is used to obtain the final form of strain energy function. Here we would like to reiterate the fact that functional form of W was not guessed a priori, neither was its functional form inspired by the experimental data. Rather the two sets of experimental data were fit with orthogonal polynomials independently and W is then derived from these two analytical fits such that the deviation from hyperelastic behavior is minimized.

Illustrative Example

To illustrate the method to calculate the deviation from hyperelastic ideal and to derive a strain energy function from the data so as to minimize such deviation we use the biaxial test data obtained from combined inflation and extension test performed on a bovine mesenteric lymph vessel. We will make standard assumptions regarding the vessel i.e. the vessel is incompressible, has orthotropic behavior at in-vivo configuration, is locally homogeneous, is axis-symmetric, thin walled and undergoes non-linear finite deformation. The hyperelastic behavior of such a vessel as mentioned earlier can be described using a strain energy function $W = W(\gamma_2, \gamma_3)$.

Specimen Preparation and Testing

A valve free segment of postnodal lymphatic vessel was harvested, using blunt dissection, from bovine mesentery within an hour of sacrifice and was stored in Ca free PBS maintained at about 4 ^{o}C till tested (within 5 hrs of harvesting). Prior to the test the attached fat and lose adventitia was carefully removed from the vessel and the daughter vessels if any were ligated using a silk suture.

The experimental apparatus used for the biaxial test and the procedure to measure the relevant parameters is described in detail in the next chapter. Briefly it consists of a test bath that has two cannulas introduced in from the opposite faces and is perfused with circulating Ca free PBS maintained at around 27 ^{o}C. The cannula at the upstream end is attached to a three way stopcock fixed on a computer controlled translational stage. One of the other two ends of the valve is connected to a reservoir filled with Ca free PBS whose height can be adjusted using a custom built computer

controlled pulley system. The cannula at the downstream end is connected to an isometric force transducer.

The axial length of the vessel was controlled with help of the translational stage. It was assumed that the change in axial length was uniform throughout the vessel and equal to the displacement of the stage. The diameter of the vessel and hence the circumferential stretch ratio under different loading conditions was estimated from the images of its central region obtained with a CCD camera. The relevant geometric dimensions of the vessel were estimated from the cross section image of a ring section cut from the vessel at the end of the test.

The no load length of the vessel (corresponding to distance between two ends of the cannula) at which it was cannulated was recorded followed by preconditioning in circumferential direction with help of 5 pressure cycles from 0 cm H_2O to 27.5 cm H_2O. The vessel was then allowed to relax for about 8 minutes before being subjected to the loading protocol. The protocol consisted of a pressure cycle, in steps of 2.5 cm H_2O, of upto 35cm H_2O for each axial stretch. The axial length was varied from no-load length to the axial length that resulted in an axial force beyond the range of the force transducer. Each step change in axial length was determined so that the axial stretch ratio increased by 5%. Since the vessel was not preconditioned in axial direction it was allowed to rest at each new axial length for 8 min prior to application of the pressure cycle. Though debatable it is our contention that the structural changes in the vessel as a result of precondition that lead to the observed repeatable behavior could also be achieved by allowing it to relax at new axial length.

Results

Parameter Estimation

The variation of $\left(\frac{\partial W_{\gamma_2}}{\partial \gamma_2}\right)_{\exp}$ and $\left(\frac{\partial W_{\gamma_3}}{\partial \gamma_3}\right)_{\exp}$ with respect to γ_2 and γ_3 as obtained from the inflation extension test on a lymphatic vessel is as shown in figure 2.2. Before approximating these variation with orthogonal polynomials as in equation 2.17, it should be noted that due to limitation of the experimental setup to precisely control the value of γ_3 with changing γ_2 the $\gamma_2 - \gamma_3$ distribution for the test mentioned above do not follow the conditions of equation 2.23. In order to obtain a distribution that confirms to these conditions, we select a region of interest from $\gamma_2 - \gamma_3$ distribution, say for γ_3 varying from 0 to some value greater than maximum of all γ_3, to model the behavior of the vessel. New values γ_3' of γ_3 are then selected so that the distribution $\gamma_2 - \gamma_3'$ follow the conditions given in equation 2.23. Spline interpolation is used to estimate values $(\partial W_{\gamma_k} / \partial \gamma_k)'_{\exp}$ of the measured variable corresponding to new values of γ_3' in the range γ_3 from 0 to maximum γ_3 for a particular γ_2. Also using spline interpolation 150 data values of measured variables are estimate in this range of γ_3 and a 3rd order polynomial function is fit to the last 50 data points in order to estimate $(\partial W_{\gamma_k} / \partial \gamma_k)'_{\exp}$ for γ_3' beyond maximum γ_3 for a particular γ_2 up to γ_3' corresponding to the upper limit of ROI. Spline interpolation was used over fitting the data with an analytical function in order to avoid Runge's error and 3rd order polynomial was used as the fit seemed to give reasonable values of $(\partial W_{\gamma_k} / \partial \gamma_k)'_{\exp}$ in this extended range. It should be noted that with use of such an approach one is excluding the data for which γ_3 is below 0 and hence the model obtained will give significant error in predicting data in that particular range. The ROI for the vessel tested, the original data and the new values $(\partial W_{\gamma_k} / \partial \gamma_k)'_{\exp}$ for the distribution $\gamma_2 - \gamma_3'$ are shown in figures 2.3a and 2.3b.

(A)

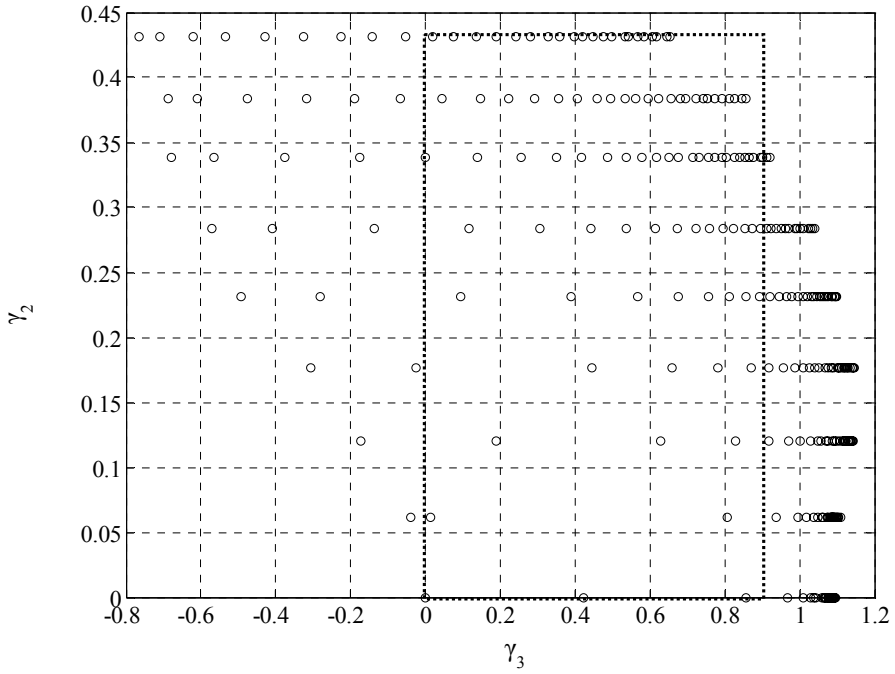

Figure 2.3a: Selection of region of interest The region of interest is selected so that the values of the variable can be confidently estimated

(A)

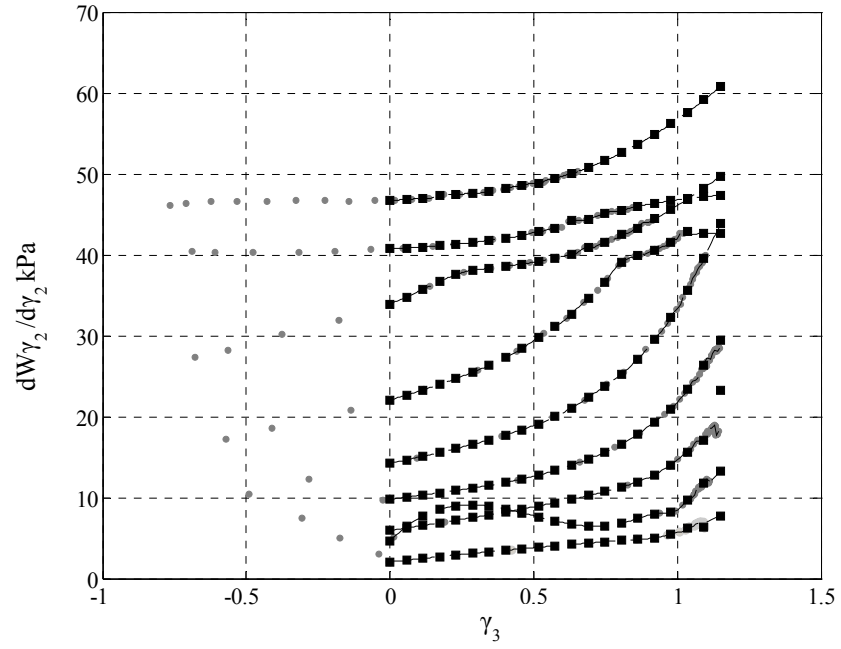

(B)

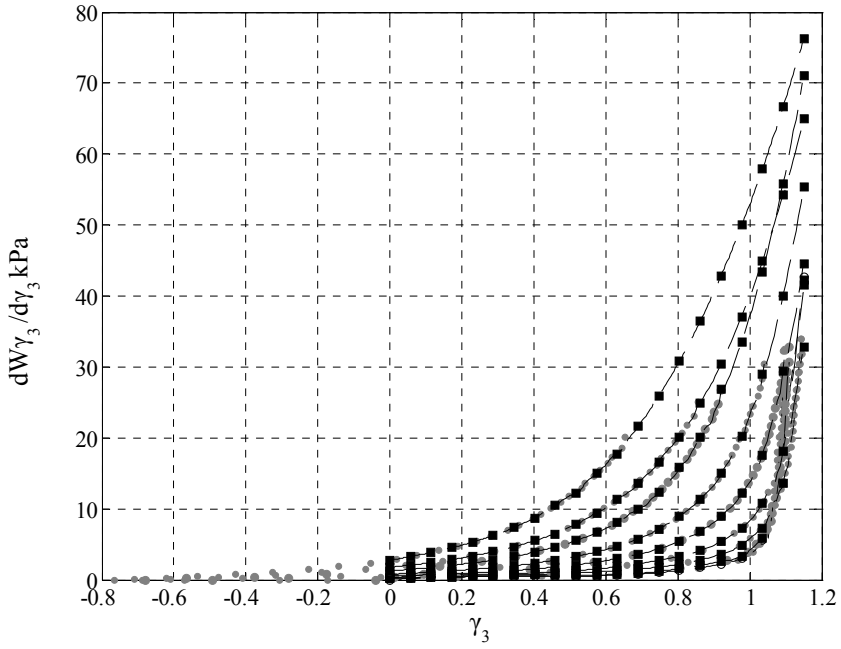

Figure 2.3b: Selection of the values of variable using interpolation and extrapolation scheme. The values are selected to meet the conditions of equation 2.23 are met. (A) The original and new values of $\left(\partial W_{\gamma_2} / \partial \gamma_2\right)$ (B) The original and new values of $\left(\partial W_{\gamma_3} / \partial \gamma_3\right)$.

The data, $\left(\frac{\partial W_{\gamma_2}}{\partial \gamma_2}\right)_{\exp}$ and $\left(\frac{\partial W_{\gamma_3}}{\partial \gamma_3}\right)_{\exp}$, is approximated with the orthogonal polynomial as in equation 2.17 and the functions $\left(\frac{\partial W_{\gamma_2}}{\partial \gamma_2}\right)_{predict}$ and $\left(\frac{\partial W_{\gamma_3}}{\partial \gamma_3}\right)_{predict}$ are obtained using equation 2.26 and 2.28 for n and m varying from 2 to 5. The goodness of fit for these analytical functions is determined using the measures defined in equation 2.24 and the results are summarized in table 2.1.

Figure 2.4 shows the data $\left(\frac{\partial W_{\gamma_2}}{\partial \gamma_2}\right)_{\exp}$ and $\left(\frac{\partial W_{\gamma_3}}{\partial \gamma_3}\right)_{\exp}$, the analytical fit $\left(\frac{\partial W_{\gamma_2}}{\partial \gamma_2}\right)_{fit}$ and $\left(\frac{\partial W_{\gamma_3}}{\partial \gamma_3}\right)_{fit}$ in terms of orthogonal polynomials and that obtained using the functions $\left(\frac{\partial W_{\gamma_2}}{\partial \gamma_2}\right)_{predict}$ and $\left(\frac{\partial W_{\gamma_3}}{\partial \gamma_3}\right)_{predict}$ for the case of n=2 and m=2.

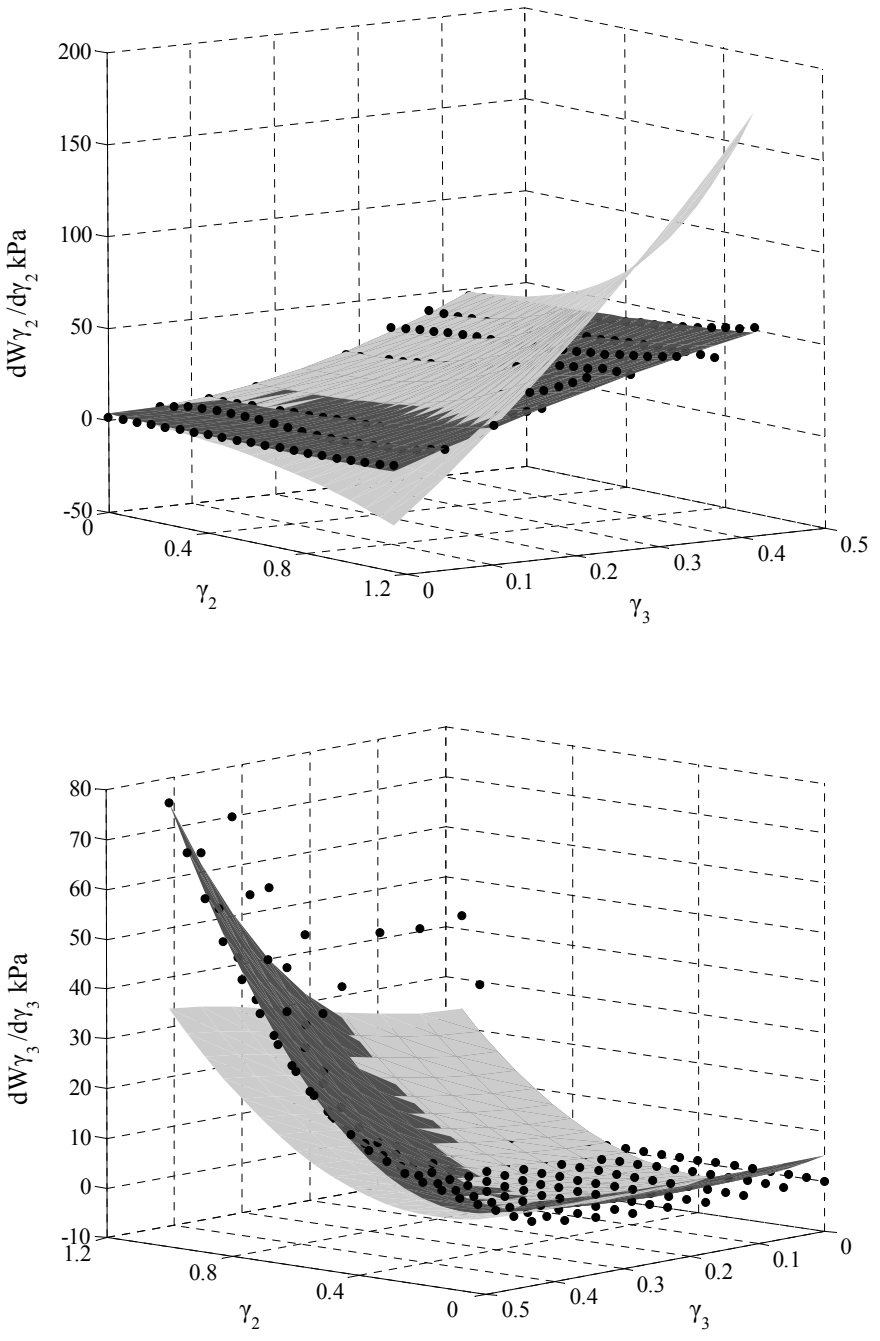

Figure 2.4: Variation of $\left(\partial W_{\gamma_2}/\partial\gamma_2\right)_{exp}$ and $\left(\partial W_{\gamma_3}/\partial\gamma_3\right)_{exp}$ with respect to γ_2 and γ_3 , and the analytical fit $\left(\partial W_{\gamma_k}/\partial\gamma_k\right)_{fit}$ and $\left(\partial W_{\gamma_k}/\partial\gamma_k\right)_{predict}$ obtained to approximate the experimental data.

Table 2.1: Values of measures used to determine goodness of fit for $\left(\partial W_{\gamma_k}/\partial\gamma_k\right)_{\text{fit}}$ and $\left(\partial W_{\gamma_k}/\partial\gamma_k\right)_{\text{predict}}$

		ε for $\partial W_{\gamma_2}/\partial\gamma_2$ Fit				ε for $\partial W_{\gamma_2}/\partial\gamma_2$ Predicted from $\partial W_{\gamma_3}/\partial\gamma_3$ Fit			
		Order γ_2				Order γ_2			
		2	3	4	5	2	3	4	5
Order γ_3	2	0.307591	0.2142768	0.195118	0.092162	1.055108	1.192975	1.217127	1.350784
	3	0.315581	0.2167399	0.197983	0.093822	1.119244	1.189581	1.211522	1.361843
	4	0.321269	0.2192898	0.200979	0.095576	1.116101	1.215037	1.244015	1.394899
	5	0.32727	0.221932	0.204114	0.097432	1.123762	1.228992	1.259211	1.422186

		ε for $\partial W_{\gamma_3}/\partial\gamma_3$ Fit				ε for $\partial W_{\gamma_3}/\partial\gamma_3$ Predicted from $\partial W_{\gamma_2}/\partial\gamma_2$ Fit			
		Order γ_2				Order γ_2			
		2	3	4	5	2	3	4	5
Order γ_3	2	0.295803	0.298264	0.294943	0.251145	0.9448	0.922912	0.953868	0.972101
	3	0.298299	0.301693	0.299275	0.255671	0.748304	0.849293	0.875049	0.891212
	4	0.30086	0.305242	0.303803	0.26045	0.835524	0.854456	0.880495	0.899623
	5	0.303487	0.30892	0.308542	0.265508	0.850716	0.871611	0.899201	0.920352

		AIC for $\partial W_{\gamma_2}/\partial\gamma_2$ Fit				AIC for $\partial W_{\gamma_2}/\partial\gamma_2$ Predicted from $\partial W_{\gamma_3}/\partial\gamma_3$ Fit			
		Order γ_2				Order γ_2			
		2	3	4	5	2	3	4	5
Order γ_3	2	786.7582	652.93387	620.2978	339.4885	1252.692	1301.936	1312.281	1354.379
	3	804.7579	660.93387	630.2978	351.4886	1283.303	1304.539	1315.026	1362.71
	4	816.7587	668.93387	640.2978	363.4886	1287.489	1316.121	1329.354	1376.775
	5	828.7539	676.93387	650.2978	375.4888	1295.074	1323.91	1338.092	1388.828

		AIC for $\partial W_{\gamma_3}/\partial\gamma_3$ Fit				AIC for $\partial W_{\gamma_3}/\partial\gamma_3$ Predicted from $\partial W_{\gamma_2}/\partial\gamma_2$ Fit			
		Order γ_2				Order γ_2			
		2	3	4	5	2	3	4	5
Order γ_3	2	428.5329	434.489	433.0258	374.9743	867.497	861.4602	876.7	886.5703
	3	434.5329	442.489	443.0258	386.9743	782.1843	833.7168	848.5886	858.9801
	4	440.5329	450.489	453.0258	398.9744	826.6281	839.5867	855.2579	867.5296
	5	446.5329	458.489	463.0258	410.9744	836.1523	850.5735	867.3523	880.8707

Table 2.2: Predicted values of the coefficients and their 95% confidence limits for the functions that define variation $\left(\partial W_{\gamma_2}/\partial\gamma_2\right)'_{exp}$ and $\left(\partial W_{\gamma_3}/\partial\gamma_3\right)'_{exp}$ using orthogonal polynomials in terms of γ'_2 and γ'_3

	$\left(\frac{\partial W_{\gamma_2}}{\partial\gamma_2}\right)'_{exp} = \sum_{i=1}^{3}\sum_{j=1}^{3} a_{ij}\phi_i(\gamma'_2)\phi_j(\gamma'_3)$			$\left(\frac{\partial W_{\gamma_3}}{\partial\gamma_3}\right)'_{exp} = \sum_{i=1}^{3}\sum_{j=1}^{3} a_{ij}\phi_i(\gamma'_2)\phi_j(\gamma'_3)$		
	$a_{ij} - a_n$	a_{ij}	$a_{ij} + a_n$	$a_{ij} - a_n$	a_{ij}	$a_{ij} + a_n$
a_{00}	25.457	25.461	25.473	10.258	10.263	10.266
a_{01}	114.278	114.286	114.393	44.966	45.012	45.034
a_{02}	131.276	131.464	132.245	161.671	162.054	162.288
a_{10}	11.672	11.690	11.712	29.958	29.976	29.992
a_{11}	16.942	17.038	17.255	103.718	103.85	103.974
a_{12}	-268.342	-267.782	-265.631	342.832	343.953	345.326
a_{20}	10.1	10.143	10.224	59.627	59.677	59.742
a_{21}	2.163	2.414	3.170	84.659	84.850	85.475
a_{22}	-238.009	-236.997	-229.106	252.041	253.676	259.861

The values of coefficients and the 95% CI are as given in table 2.2. Though not shown the residuals of the analytical fit do not confirm to normal distribution as is the general case for soft tissue behavior and hence the confidence intervals for the coefficients are determined using the bootstrapping method (Yin et al., 1986). In all 100 new data sets were created from the original one by adding random error of upto +/- 5% of the data value at each data point to the original data value. The values of coefficients for each of the data set were determined and the 95% CI were calculated using standard statistics formula. The distribution of the coefficients and the CI are as shown in figures 2.5a and 2.5b.

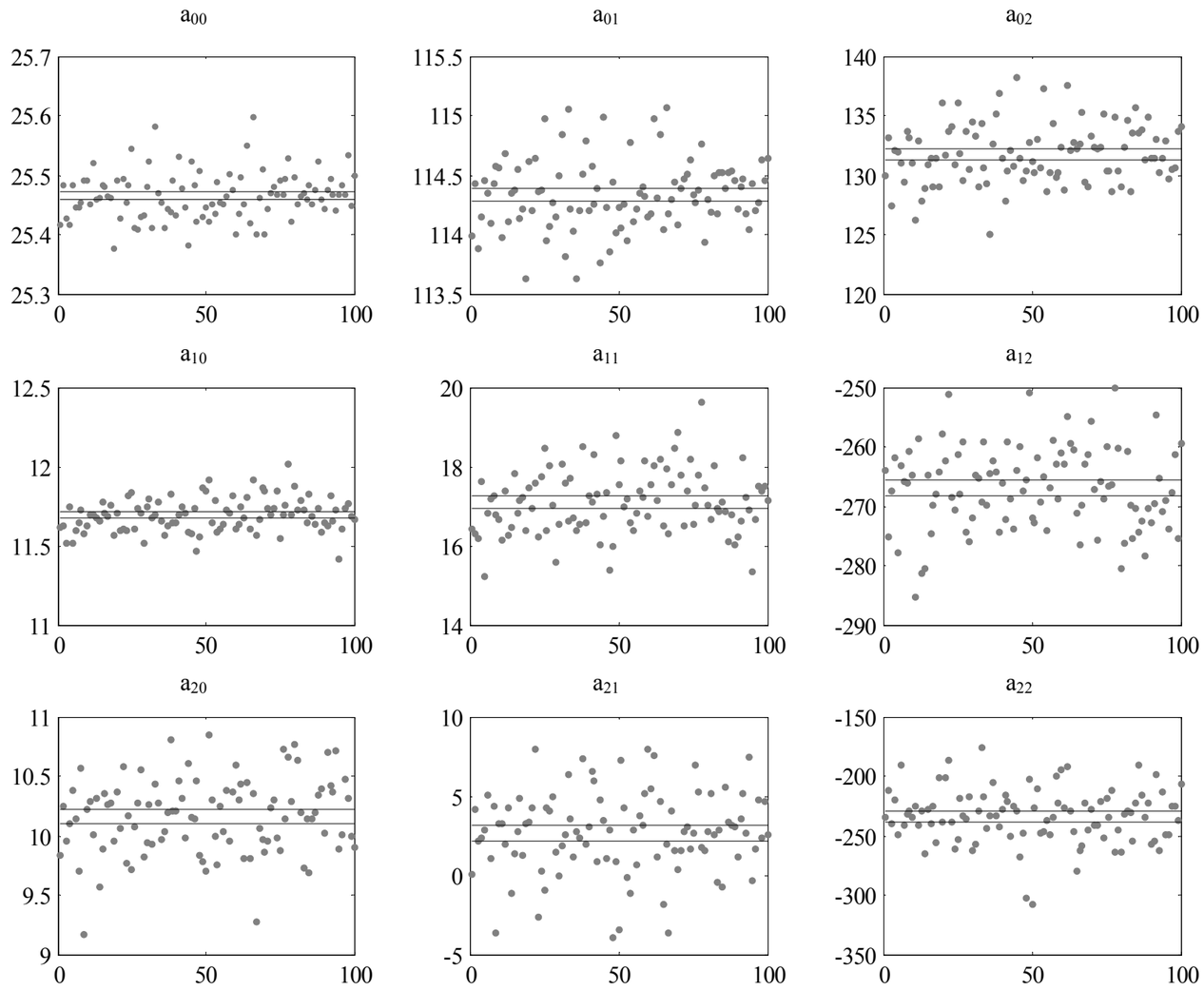

Figure 2.5a: Variation of the coefficients for the surface fits used to approximate $\left(\partial W_{\gamma_2}/\partial\gamma_2\right)_{exp}$. The 95% CI for each are estimate using bootstrap method. The new data sets were created by adding random error upto +/- 5% of the data value at each data point to the original value.

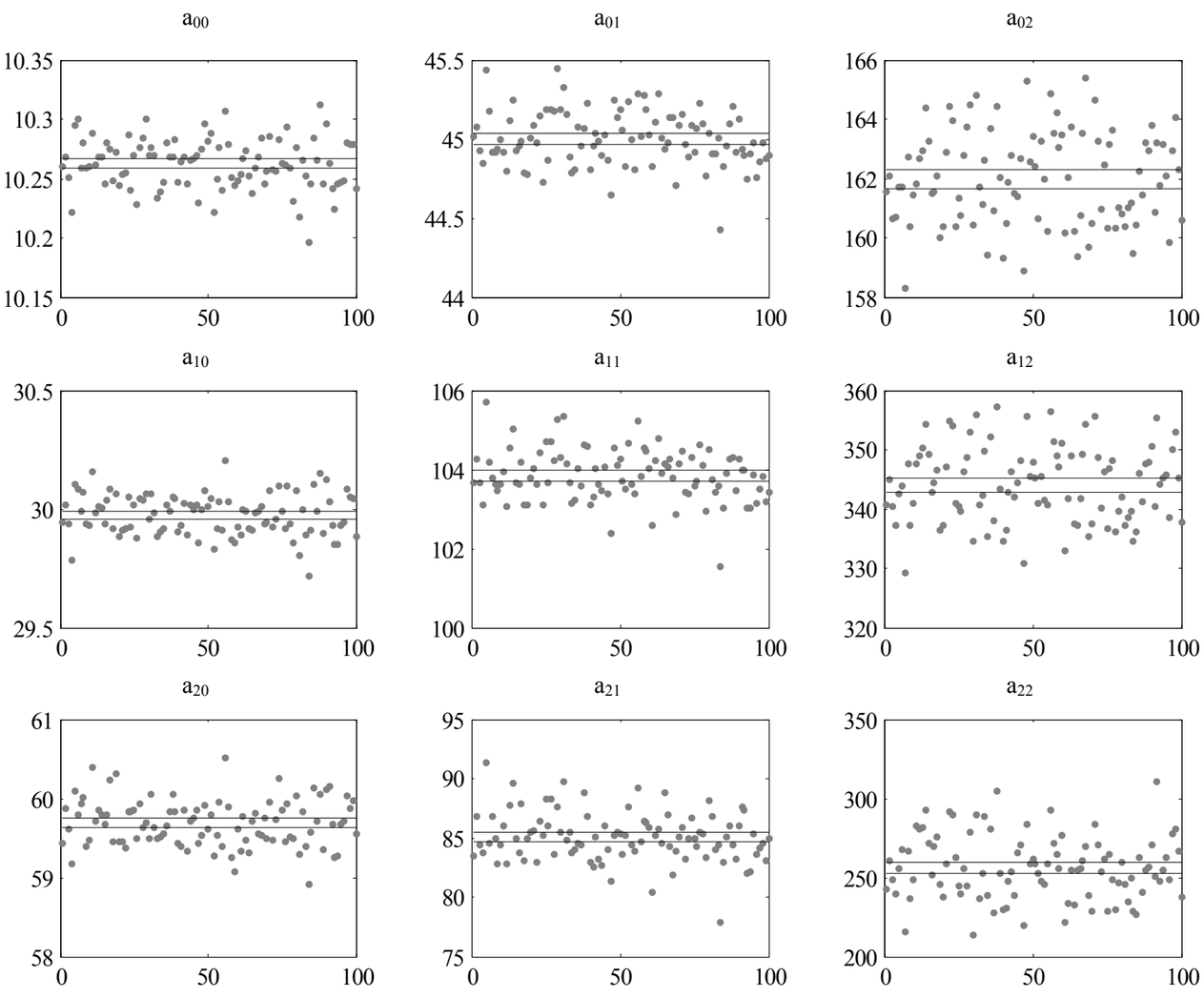

Figure 2.5b: Variation of the coefficients for the surface fits used to approximate $\left(\partial W_{\gamma_3}/\partial\gamma_3\right)_{exp}$. The 95% CI for each are estimate using bootstrap method. The new data sets were created by adding random error upto +/- 5% of the data value at each data point to the original value.

Strain Energy Function

For n=m=2 the variation of the measure that quantifies deviation from hyperelastic behavior with the weight w is as shown in figure 2.6**.** It should be evident that the deviation is minimal for w=0.1. Using the estimated value of the coefficients the form of the strain energy function simplified from the one as in equation 2.17 is as given below. The original data and the fit obtained using this strain energy function is as shown in figure 2.7.

$$W = 5.974\gamma_3 + 3.208\gamma_2 - 1.224\gamma_3\gamma_2 - 22.922\gamma_3^2 + 16.566\gamma_2^2 - 22.38\gamma_3\gamma_2^2 + 10.95\gamma_3^2\gamma_2 - 3.556\gamma_3^2\gamma_2^2 + 18.406\gamma_3^3 + 27.005\gamma_2^3 + 35.804\gamma_3\gamma_2^3 - 7.799\gamma_3^3\gamma_2 + 31.407\gamma_3^3\gamma_2^2 + 56.575\gamma_3^2\gamma_2^3$$

Table 2.3: Comparison of values of the measure to quantify deviation from hyperelastic ideal for W derived from data and similar measure determined from the total error in prediction of data.

	Order	W derived from Surface Fit	W Orthogonal Polynomial	W polynomial Function
Δ_ε	n=4, m=4	0.314	0.251	0.486
	n=3, m=3	0.301	0.266	0.479
	n=2, m=2	0.310	0.305	0.48
Δ_{AIC}	n=4, m=4	1503.082	1.27E+03	1.77E+03
	n=3, m=3	1398.524	1.27E+03	1.71E+03
	n=2, m=2	1366.03	1.33E+03	1.68E+03

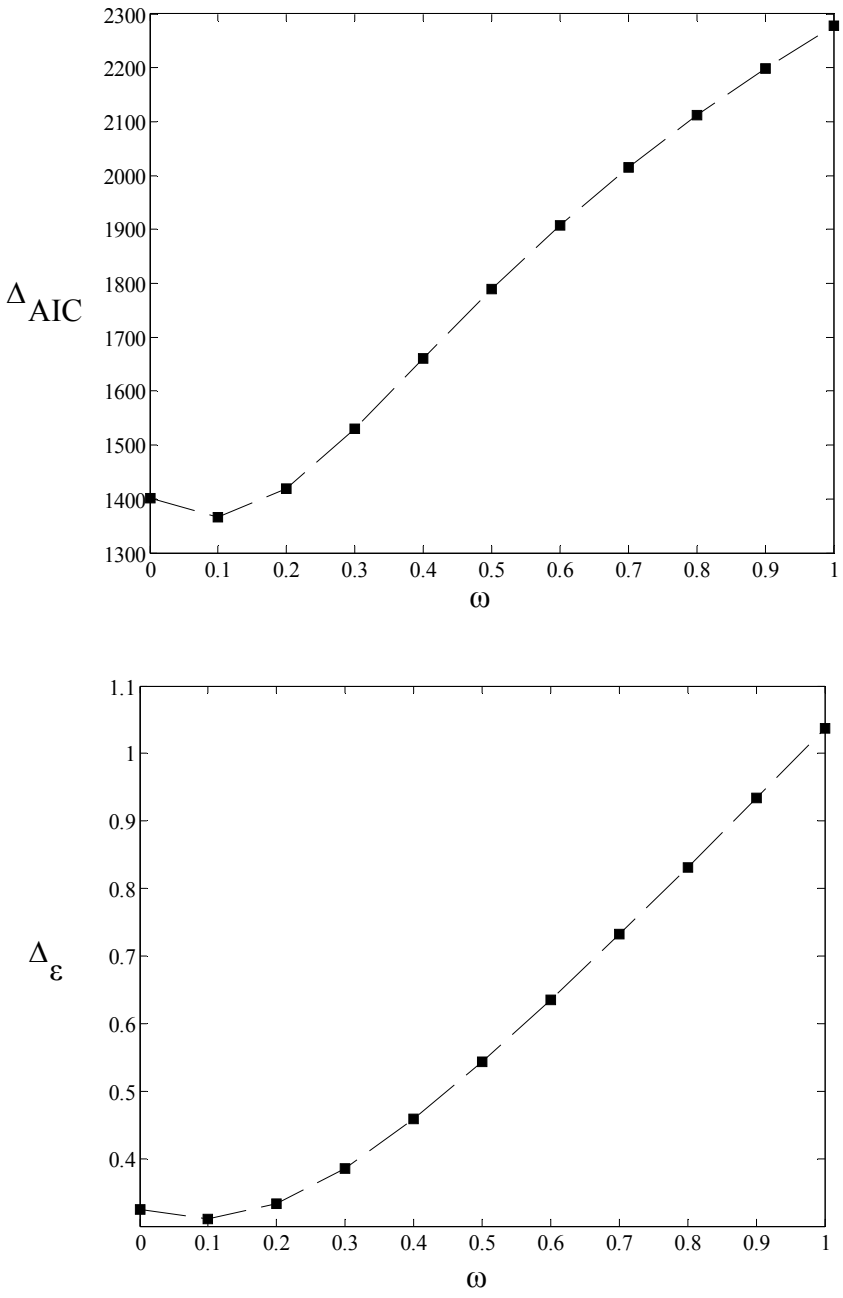

Figure 2.6: Variation of the measures of deviation from hyperelastic ideal with weight ω. The order of orthogonal polynomial corresponds to n=m=2. The weight that gives minimum deviation is used to determine the strain energy function. The line shown through the data points is not an analytical fit to the variation but is added to better visualize the trend.

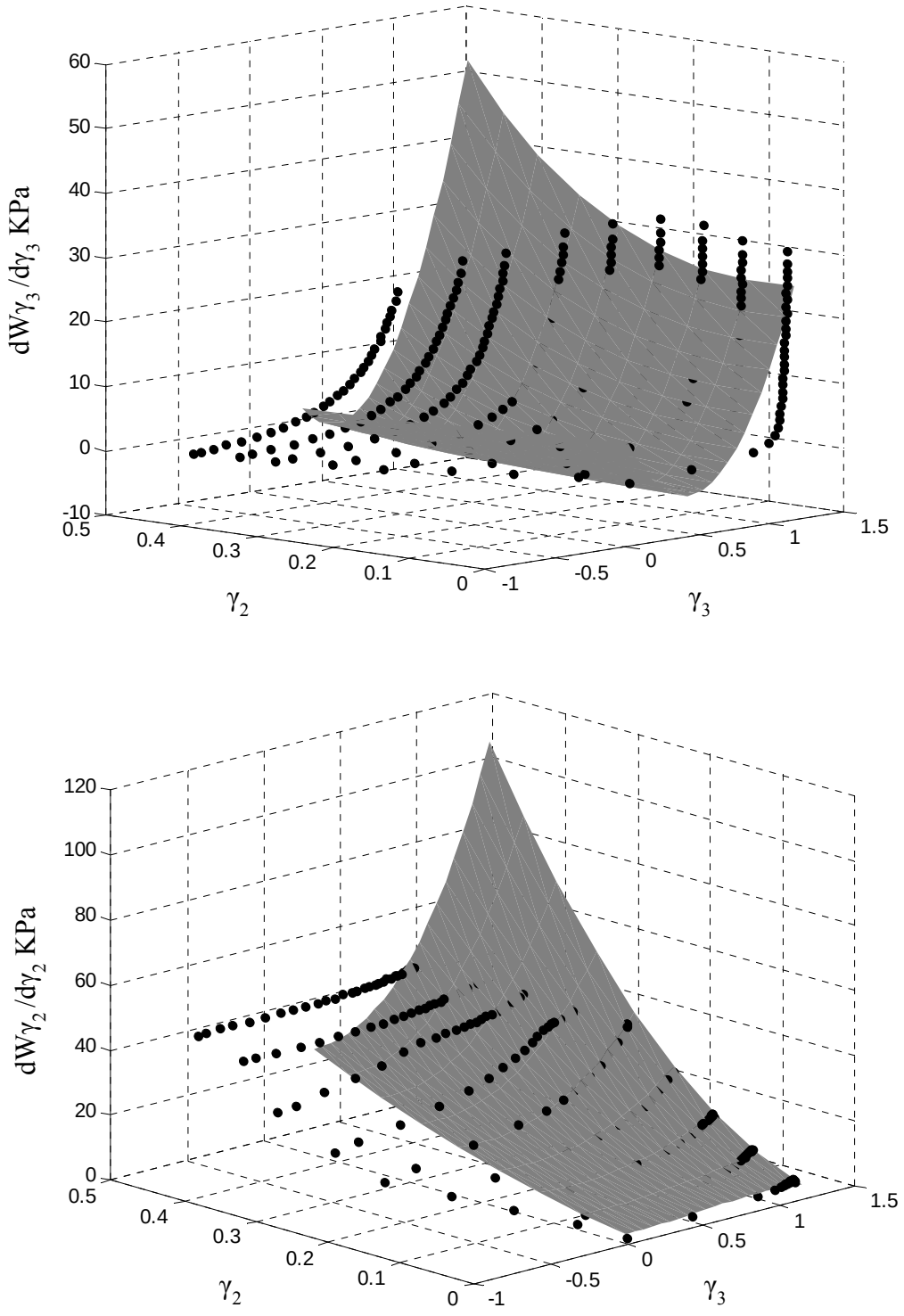

Figure 2.7: The experimental data and the surface fit. The surface fit is obtained using the strain energy function in terms of Crisione's strain attributes determined from the experimental data.

Comparison with Other Polynomial Forms

To compare the strain energy function obtained using the proposed method with that of guessing a polynomial functional form and fitting it to the experimental data, we consider two different polynomial form of strain energy and estimate the coefficients using multiple regression techniques.

W as sum of orthogonal polynomials: First W is assumed to have similar function form as that of $\partial W / \partial \gamma_k$ in equation 2.17. The data and the analytical fit are as shown in figures 2.8a and 2.8b.

$$W = \sum_{i=1}^{n} \sum_{j=1}^{m} a_{ij} \phi_i(\gamma_2) \phi_j(\gamma_3) \tag{2.32}$$

W as a polynomial function: Next we assume W to have functional form similar to that proposed by Vaishnav (Vaishnav et al., 1972). The data and the analytical fit obtained by using the estimated coefficients are as shown in figure 2.7.

$$W = \sum_{i=0}^{n} \sum_{j=0}^{n} a_{ij} \gamma_2^i \gamma_3^j \tag{2.33}$$

The deviation from the hyperelastic ideal is estimated using the measure as defined in equations 30 and 31 for n=m=2,3,4 for equation 18 and n=m=3,4,5 for equation 2.32 and 2.33. The values of the deviation are as given in table 2.3. The change in coefficients of lower order terms due to addition of higher order ones is as shown in table 2.4a and 2.4b. For the proposed method we change the order from n=m=2 to n=m=3 and for the assumed functional forms the order is changed from n=m=3 to n=m=4.

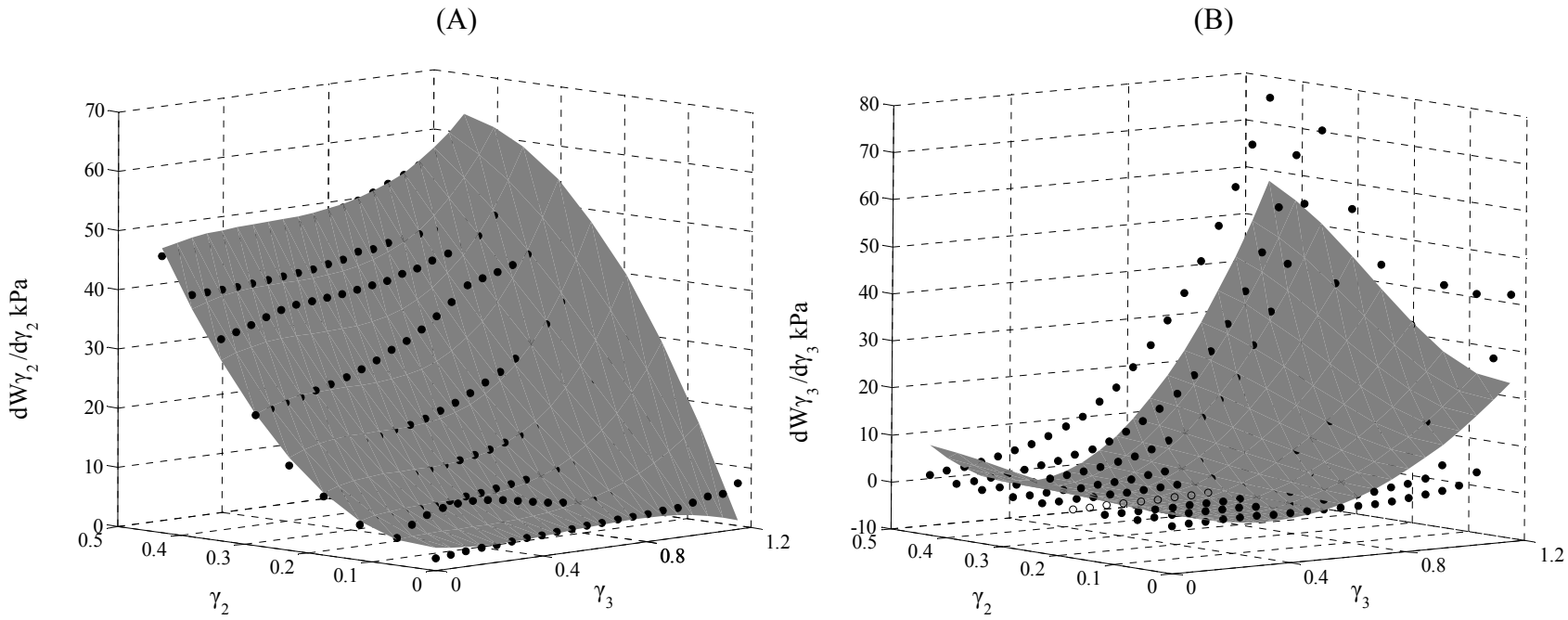

Figure 2.8a: Surface fit obtained by assuming an orthogonal polynomial as functional form of W. The predicted values of the variable using assumed functional form of strain energy function W are shown as surface plots along with the experimental data used to estimate the parameters of the functional form assumed. W is assumed to be a orthogonal polynomial as given in equation 2.32

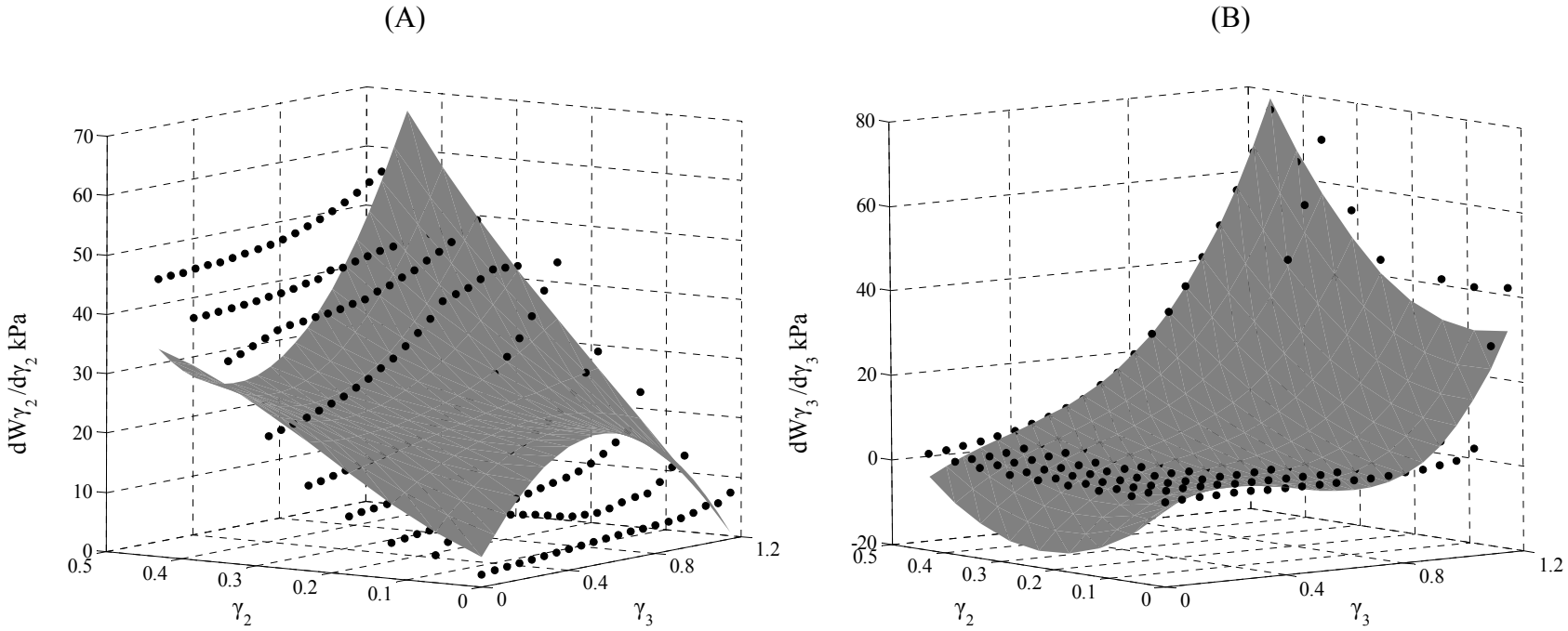

Figure 2.8b: Surface fit obtained by assuming a functional form of W as suggested by Vaishnav. The predicted values of the variable using assumed functional form of strain energy function W are shown as surface plots along with the experimental data used to estimate the parameters of the functional form assumedW is assumed to have a normal polynomial form as suggested by Vaishnav(Vaishnav et al.,1973).

Table 2.4a: % Change in the values of coefficients when a higher order polynomial function is assumed for strain energy function W.

	$W = \sum_{i=1}^{n}\sum_{j=1}^{m} a_{ij}\phi_i(\gamma_2')\phi_j(\gamma_3')$			$W = \sum_{i=0}^{n}\sum_{j=0}^{m} a_{ij}\gamma_2^i\gamma_3^j$		
	n=m=3	n=m=4	% Change	N=m=3	n=m=4	% Change
a_{00}	0	0	0	0	0	0
a_{01}	23.528	23.512	0.067	-2.148	-1.78	17.147
a_{02}	56.922	60.126	5.628	-64.386	-21.423	66.727
a_{03}	43.821	43.44	0.870	98.556	-117.386	219.106
a_{04}	-	-153.077	-	-	265.747	-
a_{10}	7.356	7.356	0	4.941	6.8	37.619
a_{11}	17.702	17.686	0.090	46.444	-13.896	129.919
a_{12}	12.818	16.827	31.278	175.325	52.501	70.055
a_{13}	-118.707	-119.193	0.409	-281.850	1404.887	598.452
a_{14}	-	-200.162	-	-	-2409.38	-
a_{20}	14.988	11.656	22.230	31.012	26.662	14.025
a_{21}	31.877	30.366	4.741	-143.071	158.183	210.562
a_{22}	22.317	21.284	4.627	-77.174	-306.768	297.501
a_{23}	-242.786	-227.745	6.195	273.485	-4032.8	1574.598
a_{24}	-	-97.0136	-	-	6989.775	-
a_{30}	19.892	19.892	0	-18.966	-14.367	24.253
a_{31}	44.793	44.802	0.019	112.028	-337.978	401.689
a_{32}	47.891	60.530	26.431	-35.828	810.942	2363.444
a_{33}	-366.067	-367.238	0.320	-15.154	3900.022	25836.08
a_{34}	-	-967.044	-	-	-7329.64	-
a_{40}	-	26.499	-	-	-1.840	-
a_{41}	-	23.619	-	-	206.944	-
a_{42}	-	174.224	-	-	-548.65	-
a_{43}	-	-613.254	-	-	-989.57	-
a_{44}	-	-3289.55	-	-	2362.593	-

Table 2.4b: % Change in the values of coefficients when a higher order orthogonal polynomial is used to fit the data and hence derive the strain energy function. The order of polynomial is changed from n=m=2 to n=m=3

	$\left(\frac{\partial W_{\gamma_2}}{\partial \gamma_2}\right)'_{exp} = \sum_{i=1}^{n}\sum_{j=1}^{m} a_{ij}\phi_i(\gamma'_2)\phi_j(\gamma'_3)$			$\left(\frac{\partial W_{\gamma_3}}{\partial \gamma_3}\right)'_{exp} = \sum_{i=1}^{n}\sum_{j=1}^{m} a_{ij}\phi_i(\gamma'_2)\phi_j(\gamma'_3)$		
	n=m=2	n=m=3	% Change	n=m=2	n=m=3	% Change
a_{00}	25.461	25.461	0	10.263	10.263	0
a_{01}	114.286	114.286	0	45.012	45.012	0
a_{02}	131.464	131.464	0	162.054	162.054	0
a_{03}	-612.307	-	-	5.002	-	-
a_{10}	11.69	11.69	0	29.976	29.976	0
a_{11}	17.038	17.038	0	103.85	103.85	0
a_{12}	-267.782	-267.782	0	343.953	343.953	0
a_{13}	-379.471	-	-	-800.66	-	-
a_{20}	10.143	10.143	0	59.678	59.677	0
a_{21}	2.414	2.414	0	84.850	84.850	0
a_{22}	-236.997	-236.997	0	253.676	253.676	0
a_{23}	1758.065	-	-	-3669.64	-	-
a_{30}	13.085	-	-	105.995	-	-
a_{31}	-69.246	-	-	-159.014	-	-
a_{32}	-134.156	-	-	-284.944	-	-
a_{33}	5244.848	-	-	-7504.42	-	-

Discussion

Orthogonal Polynomials

Use of orthogonal polynomials to fit the biaxial test data has the advantage that the independent variables are not collinear. Hence the obtained fit is not over-parameterized and therefore one does not have to carry out further analysis to identify the variables that are significant. Since such methods, the backward elimination or forward inclusion, are dependent on an individual's discretion (Yin et al., 1986) they are not too favorable in determining a strain energy function for a material behavior. The non collinearity amongst the independent variables also reduces the matrix (X^TX) of normal equation into a diagonal matrix. This is particularly useful as the unknown coefficients can be determined without the need of inverting the matrix that might be singular in certain cases. Although, as compared to the use of simple polynomial form as an analytical fit no significant reduction in error propagation is obtained, rather similar to the case of polynomials the error propagation increases with the order of orthogonal polynomial, the coefficients determined are unique and do not vary with inclusion of higher order terms.

Measure of Deviation from Hyperelastic Ideal

A common practice in development of a model to describe a phenomenon is to verify the assumption the model makes in order to understand the efficacy/applicability of the model. Though the assumptions of incompressibility, material symmetry and homogeneity of the soft tissue are often verified one seldom verifies the assumption of hyperelastic behavior. Since the soft tissue is inherently visco-elastic/non-elastic in our opinion it is essential to verify this assumption. Indeed one can use the same functional form to model two different soft tissue say aorta and great cardiac vein, but the two tissues might have different deviations from hyperelastic assumption. Hence the chosen model will be better suited to describe behavior of the tissue with lesser deviation from the assumption than the other. Also since the values of coefficients obtained are dependent on the experimental protocol one needs to decide which is more suitable to collect data in order to model the tissue with assumption of hyperelasticity. For instance

inflation extension behavior of similar tissue say rat aorta can be carried out using different test protocols like equibiaxial, randomized, inflation at constant extension or extension at constant inflation. Since all protocols are aimed at collecting data that describes behavior of tissue under combined loading of inflation and extension one needs to know which of the protocols result in minimal deviation from hyperelastic ideal. The measure that quantifies such deviation therefore would be beneficial in many ways. Finally when biaxial tests on two different specimens are carried out using similar test protocol this measure of deviation from hyperelastic ideal could be used as characteristic of tissue to compare the two behaviors. For the measure that we have proposed the closer the value to zero less the material behavior deviates from hyperelastic ideal. Currently we can use it to compare two different material behaviors but based on such measure one can define an absolute scale that would help an investigator to know if the assumption of hyperelastic behavior is acceptable.

Strain Energy Function

Since the strain energy function is not guessed but rather derived from the analytical fits to experimental data one can separate the error of fit from error of definition. Minimization of error of fit to the data will help an investigator to select the order of the analytical fit and hence that of the functional form rather than guess it. The strain energy function obtained by using the proposed method is as effective in predicting the data as the other polynomial forms of strain energy functions. It has an added advantage that the coefficients used to derive it as unique and do not vary with changes in the order of orthogonal polynomial.

Physical Significance of Coefficients

It is essential that one restricts the parameter search space in order to obtain physically realistic values (Humphrey 2001). One of the limitations of the current study is that such constraints were not enforced while estimating parameter values for analytical fit to the experimental data and hence there is a possibility that the parameter values are not realistic. For example it is possible that the negative value of the coefficients a_{12} and a_{22} (Table 2.2) for the analytical fit to the experiment data is not

realistic. The negative value could also result from non monotonic variation of the estimated values of $(\partial W_{\gamma_k} / \partial \gamma_k)^{/}_{exp}$ for distribution $\gamma_2 - \gamma_3'$. In future we aim to overcome these limitations by ensuring that we collect substantial data in ROI and by constraining the search space of the parameters.

Although a wide variety of strain energy functions are proposed to describe the non-linear material behavior of biological soft tissues, there has been little success in assigning physical meaning to the parameter values. In our opinion the task is further complicated due to the dependence of parameter values on the order of polynomial used in the functional form. Use of orthogonal polynomials that gives unique parameter values and overcomes such dependence, although does not suggest a physical meaning, is, we believe, a step forward in that direction. In our opinion the assignment of physical meaning will have to wait for detailed knowledge of structure of the soft tissue under different loading conditions and intuition gained by a large number of experiments on variety of materials with a wide range of material behavior.

Convexity of Strain Energy Function

Convexity of strain energy function is essential with regards to the local stability of the soft tissue under the dead loading conditions and in development of the numerical methods to solve the boundary value problems (Ogden and Schulze-Bauer 2003, Wilber and Walton 2002). Such a local convexity is ensured if the contours of constant strain energy for a given material are convex. One can refer to Holzapfel (2000) for a much detailed account of the convexity for the commonly used two dimensional and three dimension constitutive equations for soft tissues. It is evident that one has to place certain constraints on the parameter values so as to achieve this requirement.

For the strain energy function in terms of Criscione's strain attributes derived using the biaxial experimental data on bovine lymph vessel (illustrative example), the contour plots of constant strain energy are as shown in figure 2.9. It must be noted that the result that convexity of contours imply convexity of strain energy function, was obtained for Green Strain **E** (Holzapfel et al., 2000) and therefore one needs to substitute for γ_2 and γ_3 , and obtain the derived strain energy function in terms of E_{zz} and $E_{\theta\theta}$

Before plotting the contours. Though the performance of the strain energy function derived from the experimental data seems acceptable in the tensile region, similar to the polynomial constitutive equation proposed by Viashnav (1973), due to its dependence on the cubic powers of Criscione strain attributes it is and will not be convex (Holzapfel et al., 2000). For the strain energy function to be convex one will have to constraint the parameter search space and such constraints will result in increase in what we call error of definition. Therefore, one might have to use higher order polynomials in order to respect the convexity constraints and keep the error of definition at an acceptable value. Constraining the parameter values so that the strain energy function respects the convexity conditions and the effect of such constraints on error of definition will be studied in future.

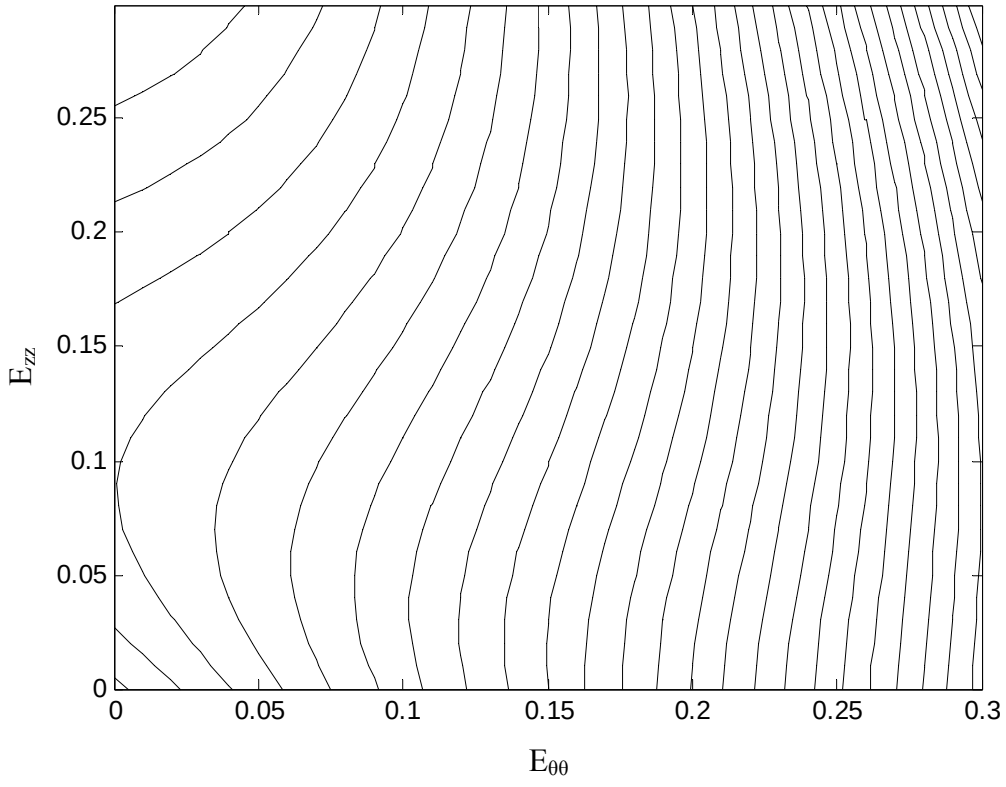

Figure 2.9: Contour plot for the strain energy function obtained from the biaxial test of a bovine lymph vessel.

CHAPTER III
ON THE BIAXIAL MECHANICAL BEHAVIOR OF THIN WALLED VESSELS – APPLICATION

Introduction

The lymphatic system, first described by Gasparo Aselli in 1672 (Swartz 2004), consists of lymph vessels interspersed with lymph nodes and is primarily involved with maintaining the interstitial fluid volume at homeostatic levels. The network returns the net capillary filtrate back into blood circulation and the inability/failure of the vessels to do so results in a pathological condition commonly known as lymphedema. The condition is characterized by local accumulation of fibroblasts, adipocytes and keratinocytes in interstitial space that leads to increased collagen deposition and outgrowth of adipose and connective tissue eventually resulting in fibrosis (Rockson 2001). The pathology can be classified as primary lymphedema and secondary lymphedema. The cause of compromised function of the lymphatic network in case of primary edema is congenital in nature where as that in the case of secondary lymphedema could be trauma, diseases or surgery and radiotherapy. American cancer society claims that of the 2 million treated for breast cancer 400,000 develop secondary lymphedema. World wide about 90 million suffer from the disease (Petrek 1998).

Though various options that include rigorous physiotherapy, use of external compression garment, pharmacotherapy and surgical procedures are generally recommended for its resolution there is no known cure for lymphedema (Brennan and Miller 1998). Recently reconstructive microsurgical procedures such as lymphatic-vein anastomosis, autologous lymphatic-venous-lymphatic shunts and autologous lymphatic transplantation have also been employed in cases where the above approaches fail to show significant improvement (Nagase et al., 2005, Matsubara et al., 2006, Campsi 2005). We also envision that percutaneous devices similar to those employed to treat various vascular pathologies could be used to resolve lymphedema caused by blocked vessels as a result of trauma. The knowledge of multiaxial mechanical properties of the lymphatic vessels and grafts would be beneficial in carrying out such microsurgical

procedures (especially with use of robotic manipulators) and in development of percutaneous devices. Also, since altered structural changes often manifest themselves in altered mechanical behavior the comparison of the mechanical characteristic of the normal and pathological vessel can also provide us with an insight regarding remodeling associated with the pathology. Such knowledge will help us better understand the disease progression and hence develop novel treatment strategies (surgical as well as pharmaceutical).

In this paper we 1) discuss the general characteristics of the bovine mesenteric lymphatic vessel relevant to its passive multiaxial mechanical behavior subjected to combined extension and inflation, 2) determine the deviation of this behavior from that of ideal hyperelastic behavior for normal, sham and venous occlusion lymph 3) we estimate the coefficients of the orthogonal polynomials used to fit the data , derive the strain energy function for these vessels and compare them to determine difference in mechanical behavior. To our knowledge data on multiaxial mechanical behavior of normal lymphatic vessels and those subjected to edematous conditions has not yet been published. The extension-inflation tests were carried out using a custom built multiaxial test device.

General Characteristics and Assumptions

Being the first study to model the multiaxial mechanical behavior of the lymphatic vessels we find it appropriate to follow the methodology suggested by Humphrey (Humphrey 2001) and start with discussion of the general characteristic of the lymphatic vessels along with the assumptions required for the formulation of the constitutive model.

Homogeneity

Figure 3.1 shows the cross section of a lymphatic vessel stained with Masson's Trichrome. Similar to blood vessels the lymphatic vessel consists of a layered architecture with innermost intima composed of a layer of endothelial cells, central media that comprises of few layers of SMC and elastin and the outermost adventia that

primarily consist of fibroblast and collagen. The constituents, their amount and their orientation vary along radial, circumferential and axial direction. Though the vessel is structurally heterogeneous we will assume that its mechanical response/behavior to be homogeneous. This assumption allows one to define a strain energy function that is independent of material coordinates (Vorp et al., 1995). Also the scale of microstructure of the vessel is very small compared to the macroscopic dimensions of the vessels, hence one can assume that the continuum hypothesis holds and thus quantities such as stress and strain can be defined at each point in the vessel wall.

Nonlinearity

Figure 3.2 shows the response of the vessel in axial and circumferential direction. It can be concluded that the vessel is capable of undergoing finite strains (>5% both in axial and circumferential direction) and that the response/deformation is non-linear. Such nonlinear behavior is characteristic of almost all soft tissues and is hypothesized to be induced due to recruitment of collagen fibers at higher strains (Ogden and Schulze-Bauer 2000). The phenomenological model developed is aimed at describing such finite non-linear behavior exhibited by lymphatic vessel under combined extension and inflation.

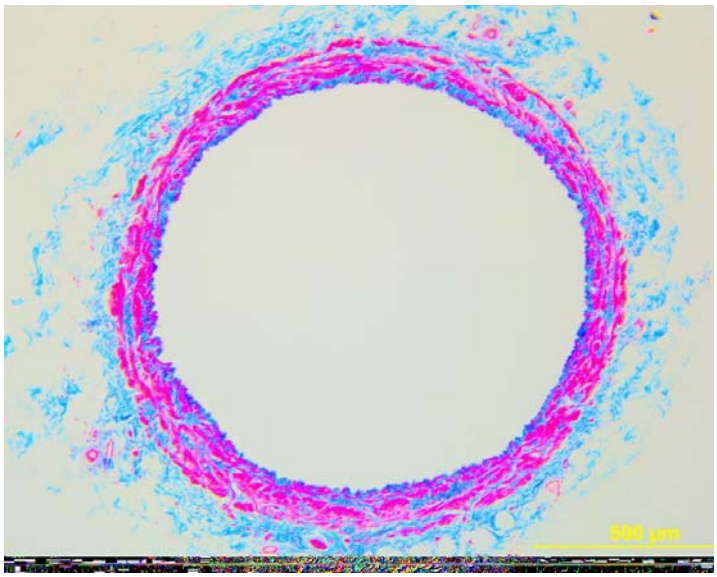

Figure 3.1: Cross section of a bovine mesenteric lymph vessel stained with Masson's Trichrome. The heterogeneous structure of SMC (stained red) and collagen network (stained blue) should be evident.

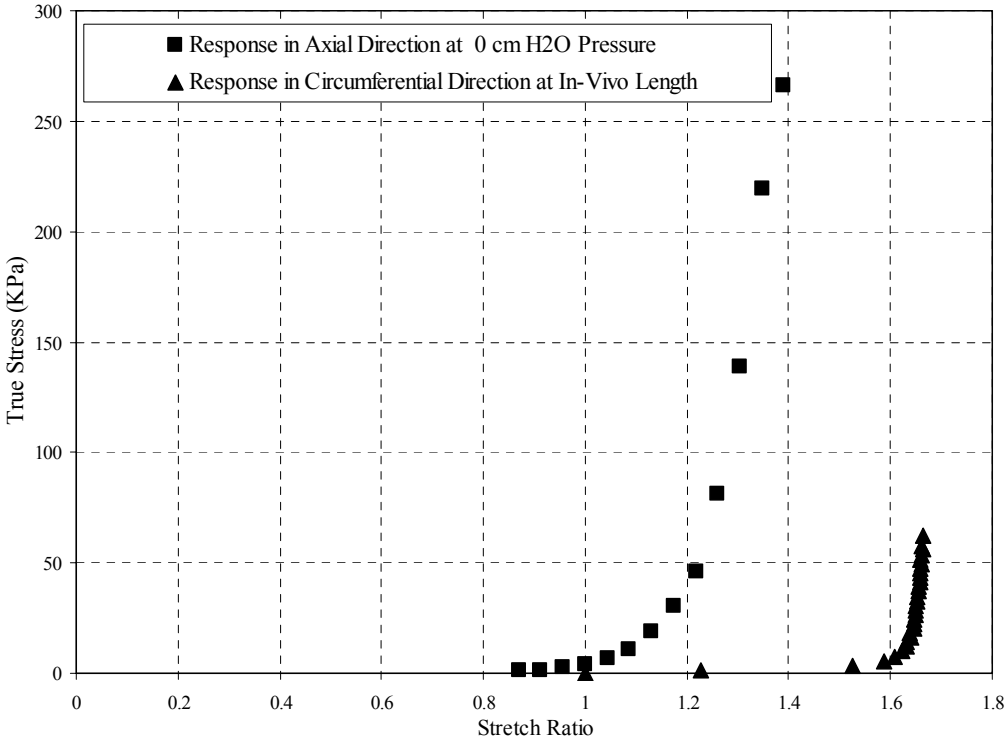

Figure 3.2: Non-linear response of bovine lymphatic vessel in axial and circumferential direction. The axial deformation is carried out at transmural pressure of 0 cm H2O and the circumferential deformation is carried out at the axial stretch ratio corresponding to the in-vivo length of the vessel (1.15 in the case with reference as no-load length). The anisotropic behavior at in-vivo length and 0 cm H2O is evident from the response.

Anisotropy

In case of biological soft tissue the material symmetry is determined by the global behavior/response of the tissue. Hence even though the vessel is locally anisotropic one can associate certain material symmetry at the macroscopic level. Figure 3.2 shows the different global behavior of the vessel in response to deformation in the axial and circumferential direction. This implies that the vessel is anisotropic at configuration corresponding to in vivo length and transmural pressure of 0 cm H2O. For formulation of the constitutive model we will assume that the behavior is orthotropic as is done for analysis of all the blood vessels. The orthotropic behavior requires that no

torsional strain be induced in the vessel due to inflation and extension as was shown by Patel and Fry in case of canine thoracic aorta (Patel and Fry 1969). Though similar tests were not carried out for the lymphatic vessels we shall assume orthotropic behavior on the basis of their structural similarity with the blood vessels.

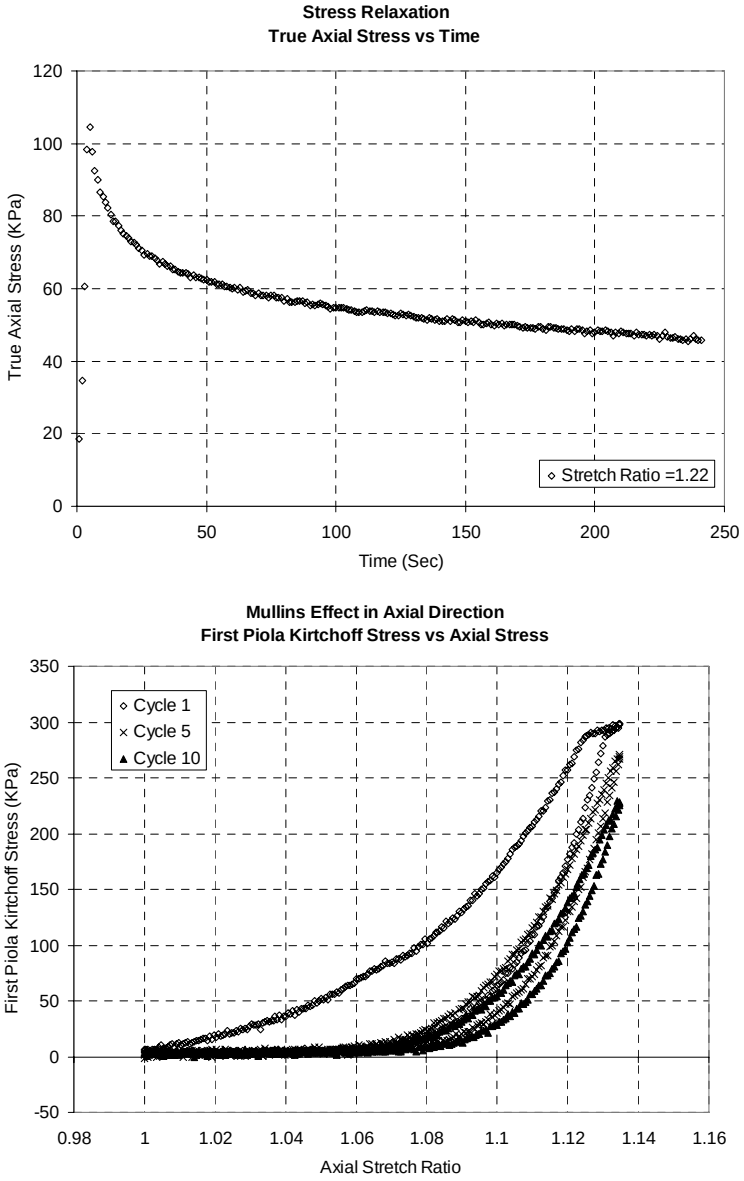

Figure 3.3: The viscoelastic behavior of the lymph vessel in axial direction: Mullins effect and stress relaxation. In case of soft tissue one often preconditioned and then assumed as pseudo-elastic i.e. its response to loading and unloading is repeatable.

Viscoelasticity

Figure 3.3 shows the stress softening and Mullins effect for a lymph vessel in the axial direction, phenomenon indicative/generally associated with viscoelastic behavior. The viscoelastic behavior is attributed to the SMC and the tangled collagen and elastin fiber. Though viscoelastic, most of the phenomenological models used to describe multiaxial mechanical behavior of biological soft tissue assume the behavior to be hyperelastic or pseudo-elastic that implies existence of a single valued potential termed as strain energy function. The assumption results in significant error between the behavior as predicted by the model and that observed during an experiment. In the present study we define a measure to estimate the deviation of the material behavior from the hyperelastic ideal and then propose a method to derive a strain energy function from the data if one assumes that the behavior is hyperelastic.

Incompressibility

The soft tissues are not truly incompressible since they contain high percentage of water by wet weight and any deformation is almost always accompanied by movement of water in and out of the tissue. Choung and Fung measured the amount of extrusion to be 0.5-1.26% of original volume of arterial tissue for compressive stresses of about 70 mmHg. This observation along with the fact that the measurement was done on tissue with open edges (condition unlike the invivo condition of tissue) has led many to believe that assumption of incompressibility is reasonable for isothermal near physiological deformation (Humphrey 2001) while it has led some to believe that such assumption is not realistic (Vorp et al., 1995). Although we did not carry out any specific experiment to confirm incompressibility of the lymphatic vessels, on the basis of structural similarity with the blood vessels and the fact that they experience maximum in-vivo radial stress of about 10mmHg we assume that the deformation (combined inflation and extension) results in very little water extrusion and hence is isochoric. This assumption also allows use to model the behavior of a three dimensional structure using two dimensional test such as combined extension and inflation (Holzapfel et al., 2000)

Residual Stresses

In general thick walled vessels such as arteries when unloaded are not stress free. Even in this no load configuration they have some pre-stress in both circumferential and axial direction. This stress is often termed as residual stress in biomechanical literature and is characterized by the opening angle of a ring section when cut along the axial direction (Chuong 1986). The residual stress is believed to be such that when under physiological loading conditions the stress throughout the arterial wall is nearly constant. The average thickness to diameter ratio of the lymph vessels tested was 0.3; hence the vessels can be considered as thin walled and the residual stresses in the circumferential direction are rather insignificant. The stresses even if present are difficult to measure as the vessels collapse under no load condition and the ring sections fail to open when cut axially. The residual stresses in axial and radial direction will also be neglected.

Geometry

As mentioned above the vessel can be considered as thin walled. Though it has been found that the vessels taper and that the thickness to diameter ratio depends on the average diameter of the vessel, a branch free lymphangion (segment of lymphatic vessel between two consecutive valves) will be considered as straight cylindrical tube/axis-symmetric tube of uniform thickness along the entire length. Thin walled/Membrane assumption also leads to assumption of plane stress and strain (Ogden and Schulze-Bauer 2000).

Passive Behavior

Under normal physiological conditions the lymphatic vessel shows/posses certain amount of tone. Indeed each segment of the lymphatic vessel called lymphangion undergoes periodic contraction that is influenced by among other factors the SMC tone. Here we do not intend to model the multi-axial contractile/active behavior of the vessel. Instead we focus on modeling the passive behavior of the vessel in distension at various axial stretches and use Ca+ free physiological solution for the purpose (Vito and Dixon 2003).

Theoretical Framework

Basic Kinematics for Combined Extension and Inflation of a Thin Walled Tube

Consider the case of combined inflation and extension of a cylindrical tube/vessel. In the reference configuration the vessel in terms of coordinates (**R, Q, Z**) is defined as (Ogden 1997)

$$R_{in} < R < R_{out} \qquad 0 < Q < 2\pi \qquad 0 < Z < L \tag{3.1}$$

Where R_{in} and R_{out} is the inner and outer radius of the vessel in the reference configuration and L is the initial unstretched length of the vessel. Assuming that the vessel undergoes combined inflation and extension such that its length is $l=\lambda_z L$ and its outer radius is r_{out} then the current configuration of the vessel in terms of coordinates (**r, q, z**) can be defined as

$$r_{in} < r < r_{out} \qquad 0 < q < 2\pi \qquad 0 < z < l \tag{3.2}$$

The deformation gradient F for the above deformation is also a function of R and is given as,

$$F(R) = \begin{bmatrix} \lambda_Z^{-1}\lambda_Q(R)^{-1} & 0 & 0 \\ 0 & \lambda_Q(R) & 0 \\ 0 & 0 & \lambda_Z \end{bmatrix}_{R,Q,Z} \tag{3.3}$$

For combined inflation-extension of axis-symmetric cylindrical segment that after deformation is still assumed as axis-symmetric the coordinates for reference and current configuration stay the same that is **r=R**, **q=Q** and **z=Z.** The strain attributes for such deformation of incompressible vessel are given as (Criscione 2004)

$$\begin{aligned} &\gamma_1 = 0, \qquad \gamma_2 = \ln \lambda_Z^{3/2}, \qquad \gamma_3 = \ln \lambda_Q^2(R) + \ln \lambda_Z, \\ &\gamma_4 = 0, \qquad \gamma_5 = 0, \qquad \gamma_6 = 0, \end{aligned} \tag{3.4}$$

Stress Power Law

In case of material/continuum with negligible body forces for mechanical processes that are isothermal, quasistatic and result in negligible body couples and reversible heat conduction, conservation of energy and stress power gives

$$\dot{W} = \mathrm{J}\, t : \dot{F}\, F^{-1} \tag{3.5}$$

Equilibrium Equations

In absence of body forces (weight of the vessel being supported by buoyant force while immersed in a tissue bath), couple moments and inertial forces (test protocol ensures slow deformation of the test specimen) the conservation of mass and linear momentum requires

$$\nabla . t = 0 \tag{3.6}$$

From equation above and considering that $-t_{rr}(r_{in})=P_{in}$ and $-t_{rr}(r_{out})=P_{out}$ where P_{in} and P_{out} are internal and external pressure respectively and equilibrium in the axial direction one can derive, for a thin walled incompressible vessels, the following equation

$$P_{in} - P_{out} = 2\frac{\partial W}{\partial \gamma_3}\frac{h}{r_{avg}} \tag{3.7a}$$

$$L_z = 3\pi \frac{\partial W}{\partial \gamma_2} r_{avg} h \tag{3.7b}$$

Where r_{avg} is the average radius of the vessel and h is the thickness of the vessel wall. Typical experimental measurements for a combined inflation extension loading of the thin walled vessel include that of luminal pressure, axial load, outside diameter of the vessel and axial stretch ratio. Using these measured values one can estimate the quantities $\left(\frac{\partial W_{\gamma_2}}{\partial \gamma_2}\right)_{\exp}$ and $\left(\frac{\partial W_{\gamma_3}}{\partial \gamma_3}\right)_{\exp}$ as defined in equation below,

$$\left(\frac{\partial W_{\gamma_3}}{\partial \gamma_3}\right)_{\exp} = \frac{(P_{in} - P_{out}).r_{avg}}{2.h} \qquad \left(\frac{\partial W_{\gamma_2}}{\partial \gamma_2}\right)_{\exp} = \frac{L_z}{3\pi r_{avg} h} \tag{3.8}$$

Where $(P_{in} - P_{out})$, is the transmural pressure difference, L_z, the measured load, r_{avg}, the average radius of the vessel wall and h is the thickness of the vessel wall.

It must be noted that no assumptions regarding the mechanical behavior of the vessel needs to be made to estimate the above quantities and that by $\left(\frac{\partial W_{\gamma_k}}{\partial \gamma_k}\right)_{\exp}$ we do not imply that the material behavior under the prescribed multiaxial loading is hyperelastic or

Green elastic. Typical variation of $\left(\frac{\partial W_{\gamma_2}}{\partial \gamma_2}\right)_{\exp}$ and $\left(\frac{\partial W_{\gamma_3}}{\partial \gamma_3}\right)_{\exp}$ with respect to γ_2 and γ_3 as obtained from the inflation extension test on a lymphatic vessel can be approximated in terms of orthogonal polynomials as follows,

$$\left(\frac{\partial W_{\gamma_k}}{\partial \gamma_k}\right)_{Fit} = \sum_{i=1}^{n}\sum_{j=1}^{m} a_{ij}\phi_i(\gamma_2)\phi_j(\gamma_3) \qquad k = 1,2 \tag{3.9}$$

Where, n and m are the order of the orthogonal polynomials used and a_{ij} are the unknown coefficients (Forsythe 1957). The coefficients a_{ij} can be estimated using least square method and minimizing the objective function

$$e = \sum_{p=1}^{N}\left[\left(\frac{\partial W_{\gamma_k}}{\partial \gamma_k}\right)_{\exp} - \sum_{i=1}^{n}\sum_{j=1}^{m} a_{ij}\phi_i(\gamma_2)\phi_j(\gamma_3)\right]_p^2 \tag{3.10}$$

Deviation from Hyperlastic Behavior

If the material behavior under the combined loading were hyperelastic then from the results of equation 3.7a and 3.7b it would be possible to determine/infer the strain energy function using the analytical function $\left(\frac{\partial W_{\gamma_k}}{\partial \gamma_k}\right)_{fit}$ and hence approximate $\left(\frac{\partial W_{\gamma_k}}{\partial \gamma_k}\right)_{predict}$ by taking the partial of strain energy function with γ_k

A measure to quantify the deviation from hyperelastic behavior of the vessel under combined loading of inflation and extension is then defined as follows

$$\Delta_{\varepsilon} = \frac{2}{mean\left(\frac{\partial W_{\gamma_2}}{\partial \gamma_{\gamma_2}}\right)_{\exp} + mean\left(\frac{\partial W_{\gamma_3}}{\partial \gamma_{\gamma_3}}\right)_{\exp}} \sqrt{\frac{e_{\gamma_2} + e_{\gamma_3}}{(2N - q_{\gamma_2} - q_{\gamma_3})}} \tag{3.11a}$$

$$\Delta_{AIC} = 2N \ln\left(\frac{e_{\gamma_2} + e_{\gamma_3}}{2N}\right) + 2.q_{\gamma_2} + 2.q_{\gamma_3} \tag{3.11b}$$

Where, $e_{\gamma_k} = \sum_{p=1}^{N}\left[\left(\frac{\partial W_{\gamma_k}}{\partial \gamma_k}\right)_{predict} - \left(\frac{\partial W_{\gamma_k}}{\partial \gamma_k}\right)_{fit}\right]_p^2$, $mean\left(\frac{\partial W_{\gamma_k}}{\partial \gamma_{\gamma_k}}\right)_{\exp} = \frac{1}{N}\sum_{p=1}^{N}\left[\left(\frac{\partial W_{\gamma_k}}{\partial \gamma_{\gamma_k}}\right)_{\exp}\right]_p$,

N is the no. of data points and q_{γ_k} is the number of parameters/coefficients.

And the strain energy function derived from the analytical fit to the experimental data is given as,

$$\begin{aligned} W = \omega & \left[\int\left(\frac{\partial W_{\gamma_2}}{\partial \gamma_2}\right)_{Fit} d\gamma_2 + \int\left(\frac{\partial W_{\gamma_3}}{\partial \gamma_3}\right)_{Fit} d\gamma_3\Big|_{\gamma_2=0}\right] \\ & + (1-\omega)\left[\int\left(\frac{\partial W_{\gamma_3}}{\partial \gamma_3}\right)_{Fit} d\gamma_3 + \int\left(\frac{\partial W_{\gamma_2}}{\partial \gamma_2}\right)_{Fit} d\gamma_2\Big|_{\gamma_3=0}\right] \end{aligned} \tag{3.12}$$

Where weight ω varies from 0 to 1 and ω that result in minimum Δ is used to obtain the final form of strain energy function.

Method

Experimental Setup

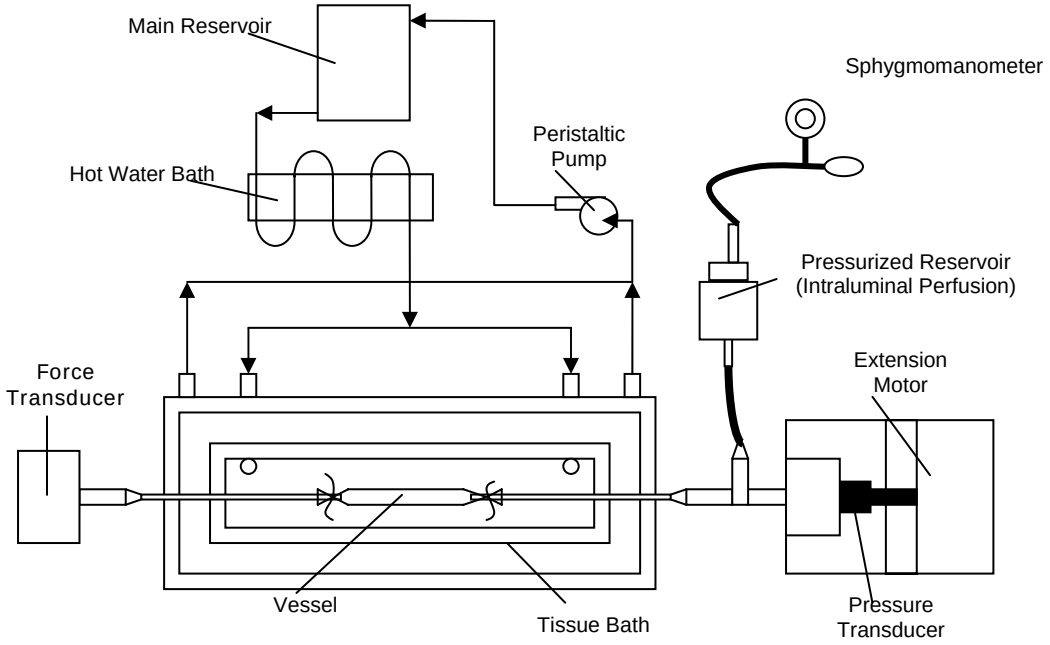

Figure 3.4: Schematic of custom built experimental set-up to carry out biaxial loading tests on thin walled cardiovascular vessels. The CCD camera used to capture images is not shown in the figure but it looks down into the plan of the paper.

The custom built experimental setup used for biaxial (inflation and extension) test on the vessel is similar, in principle, to that used by Charles Roy in 1881(Shadwick 1999). The schematic of the set-up is as shown in figure 3.4 (actual set-up is shown in figure 3.8) and each subunit of the is described separately as follows,

Tissue Bath: The custom built tissue bath (120mm X 60mm X 30mm) is similar in design as used by Humphrey et al (1994) and consists of an inner chamber (80mm X 20mm X 12mm) that hosts the tissue submerged in appropriate perfusion medium for the entire length of the experiment. As shown in figure 3.5 the bath has provision (through holes diameter 4mm) to introduce cannula from opposite walls. Since the tissue needs to be kept submerged there is a continuous outflow of the perfusion medium that is

collected in the outer chamber (10mm wide and 5mm deep) and is circulated back to main reservoir. Introduction of the perfusion medium into the inner chamber and removal from the outer chamber is attained with fluid channels (diameter: 5mm) tapped in the bottom and on the side wall of the bath respectively and fixed with appropriate barbed adapters (Small Parts: TFN-BAM093/1032 or TFN-BEM125/1032). Blunt end Needles (15GX1.5") with modified ends were used to cannulate the tissue. One can use needles of outside diameter up to 2.5 mm with the current tissue bath and hence can test tissue up to inner diameter ~ 3mm. Special connectors/adapter were fabricated to carry out tests on vessels with larger diameter but ultimately the dept of the inner chamber places an upper limit (approximately < 6mm outer diameter)on the vessel size.

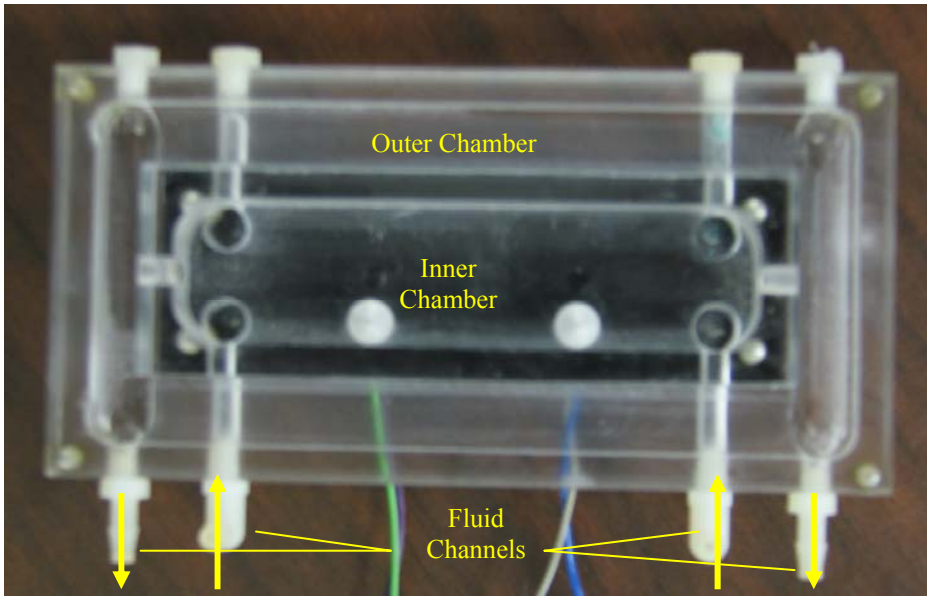

Figure 3.5: Photograph of tissue bath showing the inner and outer chamber and the barbed adapter. The black background is used for the inner chamber so to have a good contrast in the images acquired for circumferential stretch ratio. The input fluid channels open through the floor of the inner chamber.

The test bath can also be and has been used to carry out ring tests and uniaxial stretch test (ring and uniaxial stretch test of Human and Porcine coronary sinus was carried out for CardiacDimensions Inc.) with the use cannulas with appropriate modification (figure 3.6).

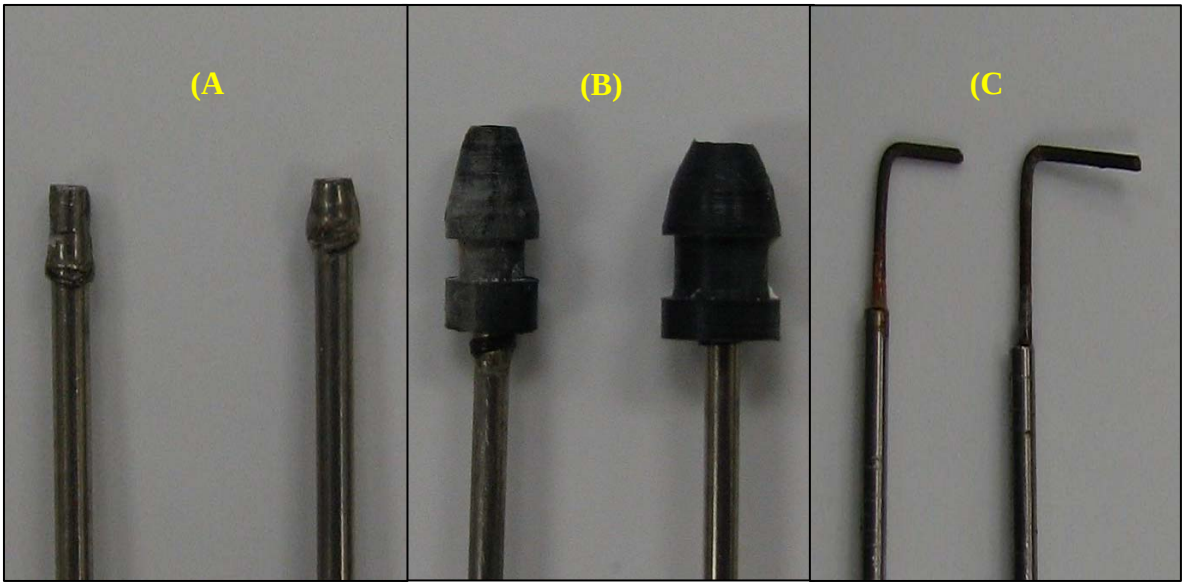

Figure 3.6: Cannula used to carry out tests on soft tissue of various sizes. (A) The end of the needle is modified for cannulation of the lymph vessel such that axial pull will not let the vessel slip. (B) Adaptors used to carry out tests on vessel sizes greater than that of the through holes through which the needles are introduced into the inner chamber. (C) The end of the needle is modified to carry out ring test on a vessel cross section.

Force and Pressure Transducer: As shown in the figure the cannula at the downstream end is connected to an isometric force transducer (Harvard Apparatus 72-4481). The transducer can be used in two modes: one with force range of 0-5 gm and second with 0-50 gm. The output of the transducer changes from 0 to 5 volts for both the modes with linearity within +/- 1%.

The cannula at the upstream end is connected to a three way stopcock that is fixed on a translational stage. One of the other two ends of the stopcock is connected to a pressure transducer (Omega PX26-001DV: Range 0-1 Psi differential) with help of a

customized connector fabricated from a standard syringe (1 ml Norm Ject, HSW) and filled with perfusion medium (without any air bubbles). The third end of the stopcock is connected to pressuring reservoir.

Axial Stretch and Luminal Pressure Control: The motion of the translation stage that has the three ways stop cock fixed on it and hence the axial stretch ratio of the cannulated vessel is achieved with help of linear actuator (Newport, CMA-25CCCl). The actuator with a displacement range of 0-25 mm, step resolution of 0.2μm and speed range of 50-400 μm is controlled with help of a Newports Universal Motion Controller (ESP Series).

The change in luminal pressure is attained by changing the height of the pressure reservoir using a custom built pulley system operated with help of a stepper motor (Japan Servo Co. Ltd: KP39HN2-025, step resolution of 3.6 deg) and thread rod assembly (Figure 3.7). The thread rod (McMaster-Carr: 98805A029, corresponding step resolution of 0.01mm) is connected to the motor with help of flexible coupling (McMaster-Carr: 6208K3). The other end of the thread rod is attached to a roller bearing (McMaster-Carr: 60355K42) fixed in a rigid support. The stepper motor is controlled using the parallel port and a standard Darlington array circuit. A customized computer interface was developed using LabVIEW to control both linear actuator and the pulley system.

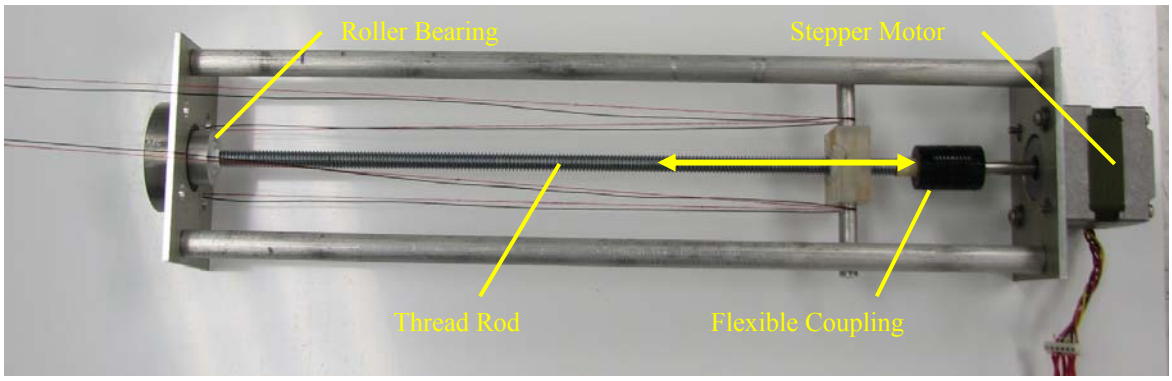

Figure 3.7: The motor and thread rod assembly. The assembly (shown in a horizontal position) is used to operate the pulley system that controls the luminal pressure.

Perfusion System: As mentioned earlier a perfusion system is used to keep the tissue submerged under perfusion medium for the entire length of the experiment. The system consists of a main reservoir that feeds (gravity feed) the inner chamber with help of Nalgene tubing (8000-0025). Gravity feed was preferred over other methods since it results in minimal disturbance in the inner chamber and hence gives better image quality and reduced error in determining the stretch ratios. The flow rate can be controlled using a valve place immediately after the reservoir. Before introduction of the medium into the inner chamber the medium is heated to a certain temperature (about 27 ^{o}C for the current experiment) by passing the tubing through hot water bath (Precision Scientific Inc. 66557-28). The medium that overflows into the outer chamber is pumped back using a peristaltic pump (Omega Engineering Inc.).

Data and Image Acquisition and Analysis: The data acquisition from both force and pressure transducer is done with help of multiplxed, 8 channel, 16 bit ADC provided with the ESP motion controller and a customized application developed using LabVIEW.

The tissue at each loading or deformation is monitored using a monochrome CCD camera (Sony XC-ST50/50CE) and an image is captured using Data Translation frame grabber Dt3162-1 and Data Translation application (DT-Acquire 2).

Both data analysis (to estimate stress values) and image analysis (to estimate stretch and reference geometry of vessel) are carried out using a customized application developed using MATLAB (MathWorks).

The photograph of the experimental set-up is shown in figure 3.8.

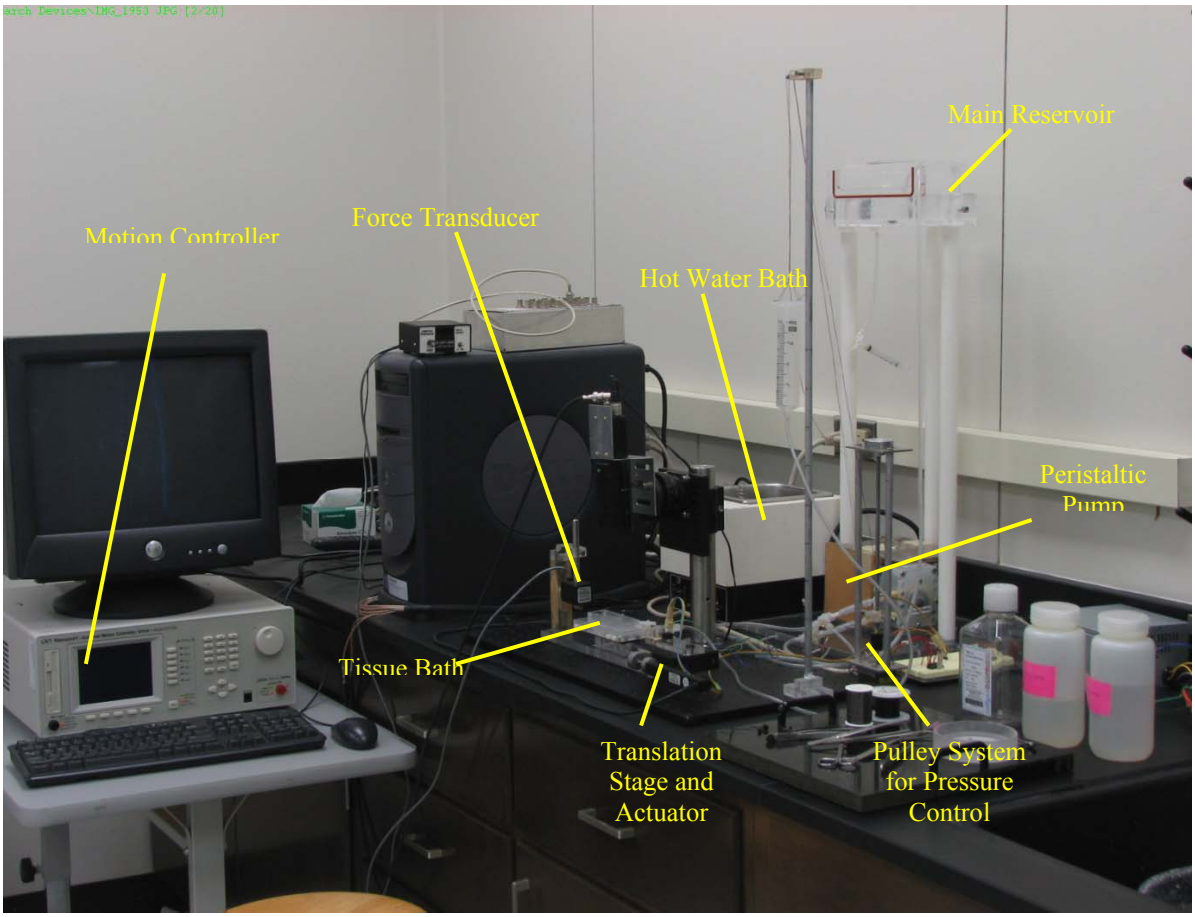

Figure 3.8: Photograph of the custom built experimental set-up showing the major subunits. The set-up is used to carry out biaxial tests on vascular soft tissue (inflation extension), uniaxial stretch tests and ring tests.

Vessel Preparation

All the vessels were harvested within one hour of sacrifice and stored in Ca+ free PBS at about 4 ^{o}C until tested. To harvest a lymphatic vessel, a blue colored dye was injected into the lymph nodes and a vessel with minimal bifurcations or branches was identified for harvesting using blunt dissection technique. It has been observed that the active and passive behavior of artery is insensitive to its storage in PBS maintained at 5 ^{o}C upto 48 hrs (Cox 1978). Though similar data is unavailable for lymphatic vessels, the biaxial tests on the vessel were carried out within 8 hour of harvesting with the assumption that the passive behavior of the vessels is insensitive storage of vessels for that period of time. Prior to testing the vessels were carefully cleaned of attached fat and lose adventitia using blunt dissection and the branches if present were ligated with help of medical suture. A valve free segment of vessel about 30mm in length was then selected for multiaxial test. Presence of a valve is indicated if the diameter of the cannulated vessel fails to return to its 0 pressure value after an inflation cycle. While cannulating the segment care was taken not to let any air bubble get trapped inside the lumen of the vessel. Ca+ free solution was used both in the bath and for inflation of the vessel in order to eliminate any effect of vessel tone.

Test Protocol

The no load length of the vessel (corresponding to distance between two ends of the cannula) at which it was cannulated was recorded followed by preconditioning in circumferential direction with help of 5 pressure cycles from 0 cm H_2O to 27.5 cm H_2O. The vessel was then allowed to relax for about 8 minutes before being subjected to the loading protocol. The protocol consisted of a pressure cycle, in steps of 2.5 cm H_2O, of upto 35cm H_2O for each axial stretch. The axial length was varied from no-load length to the axial length that resulted in an axial force beyond the range of the force transducer. Each step change in axial length was determined so that the axial stretch ratio increased by 5%. Since the vessel was not preconditioned in axial direction it was allowed to rest at each new axial length for 8 min prior to application of the pressure cycle. Though debatable it is our contention that the structural changes in the vessel as a

result of precondition that lead to the observed repeatable behavior could also be achieved by allowing it to relax at new axial length. *I*t is also observed that measurement of the axial load due to increase in pressure at a particular axial length is influenced by stress relaxation in axial direction if sufficient time is not allowed for axial force to reach a stable value

Estimation of Circumferential Stretch Ratio, Axial Stretch Ratio and Vessel Dimensions

A non-contact method is used to measure the strain/deformation experienced by the vessel under the action of combined inflation and extension. Though only the outer diameter and length at each new loading condition can be determined by using such method the value of internal diameter can be estimated from the assumption of incompressibility and the reference values of internal and external diameter.

Circumferential Stretch Ratio: An image of the vessel acquired at each loading conditions is converted into a binary image using an appropriate threshold value. A ROI (central part of the vessel) is then selected and the outer diameter is estimated by adding all the pixel values of ROI and dividing it by width of the ROI. The circumferential stretch ratio is then calculated with diameter of the vessel corresponding to no load configuration as the reference diameter.

Axial Stretch Ratio: Change in the axial length of the vessel is assumed equal to the amount of displacement of the translational stage. It should be noted that ideally one would place markers on the central region of the vessels (away from the attachment to the cannula) and calculate the stretch ratio from the knowledge of the displacement of these markers. The axial stretch ratio is then determined with length of the vessel at no load configuration as reference length.

Vessel Dimensions: To estimate the vessels dimensions (internal radius, external radius and thickness) a ring section of about 1mm thickness is cut from the vessel at the end of the inflation extension experiment and an image of its cross section is obtained. The image analysis module used requires the user to select multiple points along the inner and outer perimeter of the cross-section of the image. The centroid for the points on inner and outer diameter is then determined and using it as a center the arc length

between each adjacent points is estimated. The radius is then determined by adding all the arc lengths (essentially we estimate the inner and outer perimeter) along inner and outer perimeter and dividing it with 2π.

Determination of Reference Configuration

Since the circumferential stretch ratio and axial stretch ratio are calculated with diameter and axial length corresponding to no-load configuration of the vessel as the reference diameter and length, no load configuration is the obvious first choice for the reference configuration. However as we are not interested in modeling the buckling behavior of the vessel we will determine the axial stretch at which there is minimal change in axial force/load with change in transmural pressure as the in-vivo length of the vessel (Brossollet and Vito 1995) and use the configuration of the vessel corresponding

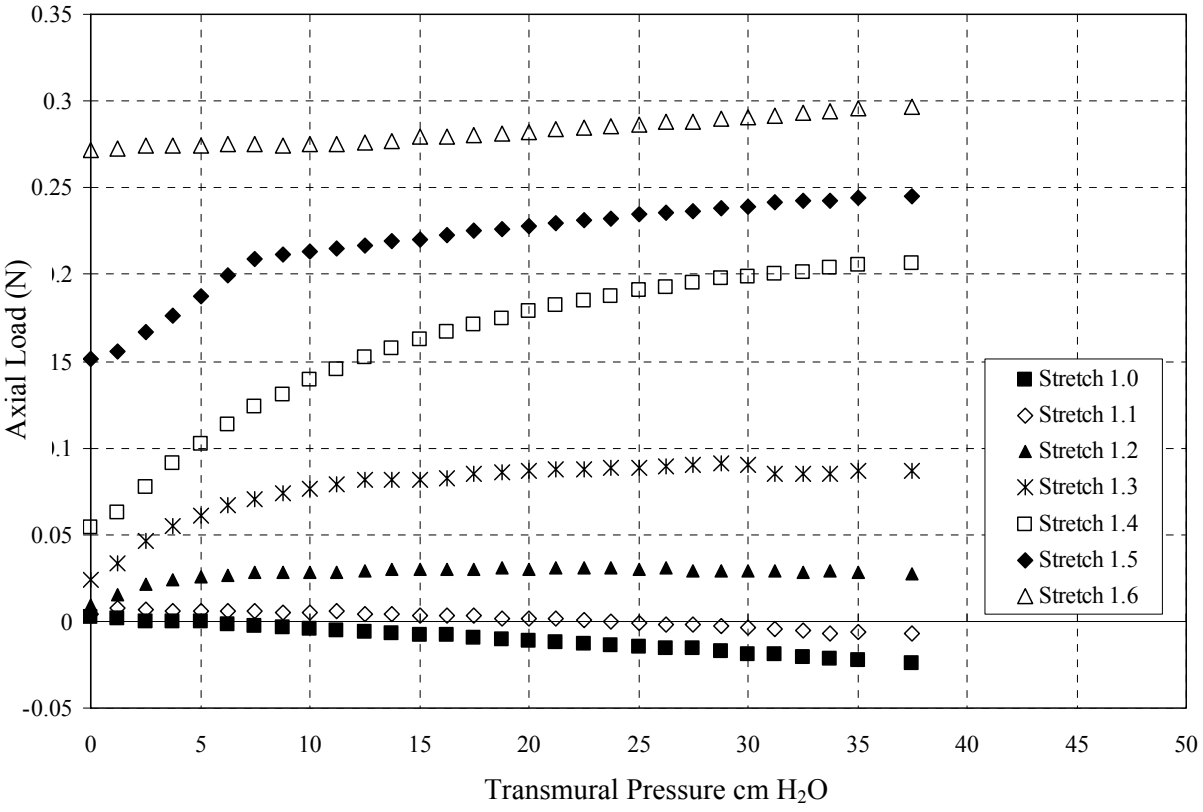

Figure 3.9: Variation of axial force with increase in transmural pressure at different axial stretch ratios. The no load configuration is used as reference configuration to estimate stretch ratios. The axial stretch ratio at which there is minimal change in axial load with increase in transmural pressure corresponds to the in-vivo length.

to that length as our reference configuration. Figure 3.9 shows the variation of the axial force with pressure at different axial stretch (no-load configuration as reference configuration) for one of the lymph vessels tested. The inside and outside diameter of the vessel at in-vivo length is determined using incompressibility condition.

Since the in-vivo length is not known a priori and the initial stretch ratio's are determined using no-load configuration as reference configuration, one has to recalculate the new stretch ratios corresponding to in-vivo configuration as new reference configuration. As shown in figure 3.10, one can relate the stretch ratios using equations 3.13.

$$(\rho_o^2 - \rho_i^2)\ell = (r_o^2 - r_i^2)l = (R_o^2 - R_i^2)L \tag{3.13a}$$

$$\tilde{\lambda}_Z = \lambda'_Z.\lambda_Z \tag{3.13b}$$

$$\tilde{\lambda}_Q = \lambda'_Q.\lambda_Q \tag{3.13c}$$

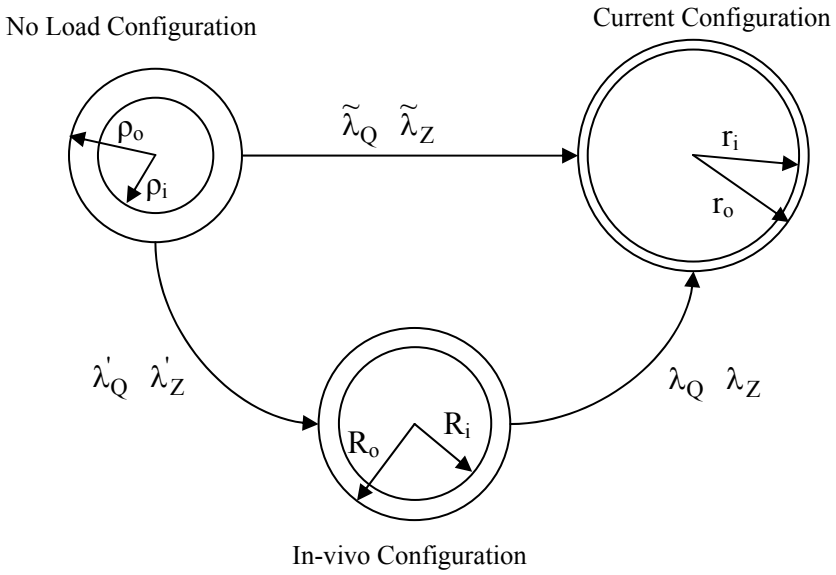

Figure 3.10: Relation between the circumferential and axial stretch ratio. The relationship is obtained when No-Load configuration and In-vivo configuration is used as a reference configuration.

Results

Variation of circumferential stretch ratio at axial stretch ratio corresponding to the in-vivo length and at approximately 1.13 with no-load length as the reference length is as shown in figure 3.11. The circumferential stretch ratio for each axial stretch ratio is estimated using diameter at zero pressure for that particular axial stretch ratio as the reference diameter.

Strain energy function to describe the biaxial test data on bovine post nodal mesenteric lymph vessels obtained from normal, venous occluded and sham were determined using the method proposed. For purpose of comparison same order (n=m=2) of orthogonal polynomial used to fit the data was selected for all the cases. The mean of the estimated coefficients is as shown in figure 3.12 and the deviation from hyperelastic ideal for each case is as in table 3.1.

Table 3.1 Values of the measure to quantify deviation from hyperelastic behavior for different lymph vessels modeled using proposed method with orthogonal polynomials of order n=m=2.

	Normal 1	Normal 2	VO1	VO 2	Sham
Δ_{ε}	0.12	0.0843	0.055	0.462	0.105
Δ_{AIC}	-163.486	257.439	130.974	825.119	-111.83

The measure proposed to quantify the deviation from hyperelastic behavior can also be used to compare two different materials provided the materials are tested over similar deformation range using same test protocol and the order of orthogonal polynomial function used to approximate the variation in data is selected so as to give almost similar total error of fit (equation). The total error of estimated using either of the two measures (ETA or AIC) is given as follows,

$$Total\ \varepsilon = \frac{1}{mean\left(\frac{\partial W_{\gamma_2}}{\partial \gamma_2}\right)_{\exp}}\sqrt{\frac{e_{\gamma_2}}{(N-q_{\gamma_2})}} + \frac{1}{mean\left(\frac{\partial W_{\gamma_3}}{\partial \gamma_3}\right)_{\exp}}\sqrt{\frac{e_{\gamma_3}}{(N-q_{\gamma_3})}} \tag{3.14a}$$

$$Total\ AIC = N\ln\left(\frac{e_{\gamma_2}}{N}\right) + 2.q_{\gamma_2} + N\ln\left(\frac{e_{\gamma_3}}{N}\right) + 2.q_{\gamma_3} \tag{3.14b}$$

Where, q is the number of parameters/coefficients $(n \times m)$, N is the number of data points, and $e_{\gamma_k} = \sum_{p=1}^{N}\left[\left(\frac{\partial W_{\gamma_k}}{\partial \gamma_k}\right)_{\exp} - \left(\frac{\partial W_{\gamma_k}}{\partial \gamma_k}\right)_{fit}\right]_p^2$.

The biaxial behavior of normal, venous occluded and sham lymphatic vessels from bovine mesentery was compared in this fashion. The total error of fit estimated using both the measures for goodness of fit and the corresponding minimum deviation for the selected order of orthogonal polynomials used is given in table 3.2 and is as shown in figure 3.13.

Table 3.2: Deviation from hyperelastic ideal for normal, sham and venous occluded vessel for order of orthogonal polynomial chosen so as the total error of fit in all the cases is comparable.

	Normal 1	Normal 2	VO1	VO 2	Sham
Total ε	5.034 E-06	2.67 E-06	3.472 E-06	3.193 E-06	2.032 E-06
Δ_{AIC}	133.038	417.55	278.469	825.112	-22.586
Δ_{ε}	0.179	0.095	0.06	0.462	0.106

	Normal 1	Normal 2	VO1	VO 2	Sham
Total AIC	-4343.343	-3568.825	-4044.463	-2562.075	-3651.325
Δ_{AIC}	2047.693	417.55	278.469	825.119	118.616
Δ_{ε}	0.179	0.095	0.06	0.462	0.122

(A)

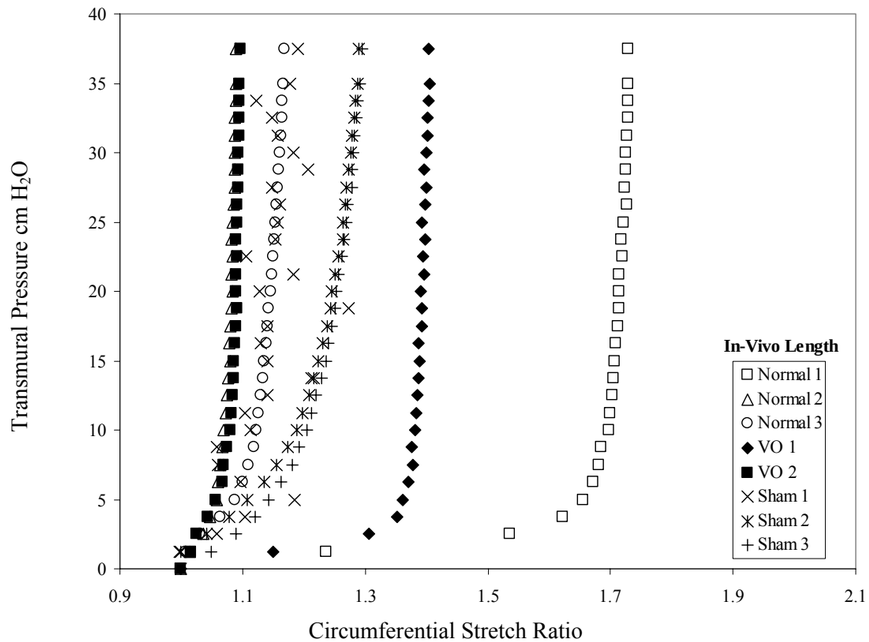

(B)

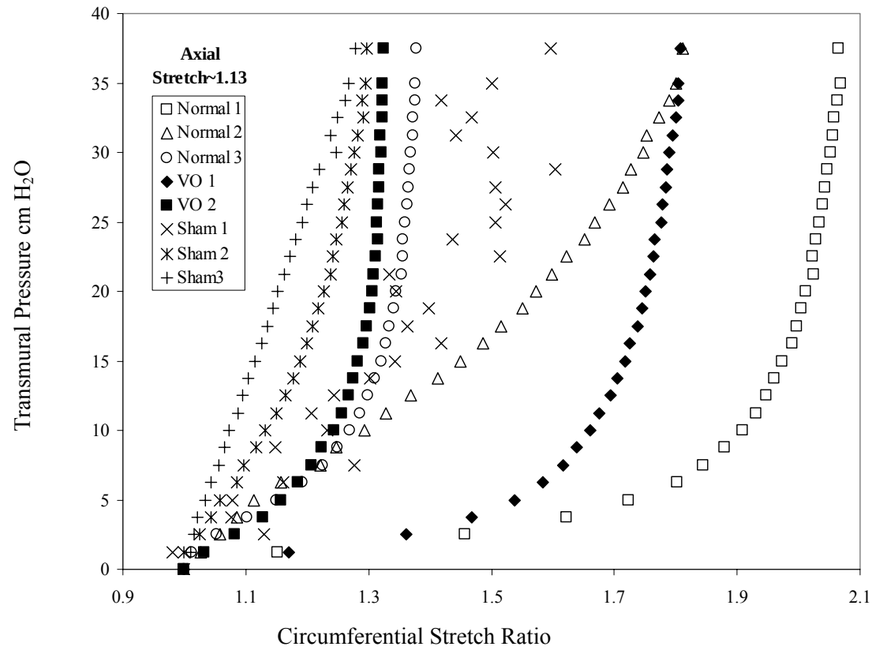

Figure 3.11: Variation of circumferential stretch ratio with transmural pressure for normal, venous occluded and sham vessels. (A) At in-vivo length (B) At stretch ratio 1.13 with in-vivo length as ref configuration.

(A)

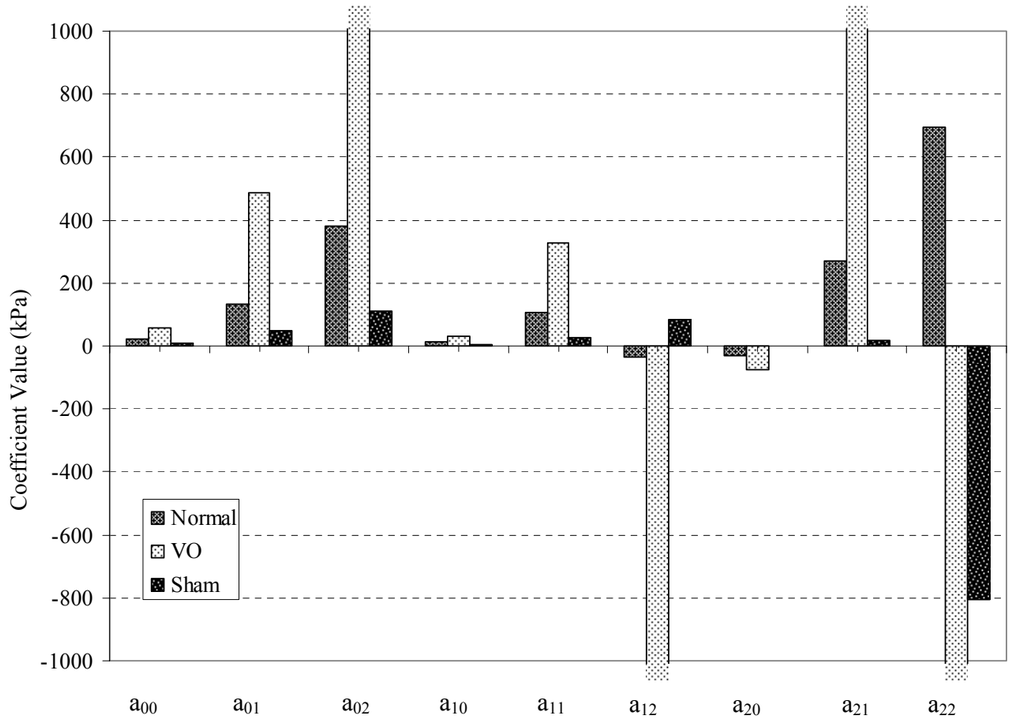

(B)

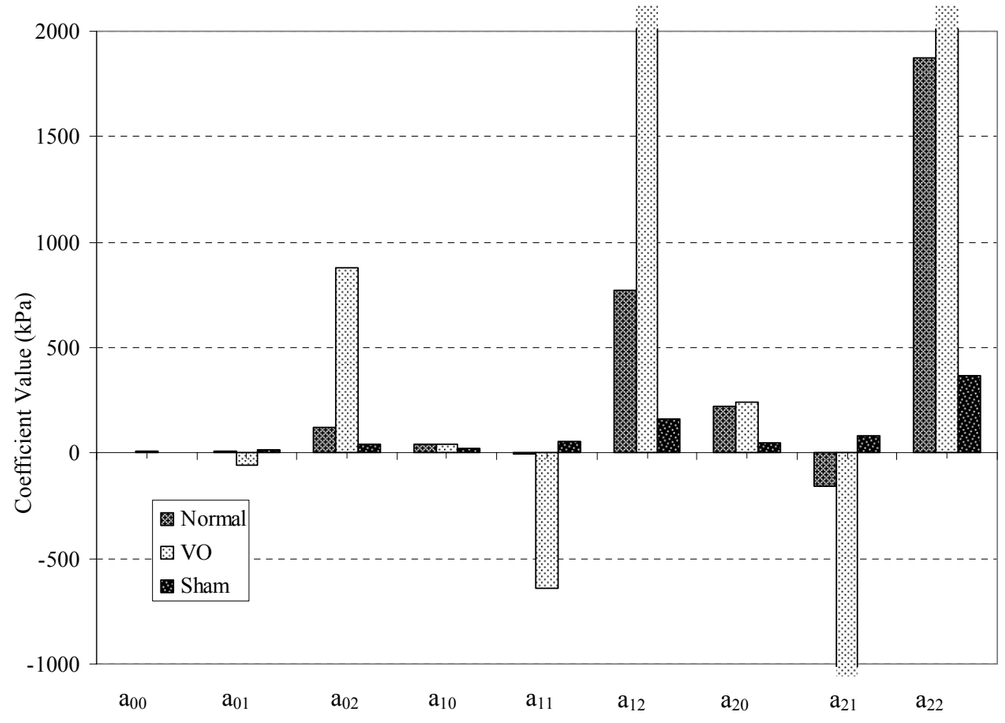

Figure 3.12: Mean values of the coefficients determined using the orthogonal fit for normal, sham and venous occluded vessels. (A) $\left(\partial W_{\gamma_2}/\partial\gamma_2\right)_{exp}$. (B) $\left(\partial W_{\gamma_3}/\partial\gamma_3\right)_{exp}$

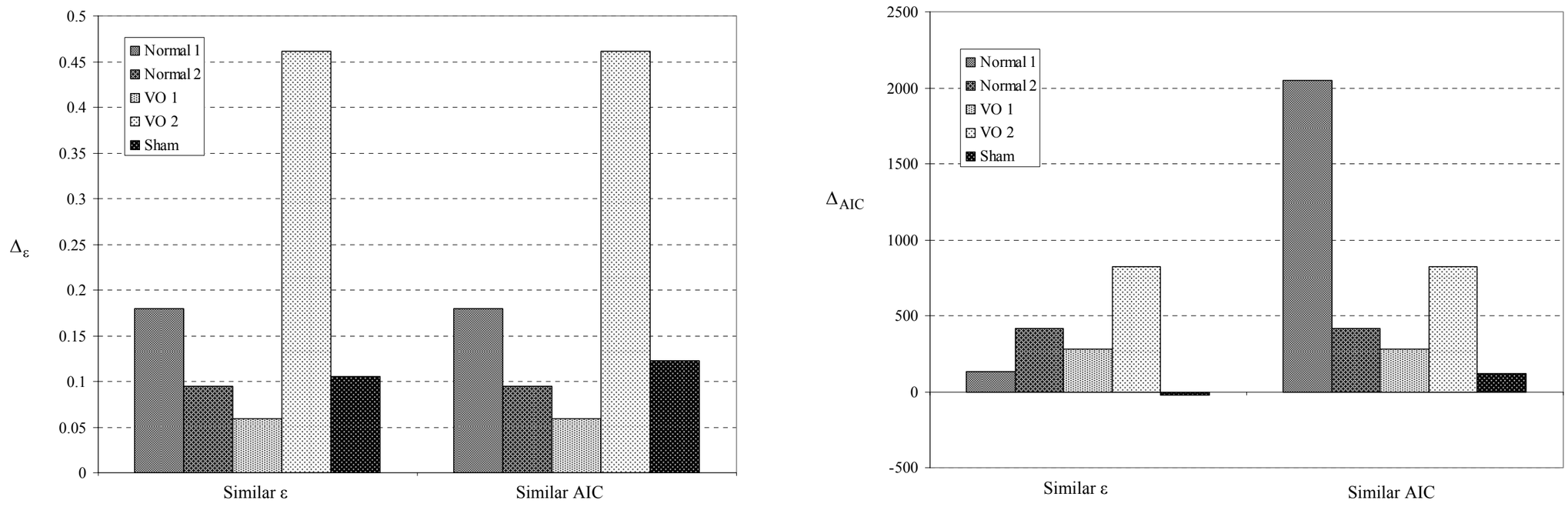

Figure 3.13: Comparison of values of Δ_ε and Δ_{AIC} for normal, sham and venous occluded vessels. These measures quantify the deviation from hyperelastic ideal as given in table 2. The order of polynomial is selected based on similarity of total error (A) determined by using the measure ε.(B) determined by using the measure AIC.

(A)

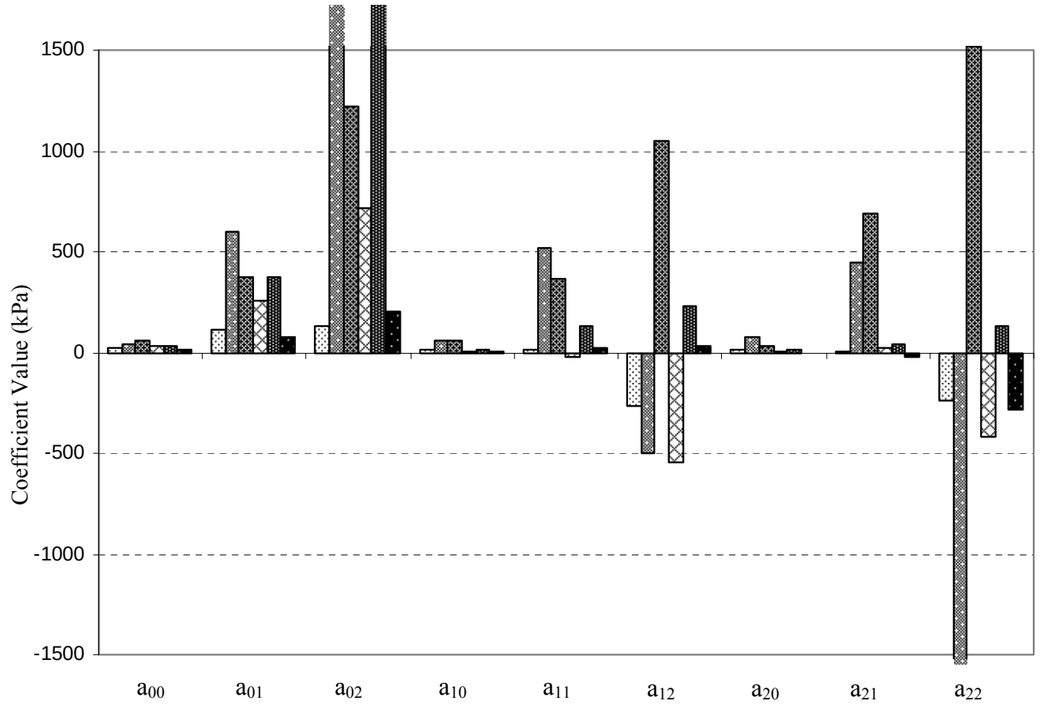

(B)

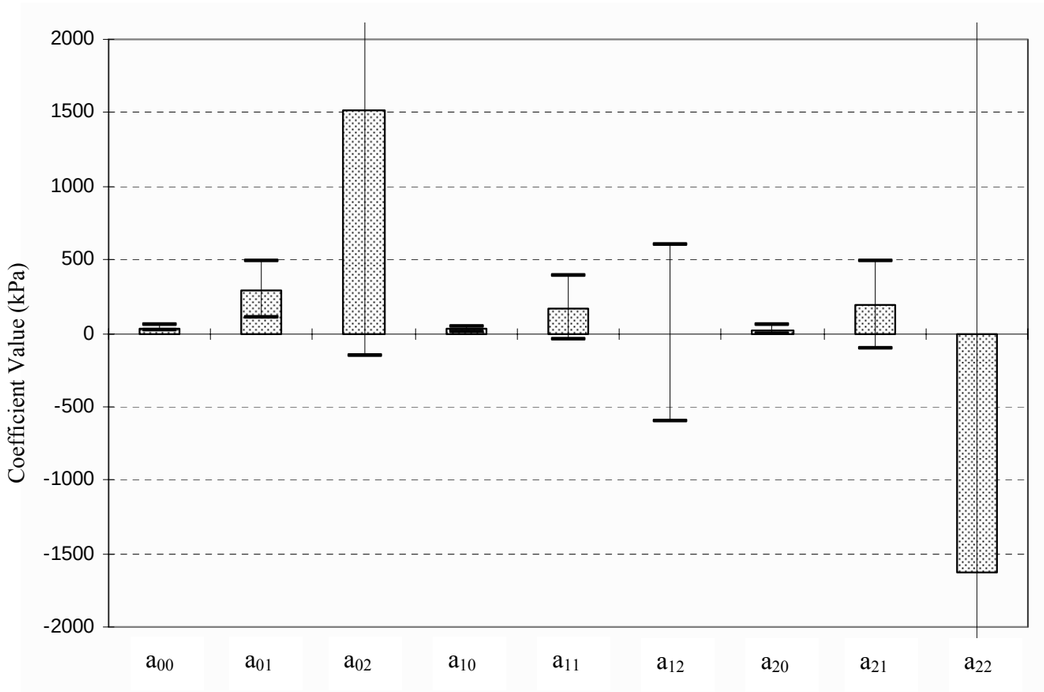

Figure 3.14: The coefficient values, their mean and standard deviation used to fit experimental values $\left(\partial W_{\gamma_2}/\partial\gamma_2\right)_{exp}$ for normal vessels (N=6). (A) Coefficient values of the orthogonal polynomials used to fit experimental values $\left(\partial W_{\gamma_2}/\partial\gamma_2\right)_{exp}$ obtained from inflation extension test on 6 normal vessels. (B) Mean and standard deviation for the coefficient values shown in figure 3.14 (A)

(A)

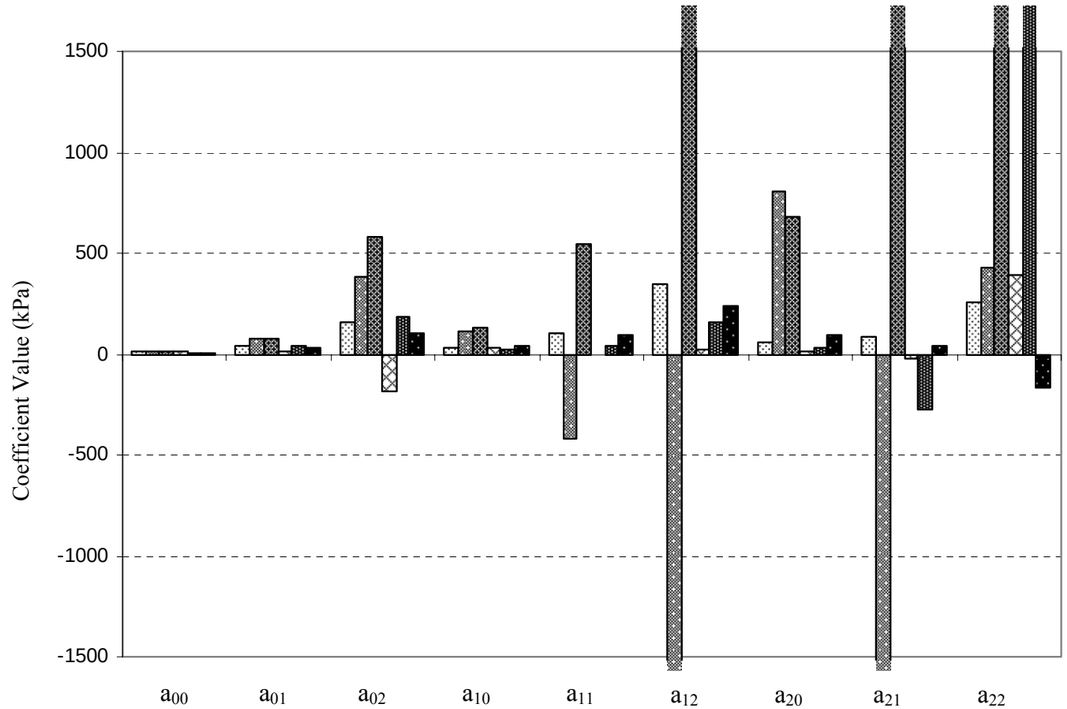

(B)

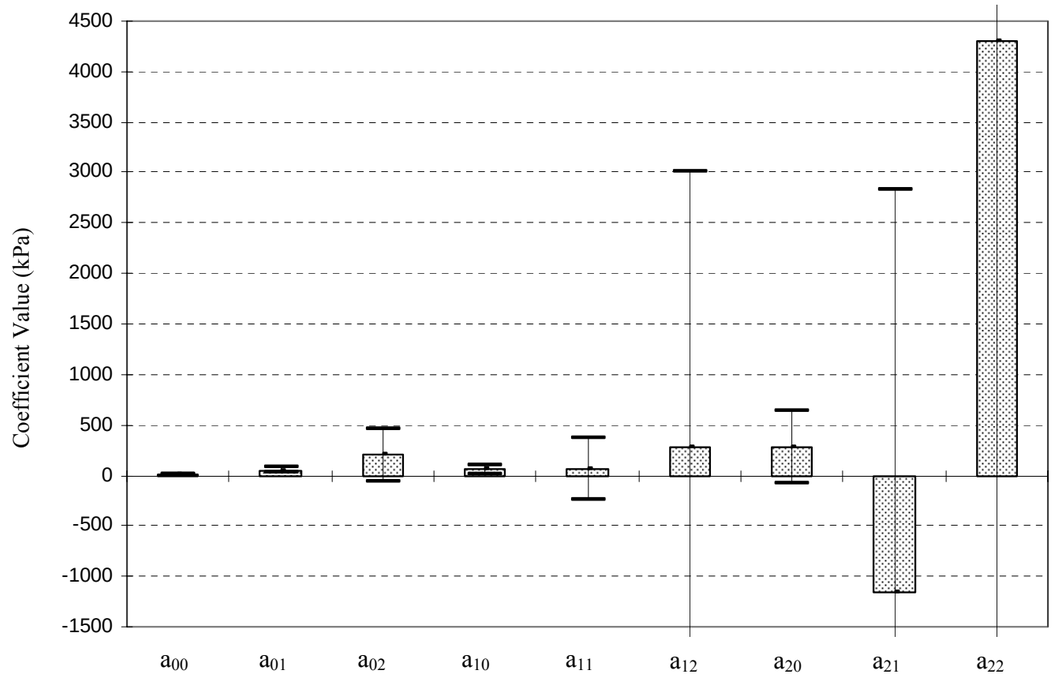

Figure 3.15: The coefficient values, their mean and standard deviation used to fit experimental values $\left(\partial W_{\gamma_3}/\partial\gamma_3\right)_{exp}$ for normal vessels (N=6). (A) Coefficient values of the orthogonal polynomials used to fit experimental values $\left(\partial W_{\gamma_3}/\partial\gamma_3\right)_{exp}$ obtained from inflation extension test on 6 normal vessels. (B) Mean and standard deviation for the coefficient values shown in figure 3.15 (A)

Discussion

General Characteristics

The post nodal bovine mesenteric lymph vessel shares lot of similarities, structural as well as mechanical or rather structural and hence mechanical with arteries and veins. On the basis of such similarity we have assumed the lymphatic vessel to be homogeneous, thin walled, axis symmetric and incompressible and that its behavior under combined inflation and extension is orthotropic and hyperelastic. Such assumptions allow us to model the behavior of the vessels from normal, sham and venous occluded animals using the proposed method. Since we have not modeled the biaxial mechanical behavior of the other two type of blood vessels using the proposed method we cannot compare or comment on how the model faired in characterizing such behavior in case of lymphatic vessels. Also due to lack of enough data on deviation of wide variety of soft tissues from hyperelastic ideal we cannot comment on the deviation observed for the vessels under consideration.

In vivo Length and Circumferential Stiffness

The length of the vessel corresponding at which there is minimal change in axial load with change in transmural pressure is assumed as in-vivo length of the vessel. In case of arteries it has been found that stretch ratio corresponding to this length changes with no-load length as the reference length changes when subjected to hypertension. In the current case no such change was found and the stretch ratio for all the vessels (Normal, VO and sham) was almost similar (~1.15). Also there was no significant/conclusive change in the variation of the circumferential stretch ratio with transmural pressure at in-vivo length or at length corresponding to stretch ratio of ~ 1.13(in-vivo length as reference). Although all the vessels seem (except two from sham) to become more complaint with increase in stretch ratio, change of compliance for each vessel was not quantified and comparison of this might give some indication of change in mechanical behavior.

Comparison of Coefficients

Since the coefficients of the orthogonal polynomials used to fit the biaxial test data can be assigned a physical meaning that is characteristic of material and are indicative of the underlying structure, comparison of their values for normal, sham and VO vessels would help us determine any difference in mechanical behavior of the vessels. Although orthogonal polynomials of order n=m=2 were used to fit the data from each vessel without any regards to the similarity of the error of fit, the coefficients obtained being unique can be compared with each other. Such comparison shows that most of the coefficients for VO vessels are higher than those for sham and normal vessels indicating that the mechanical behavior of the VO vessels for similar range of deformation is different than that for sham and normal vessels. This also implies structural remodeling of the vessels subjected to high flow/edematous conditions.

Comparison of Deviation from Hyperelastic Ideal

Since similar protocol used for biaxial test of the vessels was same, the deviation from hyperelastic behavior of the vessels for similar range of deformation estimated using the order of orthogonal polynomials that give similar error of fit can also be used to compare the vessel behavior. Although one on the VO vessel showed very large deviation compared to the other we shall refrain from making any conclusion since the deviation for the other VO vessel was similar to that of Normal and sham vessels.

From the comparison of the circumferential stretch, the coefficients and the deviation from hyperelastic ideal for the vessels we conclude that though there are indications that the behavior of VO vessels is different than those of sham and normal hence implying associated structural remodeling, it is not conclusive. We would need more data to draw any inferences especially when we consider the large error that is usually associated with the data from biaxial experiments as a result of dependence of the vessel behavior on strain history, harvesting and cleaning of the vessels using blunt dissection and selection of appropriate reference configuration. Indeed it should be evident from figure 3.14 and 3.15 that there is large variability in the coefficient values amongst the normal vessels themselves. This variation can be attributed to the different sources of error mentioned above. We believe that with use of large amount of data (biaxial experiments on more samples) the trends would become more prominent to make suitable interpretation with any certainty.

CHAPTER IV
MORPHOLOGICAL CHANGES IN BOVINE MESENTERIC LYMPH VESSEL IN RESPONSE TO INTESTINAL EDEMA

Introduction

Growth and remodeling of human tissue in homeostatic and pathological condition is dependent on the physical and chemical environment that the tissue experience. The dependence on the physical environment is rather prominent in case of cardiovascular soft tissue with stresses experienced by the tissue namely circumferential, axial, radial and shear being the most common stimuli (Langille et al., 1989, Davies 1995, Pries et al., 2005, Taber 1998). Indeed numerous studies have been done that subject a cardiovascular tissue to altered hemodynamic load, majority mimicking hypertension due to its prevalence and high mortality rate, in order to better understand the resulting morphological changes and the involved pathways (Humphrey 2001). However, little attention has been given to lymphatic vessels that help to maintain interstitial fluid at homeostatic levels.

Lymphedema is a pathological condition that is characterized by excessive accumulation of interstitial fluid as a result of compromised function of lymphatic network. The condition can be congenital or acquired with acquired lymphedema being a common side effect of chemotherapy etc aimed at treating cancer. Though various treatment options are available for edema management there is no known cure for the condition. We believe that knowledge of the morphological changes in the lymph vessels under conditions similar to edema would give us some insight into the associated growth and remodeling and help us correlate the structural changes with the observed physiological and mechanical behavior.

In the present work we report the findings, from an exploratory study, of the changes in geometry and structure of bovine mesenteric lymph vessels that were subjected to edematous conditions for 3 days. A theoretical model developed to describe the observed changes in the vessel geometry is proposed. We also discuss briefly design of a novel fixation rig that can be used for intra and extra luminal fixation of tubular

tissue at predetermined stretch ratio and transluminal pressure. The lymph vessels harvested from normal animal from local slaughter house will be called normal vessels, those harvested from the animal subjected to sham surgery will be called sham vessels and the ones from the animal induced with intestinal edema by venous occlusion will be called venous occlusion or venous occluded vessel.

Methods

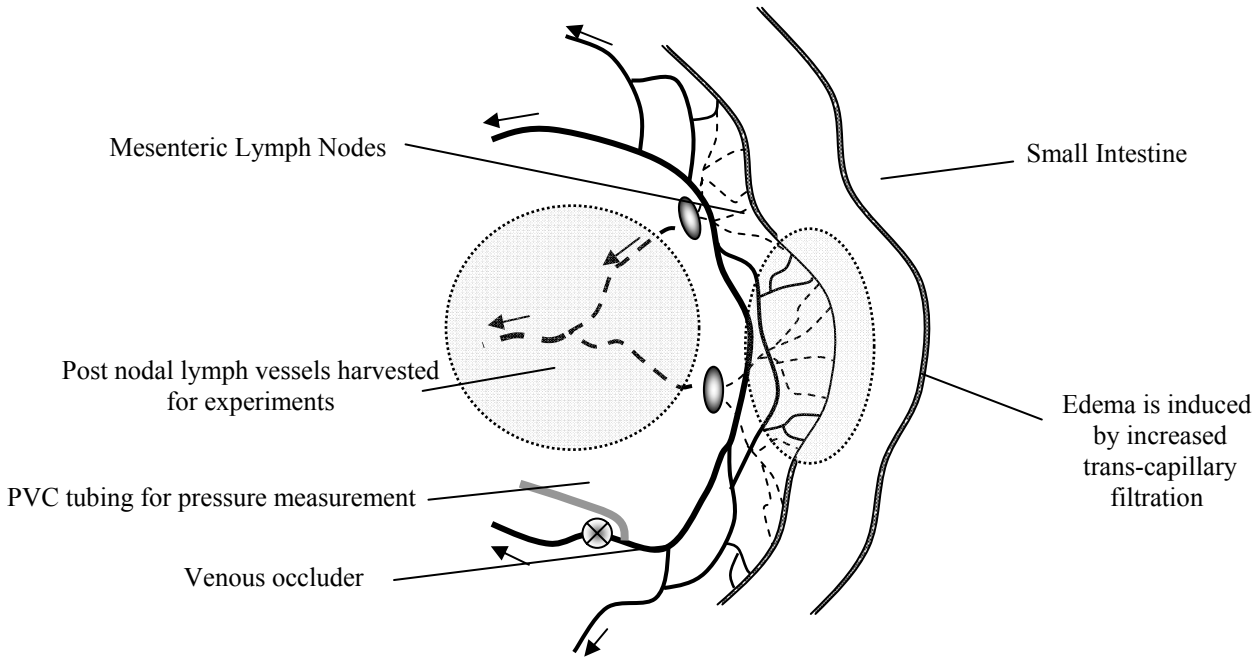

Figure 4.1: Schematic of bovine mesentery showing the lymphatic and venous vasculature. Occlusion of the vein collecting from proximal jejunal arcade results in increased microvascular pressure and microvascular filtration leading to interstitial edema. The circular shaded area shows the site from where the lymphatic vessels are harvested.

Intestinal edema as a result of increased microvascular pressure and microvascualr filtration rate was induced in the animal by surgically occluding a vein supplying the proximal jejunal arcade (Figure 4.1). The surgical procedure was carried out at Texas A&M vivarium in accordance with the animal experimentation protocols.

The right flank of each of the cows was clipped at the planned surgical site after being restrained in squeeze chute and 20 mg/kg oxytetracycline was administered

through intravenous catheter placed in its right jugular vein. It was positioned in left lateral recumbency on the surgery table following anesthesia that was induced using xylazine (0.1 mg/kg, IV), diazepam (0.01 mg/kg, IV) and ketamine (2 mg/kg). Mechanical ventilation with 100% oxygen and 1-3 % isoflurane was used to maintain anesthesia and oxygen saturation was maintained at >95% throughout the procedure.

A 25-cm incision was made midway between the tuber coxae and the last rib and was extended through the external and internal oblique, transverse muscles and peritoneum. The small intestine was exteriorized and kept moist using warmed 0.9% saline. A vein supplying the proximal jejunal arcade was identified, carefully isolated by blunt dissection, and a vascular occluder (Kent Scientific Corporation, Torrington, CT) infused with 50% dextrose was fixed around it with 2-0 polyglactin 910. A 1/8" O.D. polyvinyl chloride (PVC) tubing (VWR Scientific, Suwanee, GA) filled with heparinized saline was inserted into the upstream vein supplying the proximal intestinal arcade and secured using 2-0 polyglactin 910 for measurement of venous pressure. The PVC tubing and the tail of the vascular occluder were exteriorized through a small skin incision dorsal to the abdominal incision before replacing the jejunum in the abdomen and closing the incision in three layers using #2 polyglactin 910. The skin was closed using 0- polymerized caprolactam. For control animals a sham surgery was carried out and only the intravenous tubing for measurement of intestinal venous pressure was placed into the vein supplying the proximal intestinal arcade.

Three days following the surgery, animals were euthanized using the captive bolt method followed by exsanguination. Postnodal mesenteric lymph vessel was harvested, using blunt dissection immediately following the sacrifice of the animal and was stored in PBS at 4 ^{o}C until ready to be fixed. Prior to fixation attached fat and lose adventitia were carefully removed from the vessel using. The vessel was then fixed with zinc formaldehyde at no-load length and 10cmH_20 transluminal pressure using a rig similar to that shown in figure 4.2.

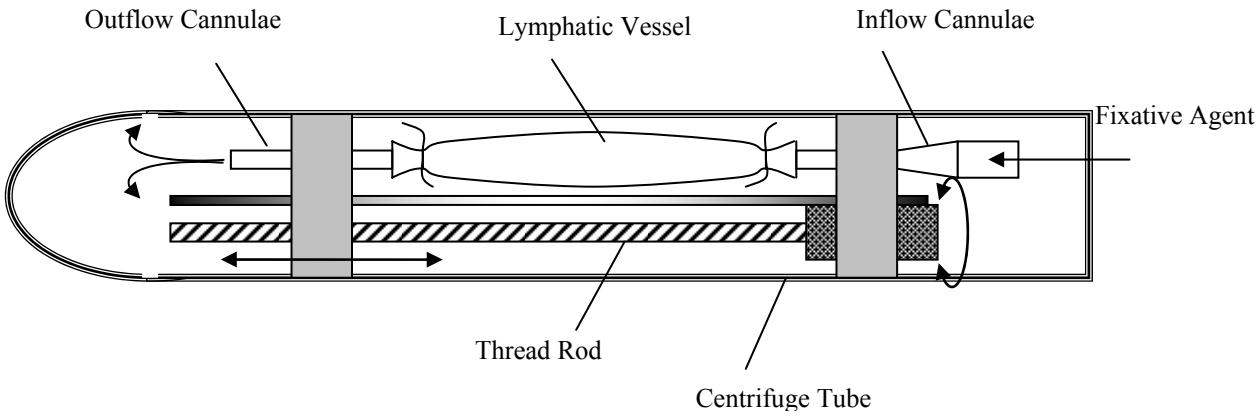

Figure 4.2: Schematic of the rig to fix vessels intra- and extra-luminally at predetermined stretch ratio and transmural pressure. In the current study the vessels were fixed with zinc-formaline at no –load length and 10 cm H20 transmural pressure.

Such a rig can be used for intra and extra luminal fixation of a vascular tissue and can be stored, along with the fixed tissue, in a standard centrifuge tube. Once the tissue is cannulated at a desired stretch ratio the rig is inserted into the centrifuge tube and the input end of the cannula is attached to a reservoir of fixative solution maintained at a desired input pressure. The cannula at the output end of the tissue has very small lumen (high resistance) so that majority of pressure drop takes place across it and the intra luminal tissue pressure is almost equal to the input pressure. The outflow from the output cannula into the centrifuge tube results in extra luminal fixation. The rig by itself can also be used, with help of a suitable microscope, to study the vessel structure (fiber orientation) and monitor changes in it at various pressure and stretch ratio. Such measurements are a common focus of majority of studies on mechanical behavior of soft tissue (Ogden and Schulze-Bauer 2000, Holzaphel 2000).

Each of the fixed vessels was then divided into two segments, one for structural analysis using histological staining with Masson's Trichrome (SMC and Collagen) and H&E (fibrous proteins) and the other for obtaining its geometric dimensions (internal and external radii).

To estimate the geometric dimensions of the vessel, the fixed vessel segment was cut, using a razor blade, into multiple cross section slices of about 1mm thickness. Image of each section was obtained using a light microscope attached with a CCD camera (Olympus). Olympus Software was used to capture and store the image. A droplet of water was added into the lumen of each section prior to capturing the image so as to keep the vessel wall from collapsing inward.

Data Analysis

A custom image analysis application developed using MATLAB was used to estimate the inner radius and outer radius from the images of the vessel cross section. Briefly the application prompts the user to select multiple points along the inner and outer perimeter of the cross section and estimates the centroid of the selected points (Figure 4.3). The total perimeter is determined by summing the arc lengths (calculated with centroid as assumed center) between the consecutive points selected along the wall boundary of the vessel. The inner and outer radius is then estimated by assuming that the cross-section is circular and that perimeter is equal to $2\pi r$.

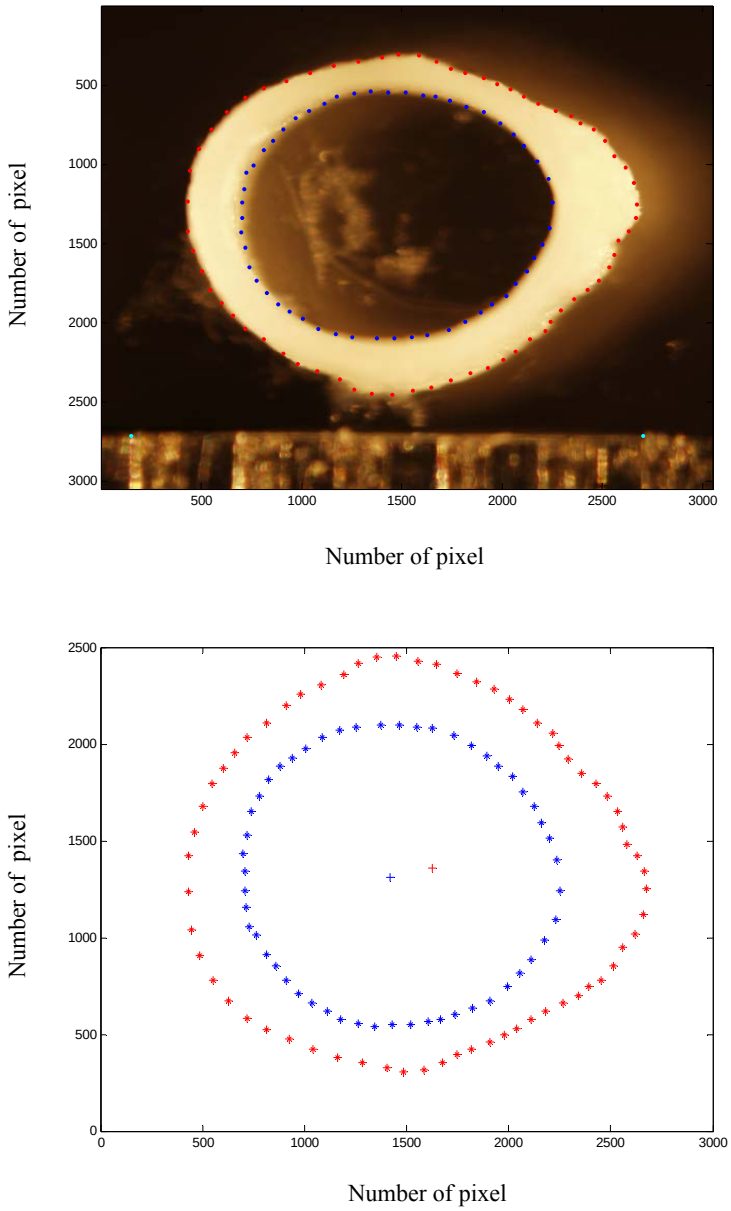

Figure 4.3: Image of vessel cross section fixed with zinc formaline at about 10 cm H_2O. A customized MATLAB code that prompts the user to select multiple point along the inner and out perimeter is used to estimate the geometric dimensions of interest

Histology

Although there are some common features the microstructure of the lymphatic vessel not only shows a great variability along the lymphatic network, but there are large interspecies and organ difference (Aukland and Reed 1993, Swartz 2001). With the exception of those in skeletal muscle bed, the collecting lymphatic vessels have layered architecture similar to that of blood vessels. The vessel wall can be divided into three layers: the innermost intima is a single layer of endothelial cells surrounded by basement membrane. The media consists of few layers of SMC with collagen and elastin fibers. The amount and arrangement of SMC within this layer is dependent on the size of the vessel. The smaller vessels have smaller amounts of SMC and lack any particular organization whereas the larger vessels have more ordered SMC oriented in circumferential direction. The outer layer, adventitia consists of connective tissue elements along with nerves and the fibroblasts (Von Der Weid 2001). For a more detailed account of the microstructure one can refer to references in for example Aukland and Reed (1993), Swartz (2001) or Hargen and Schmid-Schonbein (2000).

Vessel cross-sections stained with Masson's Trichrome and H&E are used to analyze changes in the structural components of the post nodal lymph vessel in response to intestinal edema. Images are enhanced using Picasa web (Google) and analyzed with a customized application developed using MATLAB. The analysis mainly involves filtering of the image, to identify SMC (stained red/pink) and Collagen (Stained Blue) from Trichrome stained images and Fibrous structures of Media from H&E stained images followed by thresholding to convert the filtered images to binary in order to estimate the area occupied by each constituent (Figure 4.4).

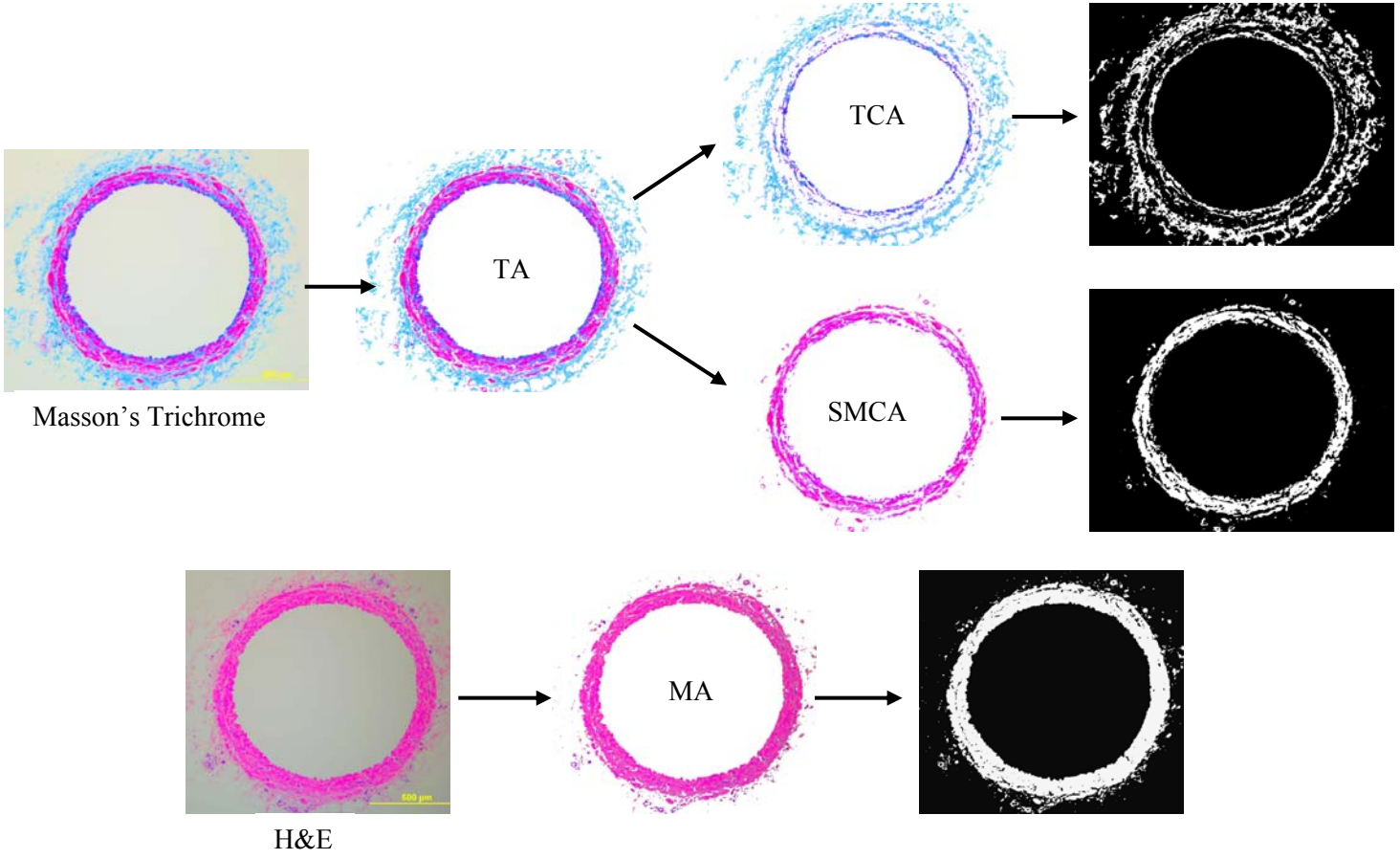

Figure 4.4: The intermediate images obtained by using the customized image analysis application. The application is developed using MATLAB to estimate the total area, medial area, area occupied by SMC and collagen. The lymphatic vessel sections stained with Masson's Trichrome and H&E were used to estimate the % area of the constituents of interest. The labels show the images used to estimate the corresponding area. TA: Total area of cross-section, TCA: Area occupied by the total collagen, SMCA: Area occupied by smooth muscle cells, MA: Area of the media. The areas are estimated using the binary images.

Theoretical Model

To explain the changes in the geometry along the length of the vessel and in response to the intestinal edema, we propose a model based on the following assumptions.

1. The circumferential stress along the length of the vessel is constant and any changes in this value acts as a stimulus for growth and remodeling.
2. The flow through lymphangion can be explained by Poisseuille's Law.
3. The flow rate through a lymphangion is proportional to its cross section area.

From Laplace law we have,

$$\sigma_c = \frac{\mathrm{Pr}}{h} = \text{constant} \tag{4.1}$$

Using assumption 2 and 3 we get,

$$P \propto \frac{Q}{r^4} \propto \frac{1}{r^2} \tag{4.2}$$

Where , σ_c is the homeostatic value of circumferential stress, P is the mean pressure of the lymphangion, r is the average radius of the lymphangion, h is the thickness of lymphangion wall and Q is the average flow rate of lymph through lymphagion

From equation 4.1 and 4.2 we get the following,

$$\frac{h}{r} \propto \frac{1}{r^2} \tag{4.3}$$

Therefore the ratio of thickness to radius is proportional to inverse of square of average radius of the lymphangion. The variation of experimental values of thickness to radius ratio with inverse of square of average radius is as shown in figure 4.5. In case of venous hypertension the flow through the lymphatic vessels increases and hence we would expect the proportionality constant to increase. The increase in flow could be achieved by increased contraction frequency (prenodal lymphangions) or due to conduit like behavior (postnodal lymphagions)(Gashev et al., 2007). The linear fit to the data obtained using least square method and constrained to zero intercept are as shown. As expected the proportionally constant for VO is higher than Normal and Sham.

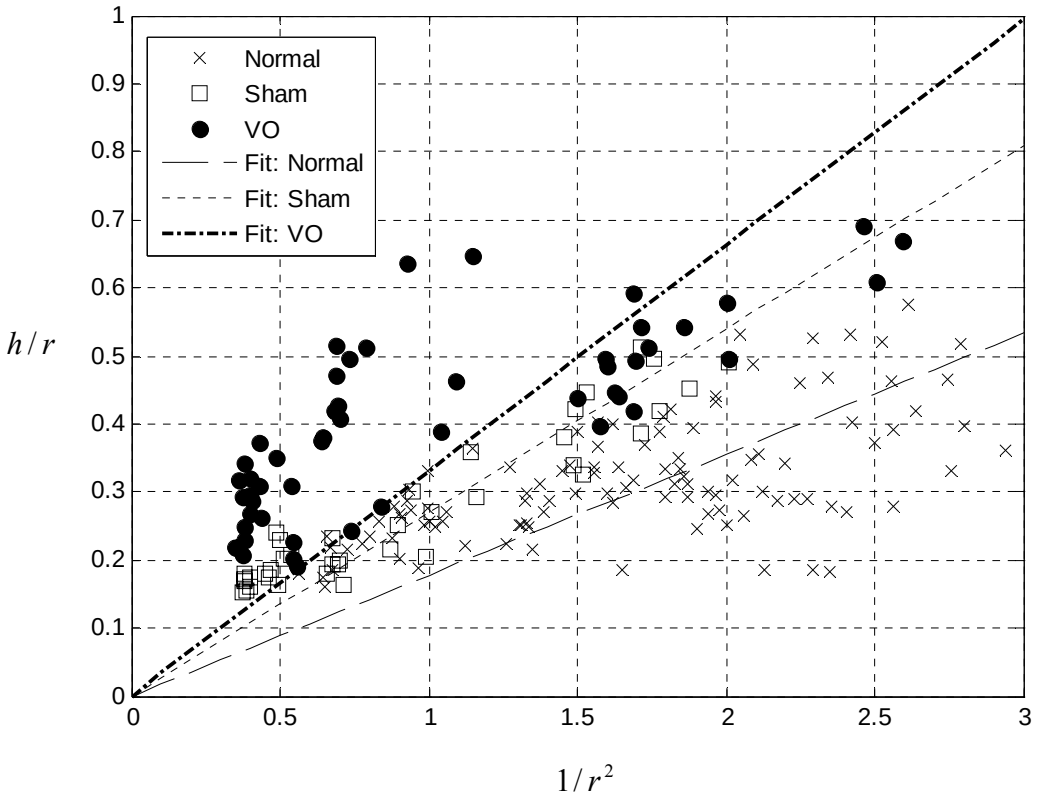

Figure 4.5: Variation of thickness to radius ratio with inverse of squared radius for normal, sham and VO vessels and the analytical fit. The analytical fit is obtained using equation 4.3. The proportionality constant for VO is greater than that for Sham and Normal as expected due to higher flow rate as a result of venous hypertension.

Results

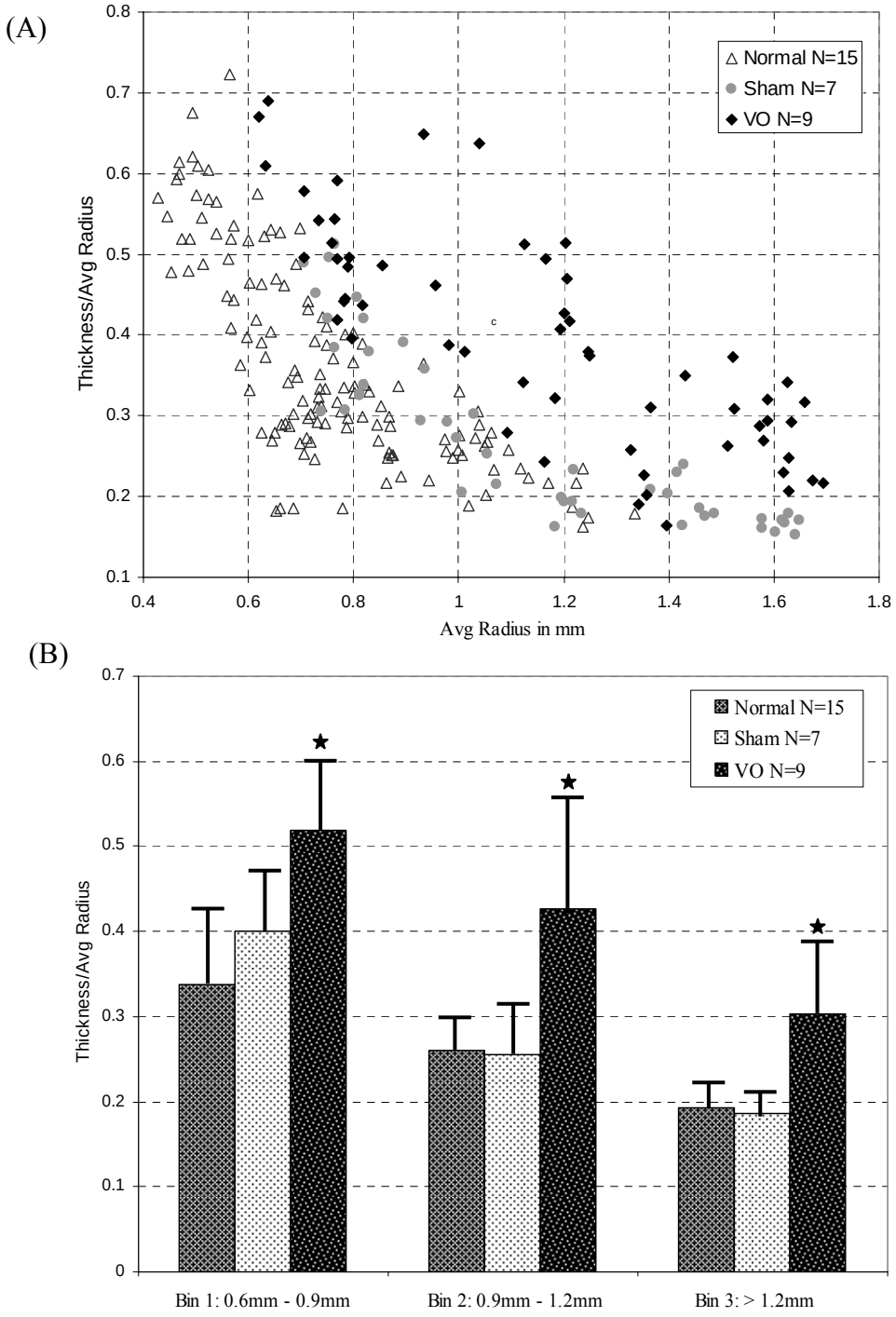

Figure 4.6: Variation of thickness to average radius ratio with the average radius for normal, venous occluded and sham vessels (A) Variation of thickness to average radius ratio with the average radius for normal, venous occluded and sham vessels. (B) The data is divided into three bins as for benefit of comparison.

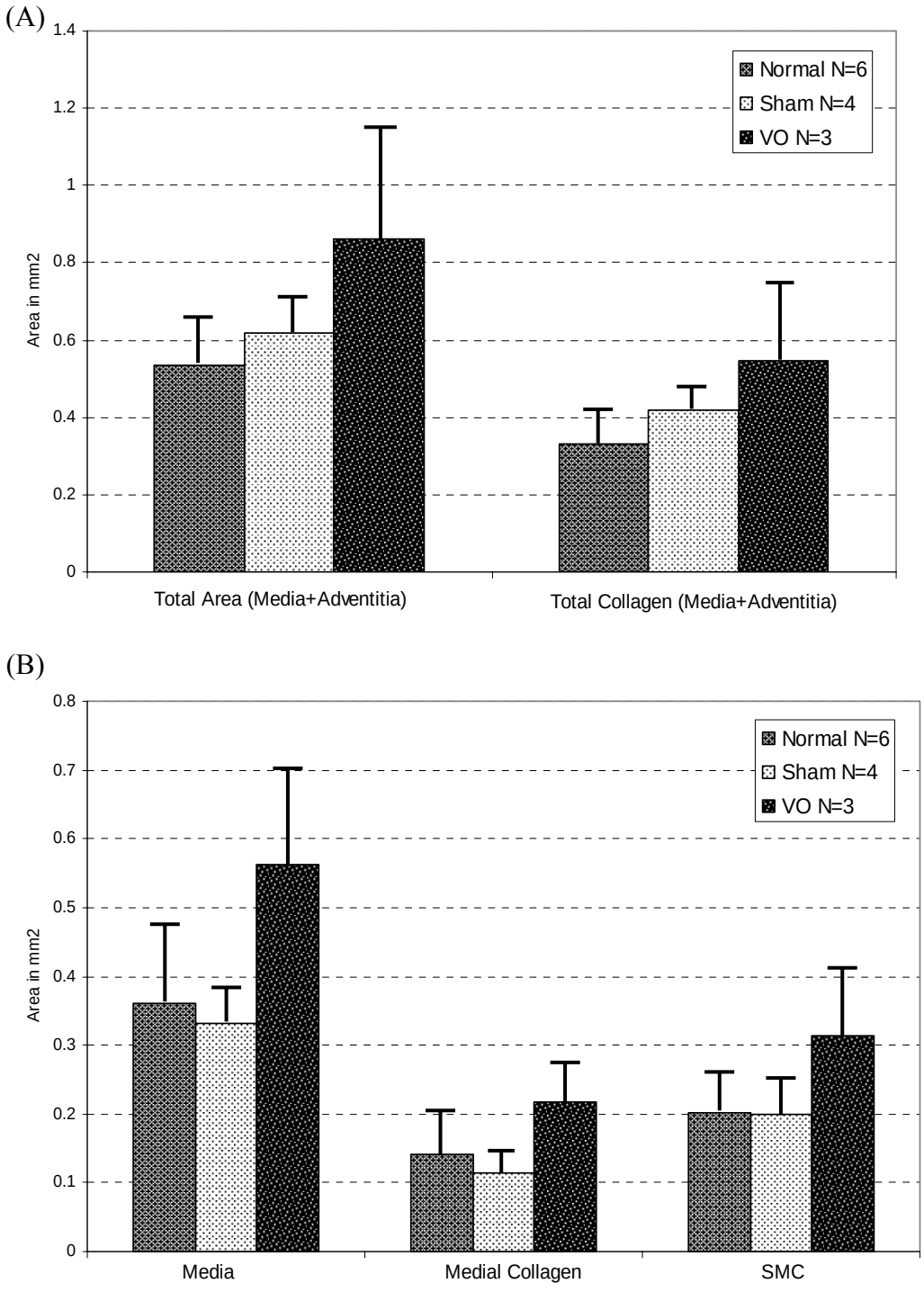

Figure 4.7: Mean and 95% CI for the total area of the constituents (A) Mean and 95% CI of the total area of cross section and the area occupied by the collagen in case of normal, sham and venous occluded vessel .(B) Mean and 95% CI of the area occupied by media, Medial collagen and SMC for normal, sham and venous occluded vessels.

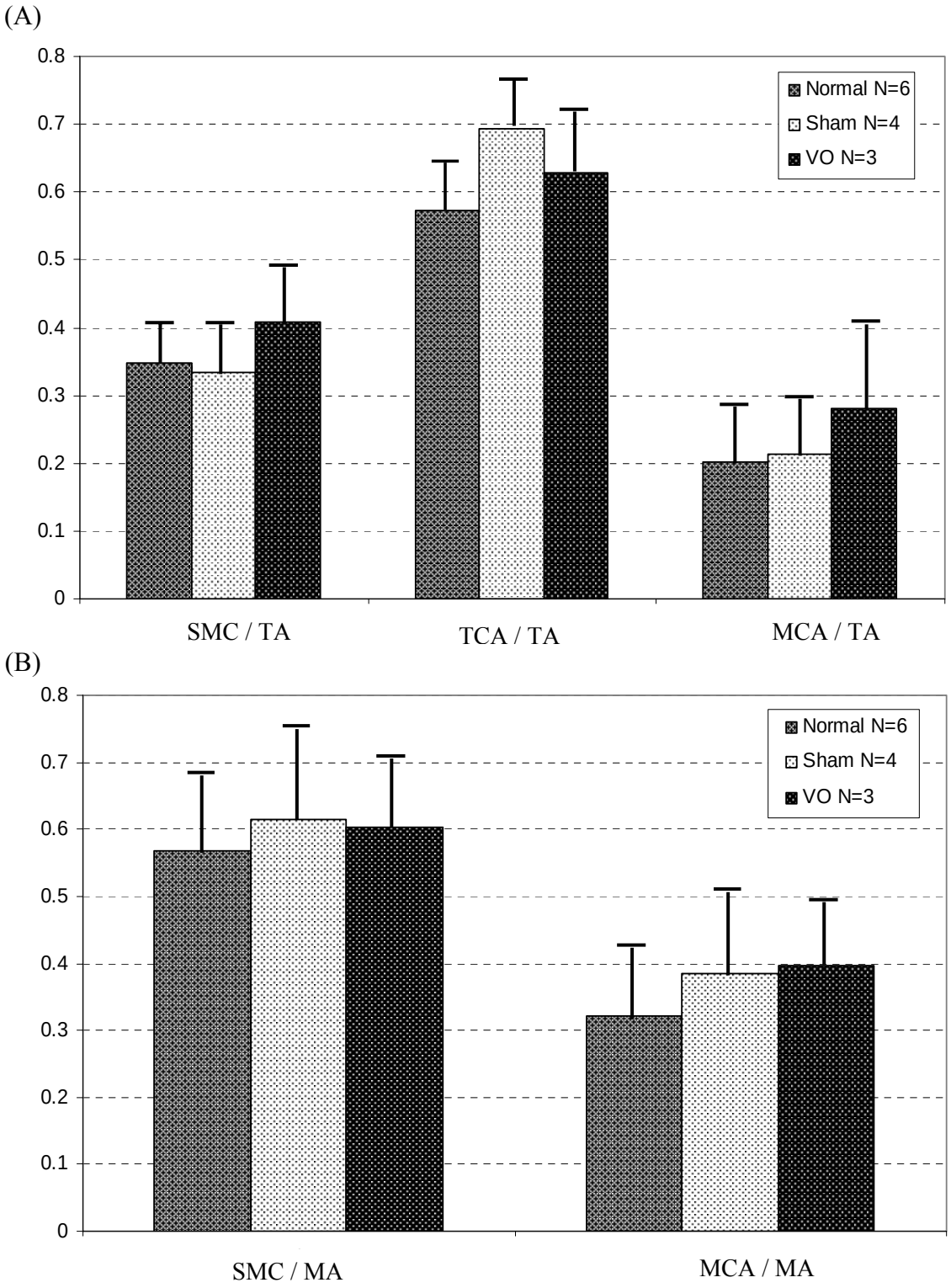

Figure 4.8: Mean and 95% CI for % area of the constituents (A) Mean and 95% CI of the ratio of total area occupied by the medial collagen and SMC with total medial area for normal, sham and venous occluded vessels. (B) Mean and 95% CI of the ratio of area occupied by SMC, Total collagen and Medial collagen with total cross section area of the vessel for normal, sham and venous occluded vessels.

Geometric Changes

Variation in thickness to average radius with the average radius of the lymphatic vessels (Normal, Sham and Venous Occluded) is as shown in figure 4.6 (A). The ratio seems to vary with the average radius with larger diameter vessels having a lower ratio as compared to the smaller diameter vessels. The variation of thickness to average radius ratio for the sham is similar to that for the normal vessel while that of the venous occluded vessels shows a slight change. The data was divided into three bins and the mean and 95% CI for each bin is as shown in figure 4.6 (B).

Structural Changes

The mean and 95% CI for total area of the vessel cross section and total area occupied by collagen estimated from the stained sections shown in figure 4.7 (A). Figure 4.7 (B) shows the mean and 95% CI of the area occupied by media, by the SMC and by collagen in the media for normal, sham and VO vessels. To have a better idea regarding the contribution of collagen accumulation and SMC hypertrophy, commonly known response to increased luminal pressure (Mulvany 2002), towards increase of thickness to radius ratio we estimate the ratio of area occupied by the individual constituents with respect to total cross section area (Figure 3.8 (A)) and total medial area of the vessel (Figure 4.8 (B)).

Theoretical Predictions

The variation of ratio of thickness to average radius with inverse of square of average radius is as shown in figure 4.5, along with the linear fit estimated using the theoretical model/ theoretical relationship between the two variables.

Discussion

Geometric Changes

The variation of thickness to radius ratio with radius of the normal lymphatic vessels shows an interesting trend. The ratio is higher for vessel of lower radius and seems to reach an asymptotic value at higher radius values. Similar trend is observed for the vessels obtained from animal that have undergone sham surgery. The variation follows similar suit in case of vessels from animals subjected to venous occlusion (the change is statistically significant at $P<0.05$, for each bin). The variation of ratio with radius can be explained with the hypothesis that the vessel geometry in case of normal homeostatic condition and in case of pathological condition is such that it keeps the circumferential stress at a fixed value. A theoretical relationship developed on the basis of this hypothesis along with some more assumptions seems to predict this variation. The higher ratio incase of venous occluded vessels can be attributed to increased flow in case of edema like conditions. Though we did not measure the change in flow in the lymphatic system due to induced intestinal edema, based on the geometric changes we can say that the vessel must have experienced a step increase. Ssimilar changes in thickness to radius ratio due to changes circumferential stress is observed in case of arteries and veins subjected to increased transmural pressure (Heagerty et al., 1993, Gusic et al., 2005).

Structural Changes

One of the most fundamental changes in cardiovascular vessels in response to change in flow and pressure is rearrangement of the matrix, especially deposition of new collagen. The changes in the total collagen content of the vessel and the collagen content of the media seems to suggest that lymph vessels are no exception. The total area occupied by media and that by SMC too shows an increase with induction of intestinal edema. Again based on the observed structural changes and drawing parallel with blood vessels subjected to hypertension we can deduce that irrespective of the response of the lymph vessel (pump of conduit) to the edematous conditions they experience a step change in pressure. The contribution of collagen accumulation and SMC hypertrophy

towards increase in vessel thickness seems to be equal as the percentage area occupied by both is similar in case of normal, sham and VO vessels. One can even draw conclusions regarding the state of remodeling by comparing the contribution of each constituent. Though we are not aware of a study that has looked into the steps involved with remodeling of lymph vessel but we speculate that the immediate response is rearrangement and accumulation of ECM and collagen and that SMC hypertrophy follows a day or two later.

Theoretical Relation

The theoretical relation between thickness to radius ratio and radius is developed on the basis of the hypothesis that the circumferential stress in a lymph vessel wall is kept at homeostatic value along the length of the vessel and in homeostatic and pathological conditions. The relation indicates that the thickness to radius ratio is proportional to inverse of radius square and that the proportional constant at a given radius is dependent on the flow through the vessel. Linear fit obtained by using the experimental data suggest that the relationship can model the variation well and as expected the proportionality constant in case of VO vessel is higher than that in case of normal or sham. The relationship developed is rather preliminary as compared to more complete model such as that of time varying elastance, the growth and remodeling proposed by Rachev (Rachev et al., 1998) or Rodriguez (Rodriguez et al., 1994).

From the present study we can conclude that there are distinct morphological changes in the lymph vessels subjected to intestinal edema. Though some of the structural changes are not statistically significant they do show a definite trend towards a change. The lack of statistical significance can be attributed to the wide variation in the data values of the vessels subjected to edematous conditions. The variation can be attributed to the fact that animal was subjected to the condition for only 3 days and the time frame might not have been sufficient for the lymph vessel to completely remodel and reach a steady structural state in response to change mechanical environment. It would be interesting to study the morphological changes in the vessels subjected to such conditions over a longer period of time.

CHAPTER V
SUMMARY AND CONCLUSION

Strain Energy Function in Terms of Orthogonal Polynomials

As have been discussed in chapter II use of orthogonal polynomials to fit the biaxial test data has certain advantages over the conventional approaches. Since the independent variables are not collinear the obtained fit is not over-parameterized. The non collinearity amongst the independent variables also reduces the matrix (X^TX) of normal equation into a diagonal matrix. This is particularly useful as the unknown coefficients can be determined without the need of inverting the matrix that might be singular in certain cases. Although, as compared to the use of simple polynomial form as an analytical fit no significant reduction in error propagation is obtained, rather similar to the case of polynomials the error propagation increases with the order of orthogonal polynomial, the coefficients determined are unique and do not vary with inclusion of higher order terms.

The soft tissues are inherently visco-elastic/non-elastic and in our opinion it is essential to verify the assumption of hyperelastic behavior that is commonly made to model mechanical behavior under biaxial loading. The proposed method allows one to separate error of definition from error of fit and hence allows one to verify the suitability of hyperelastic assumption. The measure of deviation from hyperlastic behavior was used, in the current case, to compare two different material behaviors but based on such measure one can define an absolute scale that would help an investigator to know if the assumption of hyperelastic behavior is acceptable.

Separation of the error of fit from error of definition will also help an investigator to select the order of the analytical fit and hence that of the functional form rather than guess it. The strain energy function obtained by using the proposed method is as effective in predicting the data as the other polynomial forms of strain energy functions. It has an added advantage that the coefficients used to derive it are unique and do not vary with changes in the order of orthogonal polynomial.

It is essential that one restricts the parameter search space in order to obtain physically realistic parameter values (Humphrey 2001). One of the limitations of the current study is that such constraints were not enforced while estimating parameter values for analytical fit to the experimental data and hence there is a possibility that the parameter values are not realistic. For example it is possible that the negative value of the coefficients a_{12} and a_{22} (Table 2.2) for the analytical fit to the experiment data are not realistic. The negative value could also result from non monotonic variation of the estimated values of $(\partial W_{\gamma_k} / \partial \gamma_k)'_{exp}$ for distribution $\gamma_2 - \gamma'_3$. In future we aim to overcome these limitations by ensuring that we collect substantial data in ROI and by constraining the search space of the parameters.

Although a wide variety of strain energy functions are proposed to describe the non-linear material behavior of biological soft tissues, there has been little success in assigning physical meaning to the parameter values. In our opinion the task is further complicated due to the dependence of parameter values on the order of polynomial used in the functional form. Use of orthogonal polynomials that gives unique parameter values and overcomes such dependence, although does not suggest a physical meaning, is, we believe, a step forward in that direction. In our opinion the assignment of physical meaning will have to wait for detailed knowledge of structure of the soft tissue under different loading conditions and intuition gained by a large number of experiments on variety of materials with a wide range of material behavior.

Convexity of strain energy function is essential with regards to the local stability of the soft tissue under the dead loading conditions and in development of the numerical methods to solve the boundary value problems (Ogden and Schulze-Bauer 2000, Wilber and Walton 2002). Such a local convexity is ensured if the contours of constant strain energy for a given material are convex. One can refer to Holzapfel (Holzapfel et al., 2000) for a much detailed account of the convexity for the commonly used two dimensional and three dimension constitutive equations for soft tissues. It is evident that one has to place certain constraints on the parameter values so as to achieve this requirement.

For the strain energy function in terms of Criscione's strain attributes derived using the biaxial experimental data on bovine lymph vessel (illustrative example), the contour plots of constant strain energy are as shown in figure 2.9. It must be noted that the result that convexity of contours imply convexity of strain energy function, was obtained for Green Strain **E** (Holzapfel et al., 2000) and therefore one needs to substitute for γ_2 and γ_3 , and obtain the derived strain energy function in terms of E_{zz} and $E_{\theta\theta}$ Before plotting the contours. Though the performance of the strain energy function derived from the experimental data seems acceptable in the tensile region, similar to the polynomial constitutive equation proposed by Viashnav (1973), due to its dependence on the cubic powers of Criscione strain attributes it is and will not be convex (Holzapfel et al., 2000). For the strain energy function to be convex one will have to constraint the parameter search space and such constraints will result in increase in what we call error of definition. Therefore, one might have to use higher order polynomials in order to respect the convexity constraints and keep the error of definition at an acceptable value. Constraining the parameter values so that the strain energy function respects the convexity conditions and the effect of such constraints on error of definition will be studied in future.

Biaxial Mechanical Behavior of Lymph Vessel

On the basis of structural similarity with arteries and veins we have assumed the lymphatic vessel to be homogeneous, thin walled, axis symmetric and incompressible and that its behavior under combined inflation and extension is orthotropic and hyperelastic. Such assumptions allow us to model the behavior of the vessels from normal, sham and venous occluded animals using the proposed method. Since we have not modeled the biaxial mechanical behavior arteries and veins using the proposed method we cannot compare or comment on how the model faired in characterizing such behavior in case of lymphatic vessels. Also due to lack of enough data on deviation of wide variety of soft tissues from hyperelastic ideal we cannot comment on the deviation from hyperelastic ideal observed for the vessels under consideration.

The length of the vessel at which there is minimal change in axial load with

change in transmural pressure is assumed as in-vivo length of the vessel. The stretch ratio for all the vessels (Normal, VO and sham) was almost similar (~1.15). Also there was no significant/conclusive change in the variation of the circumferential stretch ratio with transmural pressure at in-vivo length or at length corresponding to stretch ratio of ~ 1.13(in-vivo length as reference). Although all the vessels seem (except two from sham) to become more complaint with increase in stretch ratio, change of compliance for each vessel was not quantified and comparison of this might give some indication of change in mechanical behavior.

Since the coefficients of the orthogonal polynomials used to fit the biaxial test data can be assigned a physical meaning that is characterisitic of material and are indicative of the underlysing strucuture, comparison of the parameter values for normal, sham and VO vessels would help us determine any difference in mechanical behavior of the vessels. Such comparison shows that most of the coefficients for VO vessels are higher than those for sham and normal vessels indicating that the mechanical behavior of the VO vessels for similar range of deformation is different than that for sham and normal vessels. This also implies structural remodeling of the vessels subjected to high flow/edematous conditions.

Since similar protocol used for biaxial test of the vessels was same, the deviation from hyperelastic behavior of the vessels for similar range of deformation estimated using the order of orthogonal polynomials that give similar error of fit can also be used to compare the vessel behavior. Although one on the VO vessel showed very large deviation compared to the other we shall refrain from making any conclusion since the deviation for the other VO vessel was similar to that of Normal and sham vessels.

From the comparison of the circumferential stretch, the coefficients and the deviation from hyperelastic ideal for the vessels we conclude that though there are indications that the behavior of VO vessels is different than those of sham and normal hence implying associated structural remodeling, it is not conclusive. We would need more data to draw any inferences especially when we consider the large error that is usually associated with the data from biaxial experiments as a result of dependence of

the vessel behavior on strain history, harvesting and cleaning of the vessels using blunt dissection and selection of appropriate reference configuration. Indeed it should be evident from figure 3.14 and 3.15 that there is large variability in the coefficient values amongst the normal vessels themselves. This variation can be attributed to the different sources of error mentioned above. We believe that with use of large amount of data (biaxial experiments on more samples) the trends would become more prominent to make suitable interpretation with any certainty.

Morphological Changes due to High Flow Conditions

The variation of thickness to radius ratio with radius of the normal lymphatic vessels shows an interesting trend. The ratio is higher for vessel of lower radius and seems to reach an asymptotic value at higher radius values. Similar trend is observed for the vessels obtained from animal that have undergone sham surgery. The variation follows similar suit in case of vessels from animals subjected to venous occlusion (the change is statistically significant at $P<0.05$, for each bin). The variation of ratio with radius can be explained with the hypothesis that the vessel geometry in case of normal homeostatic condition and in case of pathological condition is such that it keeps the circumferential stress at a fixed value. A theoretical relationship developed on the basis of this hypothesis along with some more assumptions seems to predict this variation. The higher ratio incase of venous occluded vessels can be attributed to increased flow in case of edema like conditions. Though we did not measure the change in flow in the lymphatic system due to induced intestinal edema, based on the geometric changes we can say that the vessel must have experienced a step increase. Similar changes in thickness to radius ratio due to changes circumferential stress is observed in case of arteries and veins subjected to increased transmural pressure (Heagerty et al., 1993, Gusic et al., 2005).

One of the most fundamental changes in cardiovascular vessels in response to change in flow and pressure is rearrangement of the matrix, especially deposition of new collagen. The changes in the total collagen content of the vessel and the collagen content

of the media seems to suggest that lymph vessels are no exception. The total area occupied by media and that by SMC too shows an increase with induction of intestinal edema. Again based on the observed structural changes and drawing parallel with blood vessels subjected to hypertension we can deduce that irrespective of the response of the lymph vessel (pump of conduit) to the edematous conditions they experience a step change in pressure. The contribution of collagen accumulation and SMC hypertrophy towards increase in vessel thickness seems to be equal as the percentage area occupied by both is similar in case of normal, sham and VO vessels.

From the present study we can conclude that there are distinct morphological changes in the lymph vessels subjected to intestinal edema. Though some of the structural changes are not statistically significant they do show a definite trend towards a change. The lack of statistical significance can be attributed to the wide variation in the data values of the vessels subjected to edematous conditions. The variation can be attributed to the fact that animal was subjected to the condition for only 3 days and the time frame might not have been sufficient for the lymph vessel to completely remodel and reach a steady structural state in response to change mechanical environment. It would be interesting to study the morphological changes in the vessels subjected to such conditions over a longer period of time.

REFERENCES

Aukland K., Reed R. K. 1993. Interstetial-lymphatic mechanisms in the control of extracellular fluid volume. Physiol. Rev. 73 (1): 1-78

Brossollet L.J., Vito R.P. 1995. An alternate formulation of the blood vessel mechanics and the meaning of the in-vivo property. J. Biomech. 28 (6) :679-687

Brennan M. J., Miller L. T. 1998. Overview of treatment options and review of current role and use of compression garments, Intermittent pumps and exercise in management of lymphedema. Cancer Supplement. 83 (12): 2821-2827.

Campisi C., Bocacardo F., Zilli A., Maccio' A., Napoli F. 2001. Long term results after lymphatic-venous anastomosis for the treatment of obstructive lymphedema. Microsurgery. 21: 135-139.

Choung C.J., Fung Y.C. 1986. On residual stress in arteries. ASME J. Biomech. Eng. 108:189-192.

Cox R.H. 1978. Passive mechanics and connective tissue composition of canine arteries. Am. J. Physiol. 234:H533-541.

Criscione J.C., Humphrey J.D., Douglas A.S., Hunter W.C. 2000. An invariant basis for natural strain which yields orthogonal stress response terms in isotropic hyperelasticity. J. Mech. Phy. Solids. 48:2445-2465

Criscione J.C. 2003. Rivlin's representation formula is ill-conceived for the determination of response functions via biaxial testing. J. Elasticity. 70:129-147.

Criscione J.C. 2004. A constitutive framework for tubular structures that enables a semi-inverse solution to extension and inflation. J. Elasticity. 77:57-81

Davies P.F. 1995. Flow mediated endothelial mechanotransduction. Physiol Rev. 75(3):519-560.

Forsythe G.E. 1957. Generation and use of orthogonal polynomials for data fitting with a digital computer. J. Soc. Indust. Appl .Math. 5(2):74-88

Fung Y.C., Fronek K., Patitucci P. 1979. Pseudoelasticity of arteries and the choice of its mathematical expression. Am. J. Physiol. 237:H620-H631.

Gashev A.A., Wang W., Laine G. A., Stewart R., Zawieja D. C. 2007. Characteristics of the active lymph pump in bovine prenodal mesenteric lymhatics. Lymphatic Research and Biology. 5 (2): 71-79.

Gray H. F.R.S. 1901. Anatomy: descriptive and surgical. Bounty Books, New York.

Gusic R. J., Myung R. Petko M. Gaynor J. W., Gooch K. J. 2005. Shear stress and pressure modulate saphenous vein remodeling ex vivo. J. Biomech. 38: 1760-1769.

Hargen A. R., Schmid-Schonbein G.W. 2000. Mechanics of tissue and lymphatic transport. The Biomedical Engineering Handbook, Second Edition. Eds Bronzino J.D. CRC Press and IEEE Press, Boca Raton, Florida.

Heagerty A.M., Aalkjaer C., Bund S.J., Korsgaard N., Mulvany M.J. 1993. Small artery structure in hypertension. Dual process of remodeling and growth. Hypertension 21 (4):391-397.

Holzapfel G.A., Gasser T.C., Ogden R.W. 2000. A new constitutive framework for arterial wall mechanics and a comparative study of material models. J. Elasticity. 61:1-48.

Hu J.J., Baek S., Humphrey J.D. 2007. Stress-strain behavior of the passive basilar artery in normotension and hypertension. J. Biomech. 40:2559-2563.

Humphrey J.D., Strumpf R.K., Yin F.C.P. 1990. Determination of a constitutive relation for passive myocardium: I. A new functional form. ASME J Biomech Engr, 112:333-339

Humphrey J. D. 2001. Cardiovascular solid mechanics: cells, tissues and organs. Springer-Verlag New York.

Humphrey J.D. 2003. Continuum biomechanics of soft biological tissues. Proc R Soc Lond A 459: 3-46

Langille, B.L., Bendeck, M.P., Keeley, F.W., 1989. Adaptations of carotid arteries of young and mature rabbits to reduced carotid blood flow. Am. J. Physiol: Heart and Circulation Physiology 256, 931–939.

Malvern L.E. 1969. Introduction to the mechanics of a continuous medium. Prentice-Hall. Englewood Cliffs New Jersey.

Matsubara S., Sakuda H., Nakaema M., Kuniyoshi Y. 2006. Long-term results of microscopic lymphatic vessel-isolated vein anastomosis for secondary lymphedema of the lower extremities. Surg. Today. 36: 859-864

Mulvany M. J. 2002. Small artery remodeling and significance in development of hypertension. News Physiol. Sci. 17: 105-109.

Nagase T., Gonda K., Inoue K., Higashino T., Fukuda N., Gorai K., Mihara M., Nakanishi M., Koshima I. 2005. Treatment of lymphedema with lymphaticovenular anastomosis. Int. J. Clin. Oncol. 10: 304-310.

Ogden R.W. 1997. Non-linear elastic deformation Dover Publication, Dover.

Ogden R.W., Schulze-Bauer C.A.J. 2000. Phenomenological and structural aspects of the mechanical response of arteries. 141-156. Mechanics in Biology eds Casey J, Bao G ASME New York.

Patel D.J., Fry D.L. 1969. The elastic symmetry of arterial segments in dogs. Circ. Res. 24:1-8

Petrek J.A. 1998. Incidence of breast carcinoma related lymphedema. Cancer 83: 2776-2781

Pepper M.S., Skobe M. 2003. Lymphatic endothelium: morphological, molecular and functional properties. The Journal of Cell Biology. 163 (2):209-213.

Pries AR, Reglin B, Secomb TW 2005 Remodeling of blood vessels. Response of diameter and wall thickness to hemodynamic and metabolic stimuli. Hypertension 46:725-731

Rachev A., Stergiopulos N., Meister J.J. 1998. A model for geometric and mechanical adaptation of arteries to sustained hypertension. ASME J Biomech. Eng. 120:9-17

Rodriguez E.K., Hoger A., McCulloch A.D. 1994. Stress dependent finite growth in soft elastic tissues. J. Biomech. 27 (4):455-467.

Rivlin R.S., Saunders D.W. 1951. Large elastic deformation of isotropic materials. VII. Experiments on the deformation of rubber. Philos. Trans. R. Soc. Lond. A243:251-288.

Rockson S.G. 2005. Lymphedema therapy in the vascular anomaly patient: Therapeutics for forgotten circulation. Lymphatic Research and Biology. 3 (4): 253-255.

Rockson S.G. 2001. Lymphedema. The American Journal of Medicine 110:288-295.

Shacham M., Brauner N. 1997. Minimising the effects of collinearity in polynomial regression. Ind. Eng. Chem. Res. 36:4405-4412.

Shadwick R.E. 1999. Mechanical design in arteries J. Exp. Biol. 202: 3305-3313.

Swartz M. A. 2001. The physiology of the lymphatic system. Advanced Drug Delivery Reviews. 50:3-20.

Scavelli C., Weber E., Agliano M., Cirulli T., Nico B., Vacca A., Ribatti D. 2004. Lymphatics at crossroads of angiogenesis and lymphangiogenesis. J. Anat. 204: 433-449.

Taber L. A. 1998. An optimization principle for vascular radius including the effects of smooth muscle tone. Biophysical J. 74: 109-114.

Vaishnav R.N., Young J.T., Janicki J.S., Patel D.J. 1972. Nonlinear anisotropic elastic properties of the canine aorta. Biophysical J. 12:1008-1027.

Vaishnav R.N., Young J.T., Janicki J.S., Patel D.J. 1973. Distribution of stresses and of strain energy density through the wall thickness in a canine aortic segment. Circ. Res. 32: 577-583.

Van Trappen P. O., Pepper M.S. 2001. Lymphangiogenesis and lymph node microdissemination. Gynecologic Oncology. 82: 1-3.

Von Der Weid P.-Y. 2001. Review Article: lymphatic vessel pumping and inflammation-the role of spontaneous constriction and underlying electrical pacemaker potential. Alimentary & Pharmacology Theraputics. 15: 1115-1129.

Vito R.P., Dixon S.A. 2003. Blood vessel constitutive models 1995-2002 Annu. Rev. Biomed. Eng. 5:413-439.

Vorp D.A., Rajagopal K.A., Smolinsky P.J., Borovetz H.S. 1995. Identification of elastic properties of homogeneous, orthotropic vascular segments in distension. J. Biomech. 28-(5):501-512.

Wilber J.P. Walton J.R. 2002. The convexity properties for a class of constitutive models for biological soft tissues. Mathematics and Mechanics of Solids. 7:217-235.

Yin F.C.P., Chew P.H., Zeger S.L. 1986. An approach to quantification of biaxial tissue stress-strain data. J. Biomech 19:27-37.

VITA

Name: Akhilesh A. Kotiya

Address: Dept. Biomedical Engineering
337 Zachry Engineering Center
TAMU 3120
College Station, TX, 77843-3120

Email Address: akhileshkotiya@gmail.com

Education: B.En., Mechanical Engineering, Mumbai University, 2000
M.S., Biomedical Engineering, Texas A&M University, 2004
Ph.D., Biomedical Engineering, Texas A&M University, 2008